Delft University of Technology

Multivariate Probability Distributions for Reliability Analysis of a Submerged Floating Tunnel

Torres Alves, G.A.

Important note
To cite this publication, please use the final published version (if applicable).
Please check the document version above.

Multivariate Probability Distributions for Reliability Analysis of a Submerged Floating Tunnel

Multivariate Probability Distributions for Reliability Analysis of a Submerged Floating Tunnel

Dissertation

for the purpose of obtaining the degree of doctor
at Delft University of Technology
by the authority of the Rector Magnificus, Prof. dr. ir. T.H.J.J. van der Hagen,
chair of the Board for Doctorates,
to be defended publicly on
Thursday 26 September 2024 at 10:00 o'clock

by

Gina Alexandra TORRES ALVES

Master of Science in Hydraulic Structures and Flood Risk,
Delft University of Technology,
born in Cuenca, Ecuador.

This thesis has been approved by the promotors:

Composition of the doctoral committee:

Rector Magnificus,	chairperson
Prof. dr. ir. S.N. Jonkman	Delft University of Technology, promotor
Dr. ir. O. Morales-Nápoles	Delft University of Technology, promotor

Independent members:

Prof.dr.ir.P.H.A.J.M. van Gelder	Delft University of Technology
Prof.dr. C. Czado	Technical University of Munich, Germany
Prof.dr.ir. B.J. Leira	Norwegian University of Science and Technology
Dr.ir. G.F. Nane	Delft University of Technology
Dr.ir. M. Kok	Delft University of Technology, reserve member

An electronic version of this dissertation is available at
`http://repository.tudelft.nl/`.

Look, Dad. I made it.

Mira Pa, lo logré

Contents

Summary

Submerged floating tunnels (SFTs) represent a novel solution for challenging water crossings, particularly in locations where traditional structures such as bridges or immersed tunnels are not feasible. Despite their potential, no SFT has been built yet except for a 100 m-long prototype in Qingdao Lake, China. This lack of experience regarding the design, construction, and operation of SFTs poses significant challenges giving rise to a variety of uncertainties, especially given complex loading conditions and the potential of "cascading" failure scenarios, where multiple hazard events can lead to structural failure.

To address this gap, this dissertation seeks to investigate the application of probabilistic models such as copulas, vine-copulas, and Bayesian Networks to characterize the joint probability distribution of traffic loading, environmental conditions, and to analyze hazard scenarios. With a specific focus on a case study of a hypothetical submerged floating tunnel to be located in the Qiongzhou Strait, China, this research explores metocean loads such as wave height, wave period, and current velocities, alongside traffic loads derived from Weigh-in-Motion (WIM) data.

Regarding traffic loading, a methodology that combines copula-based models and structural models is presented to conduct a reliability analysis on a SFT (Chapter 4). The analysis focuses on how traffic loads can induce bending moments that can potentially cause structural failure in the submerged floating tunnel (SFT). Copula-based models with a focus on autocorrelation are used to characterize inter-vehicle distances, enabling the simulation of traffic flow through the SFT. This simulation, executed within a defined time frame, generates a sequence of vehicles known as a "train" of vehicles. This train includes data on axle weights, inter-axle distances, and inter-vehicle distances.

Chapter 5 presents a joint probability distribution analysis to characterize the pairwise dependence between wave height, wave period, and current velocities, employing copulas. This copula-based approach is able to capture both the linear and non-linear behavior of the data. This analysis was performed across the entire dataset and for extreme conditions. The results yield a synthetic time series of hourly values and extreme values for both waves and currents.

In the following chapters, the focus shifts to exploring multivariate probabilistic methodologies applied to the reliability and risk of an SFT. In Chapters 6 and 7, the dependence between the metocean loads and the hydrodynamic forces as a result of their combined action is investigated by using vine-copula models and Bayesian Networks respectively. The focus is on extreme values of six variables, wave height, wave period of wind waves and swell waves, and current velocities at 1 and 15 meters below the water surface. This analysis was carried out to evaluate different SFT configurations, with varying submergence depths and tube ratios.

Chapter 8 investigates the reliability of SFTs under different hazard scenarios and their potential impact on the failure of this structure. A methodology is introduced to identify and quantify scenarios that can lead to the failure of the SFT by using a discrete Bayesian

network (BN) model. The methodology adapts fault trees from previous studies related to SFTs and maritime accidents. By quantifying the conditional probability tables (CPTs) with the incorporation of data on human errors, fire occurrences, terrorist attacks, and environmental factors, we assess the probability of SFT failure under various combinations of hazard events, known as scenarios. For example, this analysis reveals that environmental loads with a 500-year return period increase the risk of failure by 40%. A similar analysis is possible for other scenarios.

This research demonstrates the importance of taking into account the complex dependence on environmental and traffic variables, among others that are of interest to an SFT. As a result, it is possible to better estimate the occurrence of extreme events and the failure of a SFT to assist decisions regarding its design. This makes it possible to support a safe and stable structure. Moreover, the primary factors contributing to the SFT failure can be identified. The flexibility of the models presented in this thesis allows them to be updated as new data is found, including information from various regions if other areas are under consideration for SFT construction. In this way, a process of continuous safety assessment can be ensured.

In summary, the applicability of copulas, Bayesian Networks, and vine-copulas to assess the reliability of an SFT can be used to make decisions that will lead to the improvement of the design of an SFT and to avoid significant damage to the structure, injuries, or loss of lives. This dissertation contributes to advancing the understanding of SFT reliability and safety, offering valuable insights for engineers and decision-makers in planning and designing stable SFT structures.

Samenvatting

Drijvende tunnels (Submerged Floating Tunnels, SFT) zijn een innovatieve oplossing voor verbindingen over water, met name op locaties waar traditionele constructies zoals bruggen of afgezonken tunnels niet realiseerbaar zijn. Ondanks hun potentie is er tot op heden geen enkele SFT gebouwd, behoudens een prototype van 100 meter lang in het Qingdaomeer, China. Het gebrek aan ervaring met het ontwerp, de bouw en de exploitatie van SFT's vormt een grote uitdaging, met name vanwege de complexe belasting scenario's en de mogelijkheid van voortschrijdende faalscenario's, waarbij meerdere gevaarlijke gebeurtenissen tot constructief falen kunnen leiden. Om deze hiaat in kennis te verkleinen, onderzoekt dit proefschrift de toepassing van probabilistieke modellen zoals copula's, vine-copula's en Bayesiaanse netwerken om de gecombineerde waarschijnlijkheid van verkeersbelasting, omgevingsomstandigheden en gevaarscenario's te karakteriseren. Met een specifieke focus op een casestudie van een hypothetische SFT in de Qiongzhou-strait, China, bevat dit proefschrift onderzoeken naar metoceaanse belastingen zoals golfhoogte, golfperiode en stromingssnelheden, naast verkeersbelastingen afgeleid van Weight in Motion (WIM) data.

Met betrekking tot de verkeersbelasting wordt in hoofdstuk 4 een methodologie gepresenteerd die copula-gebaseerde modellen combineert met constructieve modellen om een betrouwbaarheidsanalyse uit te voeren op een SFT. De analyse richt zich op de vraag hoe verkeersbelastingen buigmomenten kunnen veroorzaken die mogelijk constructief falen van de SFT kunnen veroorzaken. Copula-gebaseerde modellen met een focus op autocorrelatie worden gebruikt om onderlinge voertuigafstanden te karakteriseren, waardoor de simulatie van verkeersstromen door de SFT mogelijk wordt. Deze simulatie, uitgevoerd binnen een gedefinieerde tijdsperiode, genereert een reeks voertuigen die gecategoriseerd wordt als een "trein"van voertuigen. Deze trein bevat gegevens over asgewichten, asafstanden en voertuigafstanden.

Hoofdstuk 5 bevat een analyse van de gezamenlijke kansverdeling om de paarsgewijze afhankelijkheid tussen golfhoogte, golfperiode en stromingssnelheden te karakteriseren met behulp van copula's. Deze copula-gebaseerde benadering is in staat om zowel het lineaire als het niet-lineaire gedrag van de gegevens vast te leggen. Deze analyse is uitgevoerd over de gehele dataset en voor extreme omstandigheden. De resultaten leveren een synthetische tijdreeks op van uurwaarden en extreme waarden voor zowel golven als stromingen.

In de volgende hoofdstukken verschuift de focus naar het verkennen van multivariabele probabilistieke methodes toegepast op de betrouwbaarheid en risico's van een SFT. In hoofdstukken 7 en 6 wordt de afhankelijkheid tussen de metoceaanse belastingen en de hydrodynamische krachten als gevolg van hun gecombineerde werking respectievelijk onderzocht met behulp van Bayesiaanse netwerken en vine-copulamodellen. De focus ligt op extreme waarden van zes variabelen: golfhoogte, golfperiode van windgolven en deining, en stromingssnelheden op 1 en 15 meter onder het wateroppervlak. Deze analyse

is uitgevoerd om verschillende SFT-configuraties te evalueren, met verschillende aanleg-diepdiepdieptes en buisverhoudingen.

Hoofdstuk 8 onderzoekt de betrouwbaarheid van SFT's in verschillende scenario's en hun potentiële impact op het falen van deze structuur. Er wordt een methode geïntroduceerd om scenario's te identificeren en kwantificeren die kunnen leiden tot het falen van de SFT met behulp van een discrete Bayesiaans netwerk (BN) model. De methodologie past foutenbomen toe uit eerdere studies met betrekking tot SFT's en maritieme ongevallen. Door de 'conditional probability tables' (CPT) te kwantificeren met daarin verwerkt de gegevens over menselijke fouten, branduitbraken, terroristische aanslagen en omgevingsfactoren, beoordelen we de waarschijnlijkheid van falen van SFT's bij verschillende combinaties van accidentele gebeurtenissen, bekend als scenario's. Zo blijkt uit deze analyse dat omgevingsbelastingen met een terugkeerperiode van 500 jaar het risico op falen met 40% verhogen. Een soortgelijke analyse is mogelijk voor andere scenario's. Dit onderzoek toont aan hoe belangrijk het is om rekening te houden met de complexe afhankelijkheid van onder andere omgevings- en verkeersvariabelen die van belang zijn voor een SFT. Hierdoor is het mogelijk om de waarschijnlijkheid van extreme gebeurtenissen en het falen van een SFT beter in te schatten om beslissingen te ondersteunen met betrekking tot het ontwerp. Dit maakt het mogelijk om een veilige en stabiele constructie te realiseren. Bovendien kunnen de belangrijkste factoren die bijdragen tot het falen van een SFT worden geïdentificeerd. De gepresenteerde modellen in dit proefschrift zijn flexibel en dat maakt het mogelijk om deze te aan te passen naarmate er nieuwe gegevens beschikbaar komen, inclusief informatie uit lokale bronnen als andere gebieden worden overwogen voor de bouw van SFT's. Op deze manier kan een continu proces van veiligheidsbeoordeling worden gewaarborgd.

Samenvattend, de toepasbaarheid van copula's, Bayesiaanse netwerken en vine-copula's om de betrouwbaarheid van een SFT te beoordelen, kan worden gebruikt om beslissingen te nemen die leiden tot verbetering van het ontwerp van een SFT en tot het vermijden van aanzienlijke schade aan de constructie, verwondingen of verlies van levens. Dit proefschrift draagt bij aan een beter begrip van de betrouwbaarheid en veiligheid van SFT's en biedt waardevolle inzichten voor ingenieurs en besluitvormers bij het plannen en ontwerpen van stabiele SFT-structuren.

I

Introduction

1

Research Context

1.1 The Submerged Floating Tunnel

In civil engineering, waterway crossings are one of the most challenging structures. In the last few decades, the traffic demand and growing development of cities has increased the necessity of longer waterways that require new and more advanced technologies. One structure has already been proposed to give a solution to this problem: The construction of a submerged floating tunnel (SFT). The idea of the SFT was born in Norway in the first decades of the 1900s [6]. However, just in the last years, several preliminary designs and feasibility studies have been proposed worldwide [6–11].

An SFT is also known as Archimedes' Bridge. It is a tubular structure suspended above the sea floor and anchored by pontoons on the water's surface or by tethers by the seabed [12] (Fig. 1.1). It is based on the idea of using the load-carrying capacity of water due to Archimedes buoyancy [13].

In a tethered SFT, the main structural features of an SFT are i) the tunnel cross-section, ii) the anchoring system, iii) structural joints, and iv) the foundations [6]. The dimensions of the SFT and other key features of the SFT may depend on national codes and are beyond the scope of this research. However, design codes of similar structures can be used as a reference to define the structure's overall dimensions and target reliability. A critical structural variable to take into consideration for designing an SFT is the buoyancy-weight ratio (BWR). The BWR is defined as the ratio of Archimedes' buoyancy (B) due to the displaced water volume (W) of the self-weight of the structure (Fig. 1.2). This ratio influences the vertical stability of the SFT and governs the geometrical and material properties of the tunnel and the cables [14]. Therefore, its contribution to the safety of the SFT cannot be neglected.

When compared to traditional structures such as immersed tunnels or bridges, an SFT has the advantage of i) better environmental adaptability ii) less influence of surroundings and navigation, iii) the unit cost of an SFT is constant regardless of its total length, in the case of a suspension bridge or a submarine tunnel, their price will increase rapidly as the span increases. [15].

Parts of this chapter have been published within [1], [2], [3], [4] and [5].

1
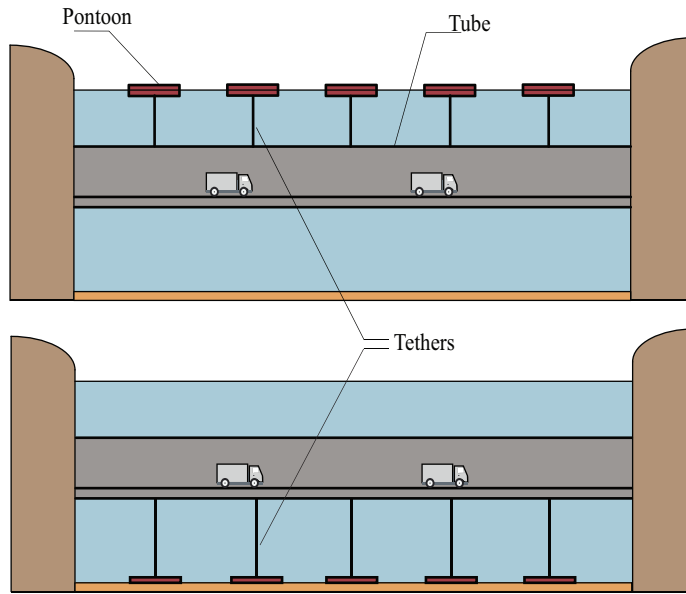
Figure 1.1: Pontoon and tethered type SFT.
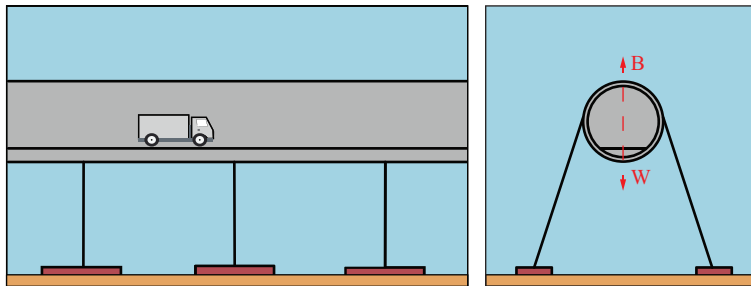
Figure 1.2: Tether type SFT.

Furthermore, the SFT shares many similarities with immersed tunnels, and offshore structures. Inside the SFT, the loads are almost the same as in any other tunnel (Table 1.1). However, as an underwater bridge, the SFT is expected to be 30m below the water's surface. This could induce further movements of the structure. Forces that can cause these movements are tides, currents, waves, traffic, or changes in water level. It is critical to consider accidental loads, for example, explosions, ship collisions, and submarine collisions. Additionally, other loads depend on the region where the SFT is located. For example, earthquakes or volcanic activity. Therefore, an SFT is subjected to a large number of loads (1.1) and the consequences regarding possible damages can be significantly different for an SFT. Consequently, it is essential to take an integrative approach to understand how different hazard scenarios could affect the behavior of the SFT.

1

Loads	Offshore Structures [16]	Immersed Tunnels [17]	SFT [7]
Permanent loads			
Self-weight	x	x	x
Permanent ballast		x	x
Marine Growth		x	x
Weight of permanent Pavement		x	x
Equipment		x	x
Weight of water absorbed by concrete			x
Hydrostatic loads	x	x	x
Deck load	x		
Variable loads due to vehicles			
Traffic		x	x
Environmental Variables			
Tide			x
Current	x	x	x
Wave induced loading	x	x	x
Wave + Current loads	x	x	x
Wave slamming load	x		
Breaking wave load	x		
Wave run-up load	x		
Internal waves	x		x
Wind			x
Snow loads		x	x
Ice loads		x	x
Accidental loads			
Ship impact		x	x
Forces generated by a passing ship		x	x
Compartment flooding		x	x
Loss of support		x	
Falling and dragging anchor		x	
Fire		x	x
Explosion		x	x
Deformation loads			
Creep and shrinkage			x
Post-tensioning			x
Temperature loads		x	x

Table 1.1: Relevant loads for offshore structures, immersed tunnels, and SFTs.

1

1.2 Knowledge gaps

Several challenges result from a lack of knowledge when studying the reliability of a submerged floating tunnel. These challenges were identified and addressed in the paragraphs below.

1.2.1 Lack of experience

Except for a prototype in Qingdao Lake in China, no SFT has been constructed to date [13]. At the same time, there are no unique features or elements in an SFT that have not been encountered in bridges, tunnels, or offshore structures. However, specific combinations of materials, design techniques, and construction methods may be required [18]. Different models to estimate the structural response of the SFT are associated with large uncertainties that are, in turn, a consequence of the lack of experience [19]. This lack of knowledge limits the assessment and validation of models, therefore it is necessary to gather information from laboratory tests on prototypes [20–25] and apply knowledge already available from similar structures to investigate the reliability of an SFT.

The first SFT to be constructed and operated may require higher acceptable risk levels compared to similar structures because of the novelty of the SFT concept and new safety issues may need to be taken into account [26]. These limitations highlight the need for further research on the safety and reliability of SFTs and suggest the need for innovative methodologies specially designed for this structure. These methodologies may combine probabilistic tools with known structural or hydrodynamic models.

1.2.2 Complex loading conditions

As mentioned in Section 1.1, the SFT is a complex structure that combines elements from other structures such as bridges, tunnels, or offshore platforms. Moreover, its particular placement within the water depth leads to complex load conditions. SFTs can span different types of waterways, for example, estuaries, rivers, fjords, lakes, straits, etc [18], and although SFTs are often focused on their use for road traffic, other applications like service or pedestrian tunnels are also of interest. Site and use-specific conditions play an important role in design choices due to their impact on the feasibility of the project and also on the behavior of the SFT under different loading/accident scenarios. Critical design conditions that are relevant for SFTs are, among others [26]: i) extreme design environmental conditions (waves, currents, tides, seismic loads, etc), ii) geology at the entrance and foundations, iii) operational conditions, iv) situations where one or more SFT elements fail or deteriorate, v) mitigation strategies and accessibility in case of repairs, etc

Different load scenarios such as the simultaneous action of traffic, currents, and waves, or the possibility of submarine accidents, lead to load combinations that rarely occur in other structures [19]. Moreover, in the design of hydraulic structures, the design values of the variables of interest are assumed to be independent and their dependence relationship is often ignored. Reliability analyses for SFTs would benefit from taking into account the dependence between variables (accidental, environmental, etc), providing, in this way, a more realistic characterization of the SFT and its surrounding environment. The need for multivariate models that can quantify the occurrence of hazard/extreme scenarios is paramount for the development of research related to SFTs. In this way, the uncertainties

1

relating to the combined action of the variables relevant to an SFT and undesired scenarios should not be overlooked

1.2.3 "Cascading" scenarios

SFTs have different consequences linked to when relevant limit states are surpassed, or when the structure fails to fulfill its intended function. Consequently, different safety costs influence selecting an optimal safety level (defined as the safety level that minimizes the total expected cost) [19]. For example, a traffic accident inside the SFT can cause leakage in the tunnel and an imbalance in the Buoyancy weight ratio (BWR). This can lead to slacking or snapping of the tethers and finally to loss of the SFT. Another example is when there is a crack opening that can lead to flooding of the structure or to corrosion of the re-bars. The lack of experience combined with the complexity of this structure regarding its loading conditions and limit states could enhance the risk perception in owners, investors, or drivers about the tunnel being lost in case of undesirable scenarios causing substantial economic damage and fatalities. It is crucial to have a design that could guarantee localized repairable structural damage. Thus, owners would be more prone to proceed with a project of this nature [27].

The safety objective is to achieve a probability of failure below an established limit. In the case of an SFT, this must be met by combining applicable standards and specific reliability analyses that consider these "cascading" scenarios. Guidelines of bridges, tunnels, or offshore structures can also be used as a reference for the design and safety assessment of SFTs, but it is crucial to consider that particular safety limits and limit states must still be developed for SFTs [19, 28].

Given the challenges described previously, it is critical to conduct thorough reliability studies to forecast the failure of an SFT and its elements before implementing this structure on a large scale. Reliability and risk studies can help identify potential factors that can lead to the failure of an SFT. Moreover, these studies can offer important information for the design and maintenance of SFTs, which can also result in increased safety and cost-effectiveness. Continued research and development in the field of submerged floating tunnels are necessary to improve the reliability of these structures and ensure their successful implementation in the future.

1.3 Motivation

Submerged floating tunnels (SFTs) are an innovative solution for waterway crossings that can potentially revolutionize transportation infrastructure. However, to this day, no SFT has been constructed yet. One of the main reasons is that its potential design, construction, and operation are not sufficiently known and understood. Moreover, given the complexity of the underwater environment, many uncertainties and risks arise about the reliability and safety of these structures. In this research, it is of interest to show the applicability of probabilistic models to study the complex dependence between the different conditions that are of importance for an SFT. This is to gain insight into the expected safety and reliability of the SFT and its elements by identifying potential risks and failure modes. Such information can be used to assist engineers and decision-makers in planning and composing a stable SFT design.

1

1.4 Research Objectives

In order to contribute towards a stable and safe submerged floating tunnel design, the main objective of this research is to investigate and develop probabilistic-based models using copulas, vine-copulas, and Bayesian networks to quantify the probability of failure of the SFT during operation under different loading conditions and hazard scenarios.

More specifically, this objective is divided into the following:

1. Identify methods that can properly characterize the dependence between loading variables that are of interest to an SFT. These variables are:

    (a) Environmental variables (waves, currents, water levels, and earthquakes).

    (b) Traffic variables.

    (c) Calamities (fire and terrorism).

2. Assess different SFT configurations to assist decision-making.

3. Compare different hazard scenarios and identify the main contributors to the failure of the SFT in the specific case presented in this thesis.

1.5 Thesis Outline

This thesis is divided into four main parts. Part I and Part IV are the introduction and conclusion. Parts II and III represent the main body of this dissertation. Part II presents the methodology and application of copula-based models to simulate traffic data passing over the SFT, as well as the simulation of normal conditions and extreme values of metocean data (waves and currents). Part III discusses methods and applications for the reliability and risk of an SFT using vine-copula models and Bayesian Network models. Part II and III comprise two and three chapters respectively. All the chapters in this thesis are based on scientific manuscripts (some published and others yet to be published) where the author of this thesis is the main author

Part I is made up of three chapters. The SFT concept and research context are presented in Chapter 1. In Chapter 2, the theoretical background to the probabilistic models employed throughout this dissertation is described. Followed by the presentation of the case study (Chapter 3).

Part II is formed by Chapter 4 and 5. Specifically, Chapter 4 is based on [3] and presents a methodology to produce a synthetic time series for traffic. Chapter 5 presents a copula-based methodology to simulate hourly and extreme values of metocean variables (waves and currents). Models for auto-correlation are also developed using copulas. This chapter is based on [1].

Part III consists of Chapter 6, 7, and 8. Chapter 6 is based on [4]. This chapter presents a methodology using vine-copulas for simulating metocean variables and their resulting hydrodynamic forces acting on an SFT. The model is also used to examine nine different configurations of the SFT (i.e. different variations of diameters and submerged depth). A similar application is presented in Chapter 7 using a methodology with bayesian networks. This chapter is based on [2]. Chapter 8 is based on [5] and presents a methodology to

identify the main contributing factors to the failure of the SFT and its elements, through a discrete Bayesian network methodology.

The chapters of this dissertation do not include the entire research output of the author. The remaining research output, in which the author was also involved, is summarized in a list of publications in the section *List of Publications*.

1.6 Research Context

This dissertation is part of the larger Submerged floating tunnel (SFT) technical research team. This joint industry project was initiated in 2018 by the Chinese engineering and construction company China Communications Construction Co., Ltd. (CCCC) as a global collaborative research project together with CCCC Highway Consultants Co., Ltd, CCCC-FHDI Engineering Co., Ltd., CCCC Third Harbor Engineering Co., Ltd, Tianjin Research Institute for Water Transport Engineering, M.O.T, Tunnel Engineering Consultants (TEC), and Delft University of Technology (TU Delft).

The SFT project aims to solve key technical issues in the design and construction of submerged floating tunnels. TU Delft's research for the CCCC-led SFT project is split over 11 work packages (Table 1.2). Three Ph.D. projects are identified in the fields of hydrodynamic effects, and risk and reliability assessments.

Code	Description
WP-01	Structural design and research
WP-02	Hydrodynamic and structural model analysis research
WP-03	Risk evaluation
WP-04	Numerical model development
WP-05	Anchoring system research
WP-06	Joints and shore connection structure research
WP-07	Construction methods and equipment assessment
WP-08	Material research
WP-09	Design and construction guideline
WP-10	Survey systems
WP-11	Physical model experiments guideline

Table 1.2: Work packages. SFT project.

This dissertation is part of the Risk evaluation work package (WP-03) and is focused on the application of probabilistic methods, specifically, multivariate probability distributions to provide a more realistic description of the complex dependence between the various loads and hazard scenarios that are of relevance for the design and reliability of SFTs.

2

Probabilistic Preliminaries

The main focus of this research, as introduced in Chapter 1, is the applicability of probabilistic models to study the complex dependence between the loads acting on an SFT to support a safe and stable SFT design. Three methodologies, copulas, vine-copulas, and Bayesian networks (BNs), have been selected for this purpose. This chapter aims to provide the theoretical basis for these methodologies so that they can be applied in the remaining chapters of this thesis. A brief description of marginal and conditional distributions is presented in section 2.1, and the basics of copula theory are discussed in section 2.3. Vine-copulas are introduced in section 2.4 and Bayesian Networks are addressed in section 2.5.

2.1 Marginal and Conditional Distributions

Probability distributions for random variables encompass both marginal and conditional probability distributions. The cumulative distribution function (cdf) of a continuous random variable X is defined as the integral of its probability density function f_X:

$$F_X(x) = P(X \le x) = \int_{-\infty}^{x} f_X(t)dt \tag{2.1}$$

Where $P(X \le x)$ represents the probability that X takes on values less than or equal to x. A definition that is necessary to understand the concepts of marginal and conditional probability is the joint probability. The joint cumulative distribution function of two random variables X and Y is defined as:

$$F_{XY}(x, y) = P(X \le x, Y \le y) \tag{2.2}$$

The conditional probability density function of X given Y is:

$$f(x|y) = \frac{f(x, y)}{f_Y(y)} \tag{2.3}$$

provided that $f(x, y)$ is the joint probability density function, $f_X(x)$ and $f_Y(y)$ are the marginal probability density functions and that $f_Y(y) > 0$. This concept can be generalized

Parts of this chapter have been published within [1], [2], [3], [4] and [5].

to $f(x_1, ... x_n)$ in case of more than two variables. The conditional probability distribution is the distribution function that provides the probability that a variable will occur given the value of another variable and is usually represented as $f(x|y)$ and the conditional cumulative distribution function of X, given $Y = y$ is defined as:

$$F_{X|Y}(x|y) = P(X \leq x|Y = y) = \int_{-\infty}^{x} f_{X|Y}(u|y)du \qquad (2.4)$$

The marginal probability density function can be computed from the joint probability distribution of several random variables, in this case, we focus on the bi-variate case. For continuous distributions, the marginal probability density function is obtained by integrating all possible outcomes of the variable, as follows:

$$f_X(x) = \int f(x, y)dy \qquad (2.5)$$

$$f_Y(y) = \int f(x, y)dx \qquad (2.6)$$

2.2 Extreme Value Analysis

In multivariate cases, sampling methods such as the peak-over-threshold (POT) can help identify extreme values within time series. In this method, one variable of the multivariate set is designated as the dominant variable, and any values that exceed a predefined threshold are labeled as extreme values. For each of these extreme values, we also extract the accompanying values of the remaining (concomitant) variables. It is important to recognize that these concomitant values do not necessarily have to be extreme themselves. The goal is to explore the relationship between the extreme events in the dominant variable and their accompanying values in the other variables. This approach ensures that the interdependence between the variables remains intact, delineating what constitutes an extreme event.

This methodology is specifically applied in this dissertation to metocean variables, including significant wave height, wave period, and current velocity, for two distinct wave systems: wind waves and swells. Additionally, current velocity data is collected at depths of 1 and 15 meters from the water's surface. A detailed description of this approach is presented in Chapter 6.

Understanding the frequency and magnitude of extreme events is crucial for risk assessment and infrastructure planning. This is often quantified using the concept of return period (T_R), which provides a quantitative measure of the probability that a particular extreme value will occur. Return period analysis provides valuable insights into the frequency and impact of extreme events. Suppose that an extreme event occurs if the extreme value random variable X is greater than or equal to some magnitude x, then the return period (T_R) is defined as:

$$T_R = \frac{1}{P(X > x)} \qquad (2.7)$$

Here, $P(X > x)$ represents the probability of observing an extreme event. The longer the return period T_R, the less frequent the event ($P(X > x)$), and the larger the magnitude of the random variable x. Equation 2.7 assumes that the probability of the event is independent of past events and does not vary over time. In other words, it is defined as the average time interval between the occurrence of a specific event or phenomenon. For example, if an event has a probability p of 0.01 (or 1%), it suggests that on average, $1/p = 100$ trials would need to be conducted before experiencing that event once. Note that this does not mean that this event will occur every 100 years or only once in 100 years. It means that a 100-year event may occur once, more than once, or not at all in any given 100-year period.

In this dissertation, the return period for the dominant variable is computed using Eq. 2.7. However, this concept can not be applied directly to the concomitant variables because they may not follow an extreme value distribution.

Consider a case with three continuous random variables X, Y, and Z. Where X is the dominant variable, and Y, and Z are the concomitant variables. Let u represent the threshold value. The cumulative distribution function (CDF) F_u of X over the threshold u for the dominant variable is defined as:

$$F_u(x) = P(X - u > x | X > u) \tag{2.8}$$

The random variable $X - u$ is the "excess" over the threshold u. In this context, the CDFs of the concomitant variables Y and Z, given the dominant variable X exceeding a threshold u, can be expressed as:

$$F_{Y|X}(y|x) = P(Y \leq y | X > u) \tag{2.9}$$

$$F_{Z|X}(z|x) = P(Z \leq z | X > u) \tag{2.10}$$

These equations capture the relationship between the concomitant variable and the extreme values of the dominant variable.

2.3 Copulas

Variables such as significant wave height, wave period, and current velocity, alongside traffic loads, collectively shape the operational conditions of submerged floating tunnels. Copulas provide a flexible framework for modeling the joint distribution of these variables, capturing dependencies that may exist beyond simple linear correlations. By applying copulas in SFT studies, engineers and researchers can gain a deeper understanding of how environmental conditions and traffic patterns interact to influence the structural integrity and safety of the structure.

Despite the potential of these models, their application in submerged floating tunnels remains largely unexplored. Usually, copulas are commonly applied in bi-variate cases across various fields. In hydrology, [29] used copulas to estimate the annual instantaneous maximum flows at three tributaries in the Euphrates River Basin, Turkey. Similarly, in [30, 31], the authors characterized floods by modeling flood event properties such as hydrograph duration and volume and peak discharge. In transportation and traffic studies,

[32] suggested a copula-based model to investigate the relationship between vehicle type choice and usage (miles traveled). The effects of travel behavior are examined in [33] by studying the dependence between residential neighborhood choice and daily household vehicle miles per travel (VMT). Additionally, [34] employed a copula-based model to describe the relationship between vehicle speed, headway, and length.

In structural engineering, copulas find application in diverse contexts. In [35] copulas are used to characterize corrosion growth for the assessment of steel girder bridges. Environmental load modeling is another area of interest as evidenced in [36], where a copula model is used to characterize the joint distribution of wind speed and rain intensity to perform a failure analysis of a transmission line. The relationship between wind speed and air temperature is studied to assess long-span bridges [37]. Copulas have also been applied to describe spatial correlation in estimating wave height records [38] and to capture the asymmetric dependencies between met ocean data [39]. Similar dependencies have been used for the design and risk assessment of offshore engineering applications [40]. Finally, [41] presented an application of copula-based models and reliability analysis to investigate the failure of a dike by overflow.

Sklar's theorem [42] states that any multivariate joint distribution of continuous random variables can be written in terms of a set of univariate marginal distribution functions and a copula that describes the dependence between the random variables. For the case of two random variables, the bi-variate copula (C) is defined as:

$$H_{XY}(x, y) = C\left(F_X(x), G_Y(y)\right) \tag{2.11}$$

Here, $H_{XY}(x, y)$ is the joint distribution of the two continuous random variables $(x, y) \in \mathbb{R}$ with marginal distributions $F_X(x)$ and $G_Y(y)$ in the interval $[0, 1]$. The copula takes values from the unit square $I^2 = ([0, 1] \times [0, 1])$, such that for all (x, y) Eq. 2.11 is satisfied. If F and G are continuous, then C is unique. For a complete overview of copula modeling the reader is referred to [43] and references therein.

Furthermore, it is of interest to consider the auto-correlation of a particular set of variables. By examining the transition distribution between consecutive observations, we can assess the temporal dependence of the variables. This analysis is particularly relevant when dealing with metocean variables and traffic loads to assess their impact on the structural integrity of SFTs. For instance, autocorrelation in traffic loads may help identify patterns of heavy vehicle traffic, that can lead to fatigue and structural degradation over time. For a random variable X with distribution F_X, where the associated time series is X_t, $t \in \mathbb{N}$. The transition distribution is given by equation 2.12.

$$\begin{aligned} H(x_t|x_{t-1}) = P(X_t \le x_t|X_{t-1} = x_{t-1}) = \\ C\left(F(x_t)|F(x_{t-1})\right) \end{aligned} \tag{2.12}$$

Where $C_{\theta_X}(u|v)$ is the conditional copula. Notice that the parameter θ_X would model the auto-correlation of order 1 for the time series of interest. This procedure is performed to characterize the correlation of the variables over a determined time domain that allows the generation of a synthetic time series that more accurately reflects the actual temporal patterns. The application of copulas for the context of the SFT is described in more detail in chapter 4 and 5.

Copulas can be powerful tools to characterize multivariate distributions. However, for the n-dimensional case ($n \geq 3$) this can be a difficult task because there are no simple extensions to such cases. In [44–46] the problems associated with the construction of n-copulas are treated in detail. However, copulas can be used as building blocks for multidimensional probability distributions such as vine-copulas and Bayesian networks. In the following sections, a brief introduction to vine-copulas and Bayesian networks is presented.

2.4 Vines

Particularly with high-dimensional datasets, multivariate copulas often struggle to adequately capture the full spectrum of dependency structures within a random vector to a satisfactory level [47]. This limitation underscored the preference for vine-copulas over multivariate copulas in such situations.

Vines are graphical tools used to model high dimensional distribution functions, in which the variables involved have a complex dependence structure. Vines were first introduced by [44] and further developed by [48–50].

A vine with n variables $V = (T_1, \ldots T_{n-1})$ is a nested set of trees where the edges of the tree T_j are nodes of the tree T_{j+1} [51]. A regular vine (R-vine), is one where an edge in T_{j+1} connects two edges from T_j, only if they share one node in T_j. If this condition is not met, the vine is called a non-regular vine.

There are many kinds of regular vines but two main types, canonical (C-vines) and drawable vines (D-vines). Each tree in a C-vine is a star (in the graph theoretical jargon) while each tree in a D-vine is a line (Fig. 2.1). On each edge of a vine, there is a constraint, conditioned and conditioning set [52]. The constraint set of an edge is the nodes on the first tree reachable from a given edge via the membership relation. The conditioning set is the intersection of the constraint sets of two edges on T_j that are joined by another edge on T_{j+1}. Finally, the conditioned set of that edge is the symmetric difference of the constraint sets [52]. The label of each edge denotes the conditioned and conditioning sets as shown in Fig. 2.1. For example, in T_2 the edges $1,2$, and $2,3$ form the constraint set of edge $1,3|2$ while the symmetric difference is $\{2\}$. For more details, the reader is referred to [51, 52].
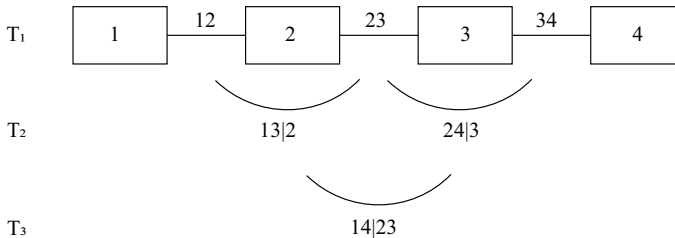
Figure 2.1: A 4-variable D-vine with its corresponding conditioned and conditioning sets. For example, for edge 13|2, the conditioned set is 1,3 and the conditioning set is given by node 2.

In many applications, especially in engineering, it is crucial to understand the physical properties of variables and how they relate to each other. This knowledge can help

determine the first tree of a regular vine. However, selecting the subsequent trees and ultimately defining a regular vine structure to characterize multivariate data sets can be challenging. To fully define a vine-copula model, three things are required [53, 54]: i) selection of a regular vine structure. In other words, selecting which (un)conditioned pairs to use, ii) determining the bivariate copula families for each pair copula chosen in (i), and iii) estimating the parameters for the copulas selected in (ii). Thus, selecting a regular vine structure for a dataset would involve fitting all possible regular vines to the dataset. However, the number of possible regular vines on n nodes increases substantially as shown by [55]:

$$\binom{n}{2} \times (n-2)! \times 2^{\binom{n-2}{2}} \tag{2.13}$$

In their work, [55] introduced a catalog classifying regular vines based on their tree equivalent class. Subsequently, in [56] this catalog is made accessible as datasets, providing all regular vine structures up to 8 nodes, in the form of matrices. The data sets are compatible with R, MATLAB, and Python. Additionally, the catalog's potential is demonstrated by fitting all regular vines to synthetic data. For further details into the catalog's construction and use, readers are directed to [55–57].

In contrast, [54] introduced a sequential "top-down" methodology for selecting the tree structure of regular vine-copulas. The term "top-down" means that the method starts with selecting the first tree T_1 and continues tree by tree up to the last tree T_{n-1}. Each tree is chosen in a way that prioritizes modeling the strongest pairwise among the variables. Since each tree is examined separately, there is no guarantee of finding a global optimum, for example in terms of model fit metrics like the Akaike Information Criterion (AIC) or the Bayesian information criterion (BIC). This approach acknowledges that the copula families specified in the first tree of the regular vine have a significant influence on the model fit. For further details on this methodology, the reader is referred to [53, 54].

The goodness of fit for regular vines is often assessed with likelihood-based measures such as Akaike's Information Criterion (AIC), the Bayesian Information Criterion (BIC), and the negative log Likelihood (NLogL). Throughout this research, we use the AIC [58] coefficient as a goodness of fit (GOF) measure because it considers the number of parameters and the likelihood of the model where models with fewer parameters are preferred. Visual inspection is also used to assess the goodness of fit.

Vine-copulas have gained popularity in a variety of different fields. Vines are frequently employed in hydrology to simulate rainfall [59–61] or to model multivariate return periods [62]. In [63], models to predict water flow discharge in locations like George Island in Antarctica are presented. In the North Sea, large series of wave heights and periods have been produced using vines [64]. In [65], a vine-copula model was applied to generate a maintenance plan for offshore infrastructure considering variables such as wave height and period, wind speed, and current velocity. In this dissertation, vine-copulas are used to investigate the dependencies between waves, currents, and their corresponding resulting hydrodynamic forces (Chapter 6). A regular vine on six nodes is proposed, resulting in 23040 possible regular vines that can characterize the data set. Fitting 23040 regular vines poses a significant computational challenge, especially on a standard laptop computer. In this research, both approaches, the sequential methodology from [54] and fitting all pos-

sible vines as per [56] were applied to select a vine for describing the data. This analysis is further expanded to study nine different SFT configurations, defined by combinations of different tube diameters and submergence depths.

2.5 Bayesian Networks

In risk and reliability analyses, Bayesian networks offer a viable alternative to fault trees or event trees. Since the introduction of fault trees by [66], they have found applications in a variety of fields. However, their applicability is limited, particularly when modeling complex systems [67]. Bayesian Networks allow for a comprehensive assessment of how intervention impacts a system or how changes in variables influence each other. This transparency in representing dependencies enhances the understanding of safety analyses. Additionally, Bayesian Networks facilitate the incorporation of prior knowledge or expert opinions through prior distributions, a feature not present in fault trees. Moreover, when dealing with systems with numerous variables and dependencies, Bayesian Networks offer computational efficiency advantages over fault trees. The choice between the two techniques depends on the study's nature, system complexity, and data availability. Given these considerations, Bayesian Networks emerge as a valuable tool for studying the safety of submerged floating tunnels.

BNs have been used in the study of emergency scenarios. For example, [68] presents a dynamic BN framework to simulate emergency events such as the 2011 Fukushima nuclear accident and the COVID-19 pandemic, supporting rapid decision-making. In hydrology, BNs were used to predict monthly regional rainfall with local meteorological drivers in India [69]. In [70], a BN model is introduced to estimate extreme river discharges in Europe. Regarding risk and reliability analyses, [71] implemented a non-parametric Bayesian network (NPBN) model based on Gaussian copulas, to generate synthetic storm events for assessing flood risk in a coastal watershed. [72], applied a BN approach to study urban risks, including food security, water availability, landslides, and floods, in developing cities facing climate change with limited information. [73] modeled multi-hazard hurricane damages by linking hazards to observed building damages in New York. [74]. [75] and [76] provide a thorough explanation of BN theory and how it applies to risk assessment. In water management, [77] provides a comprehensive literature study about the extent of applying Bayesian Networks to water management issues in South Africa. Another field of application of BNs is the study of the influence of human errors [78] and waves [79] in the occurrence of ship accidents. In cases where boolean variables are not sufficient to perform an adequate risk analysis, hybrid BNs (formed with continuous and discrete variables) can be effective tools, especially in situations where data is scarce. However, evaluating these networks can be challenging [80]. [81] presents a hybrid methodology that combines the modeling flexibility of continuous BNs with the fast-updating algorithms of discrete BNs. For example, this methodology has been applied in [82] to simulate hydrological dynamics to forecast the maximum daily river discharge in catchments in the United States.

Bayesian Networks (BNs) are directed acyclic graphs (DAG) formed by nodes and arcs that represent the joint distribution of a set of variables [83, 84]. The nodes represent random variables that can be either continuous, discrete, or functional and the arcs represent the probabilistic dependence between the variables. No direct arcs between nodes

represent a set of (conditional) independence statements.

The direct predecessors and successors of a node are called parents and children respectively. Each node with no parents is characterized by a marginal distribution while nodes with parents are represented by conditional distributions [84]. The conditional and marginal distributions provide quantitative information about the strength of the dependencies between the variables. The main advantage of BNs is that they allow to update distributions given observations, this is known as inference. A Bayesian Network G on $X_1, ..., X_n$ defines a joint probability density function f_G as [85]:

$$f_G(x_1, ..., x_n) = \prod_{i=1}^{n} f(x_i | pa(X_i)). \tag{2.14}$$

Where n is the number of variables and $pa(X_i)$ is the set of parents of X_i. This dissertation explores the application of Gaussian copula-based Bayesian Networks (GCBN) for investigating continuous random variables (Chapter 7) and discrete BNs for discrete random variables (Chapter 8).

Gaussian copula-based Bayesian Networks (GCBNs) associate nodes with random variables, and arcs with one-parameter conditional copulas, which are parameterized by rank correlations (r). This correlation describes the strength of the monotonic relation between the variables. Let X_1 and X_2 be two random variables, with cumulative distributions F_{X_1} and F_{X_2}, then r is computed following Eq. 2.15:

$$r(X_1, X_2) = \rho \left[F_{X_1}(X_1), F_{X_2}(X_2) \right] \tag{2.15}$$

where ρ is the product-moment correlation of the random variables. While any copula with the zero-independence property (i.e., zero correlation implies independence) could be employed to represent the arcs, only the Gaussian copula can reduce computation and inference times when working with large and complex problems [84]. Thus, in [81], GCBNs were further developed to use Gaussian copulas to capture the dependence structure defined by (conditional) rank correlations. The reader is referred to [84] and its references for a comprehensive description of BNs based on Gaussian copulas.

Once the DAG of the Bayesian network is established, the marginal distributions of the variables and the (conditional) rank correlations must be quantified. This can be achieved using data (from physical models or observations) or via structured expert judgment.

In discrete BNs, the nodes represent discrete random variables. Marginal distributions are specified for nodes without parents, while conditional probability tables (CPTs) are used for child nodes [84]. This dissertation focuses on binary nodes, where each node has two states (Chapter 8). For example, in the BN shown below (Fig. 2.2), X_1 has an edge adjacent to X_2. Both X_1 and X_2 take values on the set $\{T, F\}$. The quantification of such a simple model would require one marginal probability for X_1 and four conditional probabilities for X_2. Notice that only two of these four probabilities need to be specified since the remaining may be computed by difference since conditional probabilities must add to one.

X_1	$P(X_2{=}T| X_1)$	$P(X_2{=}F| X_1)$
T	0.2	0.8
F	0.6	0.4

$P(X_1{=}T)$	$P(X_1{=}F)$
0.5	0.5
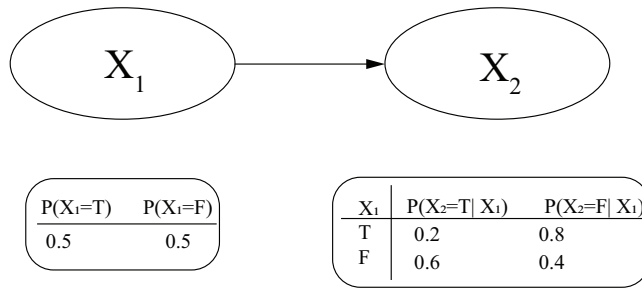
Figure 2.2: Example of a BN

CPTs are typically quantified with data or expert judgment. However, the size of CPTs (2^k) grows exponentially with the number of parent nodes (k), posing challenges, especially in complex problems with sparse data. Quantifying the correlations becomes more complex with large CPTs and multiple parents [86].

In this dissertation, a Gaussian copula-based Bayesian Network (GCBN) consisting of seven nodes is used to model the multivariate joint distribution between significant wave height and period for two wave systems (wind waves and swell waves), as well as current velocities at two different depths below the surface (1m and 15m), and the resultant forces acting on the SFT due to the combined action of waves and currents. Additionally, a discrete Bayesian Network consisting of 51 nodes is employed to quantify potential scenarios that can lead to the failure of the SFT. This involves estimating the conditional probability of failure of the SFT given different combinations of hazard events referred to as scenarios. Details of the implementation of these Bayesian Networks are found in Chapter 7 and Chapter 8.

3

Case study: The Qiongzhou Strait

This chapter presents a comprehensive overview of the proposed site for an SFT and the data that were used throughout this dissertation. In this dissertation, we pay attention to an SFT that is planned to be built at the Qiongzhou Strait in China. The relevant data include wind waves, swell waves, currents, and traffic. Wind waves are formed by local winds that blow over the water surface, whereas swell waves are waves that have traveled out of their area of origin [87]. Wind and swell waves are characterized by their significant wave height and mean wave period. Currents are characterized by the speed at two levels from the water surface (1m and 15m). Traffic at the SFT is described using WIM (Weigh-in-motion) data from heavy vehicles (heavier than 3.5 tons).

This chapter is organized as follows: Section 3.1 introduces the proposed location for the SFT. Next, a description of the metocean data (waves and currents) is presented in Section 3.2 followed by a description of traffic data in Section 3.3.

3.1 The Qiongzhou Strait

Possible locations to build an SFT are divided into inland and coastal regions. Regarding inland regions, an SFT is an attractive proposition for crossing lakes. While in coastal regions, an SFT can be used to cross fjords, and straits, or as a way to connect islands. One location for an SFT is the Qiongzhou Strait in China (Fig. 3.1), which connects the Gulf of Beibu (Gulf of Tonkin) on the west and the northeastern South China Sea Basin on the left. The goal of this SFT is to connect mainland China to Hainan Island. The strait has a length of 70 Km and a width that ranges from 20 Km to 40 Km. The average depth of the strait is 40 m and the deepest central trough is 120 m.

Hainan Island is part of the Guangdong province and forms the extreme southern limit of the People's Republic of China. This island lies between longitudes 108°30' and 111° east and latitudes 18° and 20°31' north. This region is very dynamic and characterized by complex physical processes and it is frequently affected by tropical cyclones [88]. The wet season from May to October has an annual precipitation of 1500 ml, and from May

Parts of this chapter have been published within [3], and [4]

Figure 3.1: Overview of the area of study.

to November is typhoon season, especially in September [89]. These extreme events can jeopardize the construction and operation of an SFT in this location.

Since the 1980s, research to assess the feasibility of building a water crossing at the Qiongzhou strait started, and it keeps going today [89]. For this purpose, the Ministry of Transport and former Ministry of Railways, Guangdong province, and Hainan Province have collected a great number of data on social economy, transportation, meteorology, hydrology, landform, geology, earthquakes, and other aspects [90].

At the moment, tourists travel to Hainan Island via plane or ferry. Congestion usually peaks during the Spring Festival or summer holidays. For example, due to bad weather conditions during the 2018's Spring Festival, services were shut down causing week-long traffic jams and delays [91].

The need for a cross-sea passageway at the strait is urgent and much needed. According to [90], by 2050, the number of passengers in the area will be 3 times larger than in 2018. The purpose of building an SFT in the region is to solve the bottleneck problem of travelers and cargo traffic flow volume and to ensure the all-day navigation safety of both shores under bad conditions [90].

Several locations within Qiongzhou Strait are proposed for the SFT. They are categorized into 3 main lines: east, central, and west [89, 90] (Fig.3.2). This dissertation is focused on the central line. The main advantages and disadvantages of this alignment are further discussed in [89].
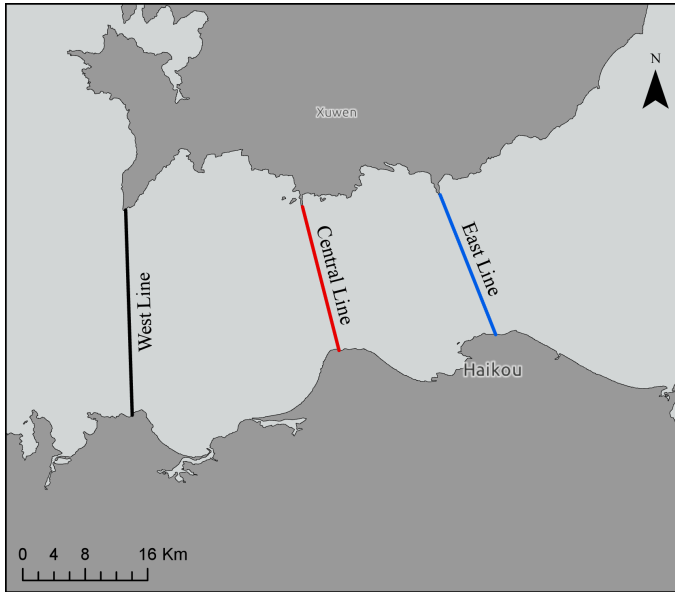
Figure 3.2: Line's proposal for the SFT project. Adapted from Jiang, Liang, & Wu (2018).

3.2 Metocean Data

Hourly values of significant wave height and wave period, and 3-hour values for current velocity are available for the Qiongzhou Strait. The data were retrieved from ERA5 [92] and the Copernicus Marine Environment Monitoring Service [93], for waves and currents respectively. Both sources provide climate reanalysis data sets. Table 3.1 presents a description of the data sets. As mentioned previously, two types of waves are considered, i) wind-sea waves (WW), and ii) total swell (TS). The term total includes all the swell partitions that occur at a specific location. Current velocity data is also classified into two sets, the current velocity at 1 meter (U_{1m}) and 15 meters (U_{15m}) below the water surface. Current data is retrieved as vectors of velocity, i) the zonal velocity (Velocity along the latitudinal circle East-West direction), and ii) the meridional velocity (velocity along the longitudinal circle North-South direction). These vectors were transformed into the resultant current velocity and direction. The nomenclature used throughout this thesis is presented in Table 3.2 and illustrated in Fig. 3.3.

Different temporal and spatial resolutions are present in the wave and current data sets, as well as different temporal coverage (Table 3.1). As a result, the date of observation was used to match the temporal coverage between the data sets. In this way, the same number of observations were obtained for both waves and currents. Only dates where all variables were available were considered in this study. The total amount of observations spans from January 2000 to February 2019.

To address the disparity in spatial resolution, the grid for currents was resized to match the grid from waves. The *resample* function from the "raster" package [94] in R [95] was used to do this. This resulted in geographic coverage for both data sets between 20°0'-

	Waves: Wind & Total Swell ($H_s\,[m]$, T [s])	Current Velocity [m/s]
Product Name	ERA5 hourly data on single levels (1979-present)	MULTIOBS_GLO_PHY_REP_015_004
Geographical Coverage	Global	Global
Observation/models	Reanalysis	Numerical model Satellite-Observation
Spatial resolution	0.5x0.5 Degrees	0.25x0.25 Degrees
Vertical coverage (number of vertical levels)	-	From -15m to 0.0m (2 levels)
Coordinate reference system	WGS 84 (EPSG 4326)	WGS 84/ Simple Mercator (EPS41001)
Feature type	Grid	Grid
Temporal coverage	1979-01-01/2019-06-30	1993-01-01/ 2019-10-15
Temporal resolution	Hourly	3-Hourly
Original file format	NetCDF-4	NetCDF-4

Table 3.1: Product description for waves and currents data

Variable	Standard Name	This thesis
Wave height (WW) [m]	H_s	$X^{(1)}$
Wave period (WW) [s]	$\overline{T}$	$X^{(2)}$
Wave height (TS) [m]	H_s	$Y^{(1)}$
Wave period (TS) [s]	$\overline{T}$	$Y^{(2)}$
Velocity (1m depth) [m/s]	U_{1m}	$Z^{(1)}$
Velocity (15m depth) [m/s]	U_{15m}	$Z^{(2)}$

Table 3.2: Name and description of the variables

20°50'N and 108°25'-112°75'E. This area includes a total of 9 grid points (Fig. 3.4) that cover the entire strait and the area just outside the strait. The SFT is aimed to be located on grid point 4 [15].

To ensure the quality of the data sets, the time series were checked for outliers. According to [96], an outlier is an observation that i) deviates more than 7 times the standard deviation of the monthly data from its mean, or ii) more than 3 times the standard deviation of the monthly data from the previous observation. These two approaches were applied to the data. A total of 800 outliers were identified and removed.

Furthermore, data availability is not consistent for all grid points. This is the case of grid points 4, 5, and 6. Gridpoint 4 has no data for waves while grid points 5 and 6 have no information on currents. Focus is on grid point 4 because this area covers the SFT's central line proposal (Fig. 3.2) [15]. For this purpose, a "hybrid" grid point 4 is formed by combining the data of currents at that location and wave data from point 5. This results in a total of 7 grid points available for analysis (grid points 1-4 and 7-9).

Wind waves ($X^{(1)}$, $X^{(2)}$)
Total swell ($Y^{(1)}$, $Y^{(2)}$)

Currents
1m depth $Z^{(1)}$

Currents
15m depth $Z^{(2)}$
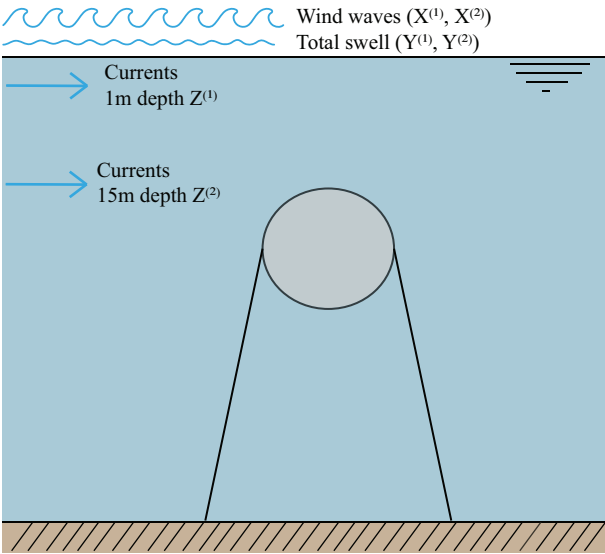
Figure 3.3: Scheme of the SFT and relevant variables.

1 2 3 4 5 6 7 8 9

0 20 40   80 Km
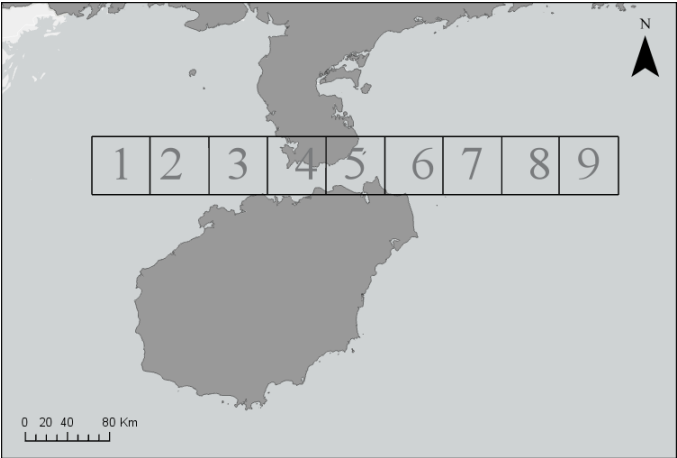
Figure 3.4: Overview of the grid at the strait.

3.3 Traffic Data

Traffic data is formed by two data sets, namely WIM and VH. The WIM (Weigh-in-Motion) data set, consists of measurements of heavy vehicles at the National Highway A12 (km 42) in Woerden (The Netherlands) for two lanes (RW-12-L-2 and RW-12-L-3) [97]. These measurements include the time of measurement, vehicle category, lane, speed, the total length of the vehicle, the total weight of the vehicle, axle weight, and inter-axle distance. This data is available for 27 days in the month of April 2013 (from the 3rd to the 30th) with a total of 157.000 vehicles approximately divided into 26 vehicle categories (Appendix A.1). For details regarding the accuracy of the data, the reader is referred to [97].

In this thesis, all vehicle categories are considered for analysis. The proportion of each vehicle category in the data set serves as the foundation for traffic simulation. In this data set, congestion was filtered automatically. In other words, measurements were neglected if the traffic had a velocity lower than 40[km/h]. This specific WIM data set was chosen because is used as an input for the model developed by [98] from where the second data set (VH) is obtained.

The second data set (VH) is the result of a Bayesian Network-based (BN) model developed by [98]. The BN was implemented in Python with the toolbox BANSHEE [99]. The data set is a collection of approximately 300.000 vehicles with their corresponding axle weights and inter-axle distances (that consequently define the number of axles per vehicle) that were randomly generated using the BN model. The VH data set and procedure used to generate it are further discussed in Chapter 4.

WIM data is defined by four variables, i) Axle weight, ii) inter-axle distance iii) inter-vehicle distance and, iv) number of axles per vehicle (Fig. 3.5). In Fig.3.5, D_t refers to the inter-vehicle distance (in kilometers). $AX1$ and $AX2$ are the weights of axles 1 and 2 [KN]. $DTF1$, $DT12$, and $DTLAE$ are the distances between axles (in meters).
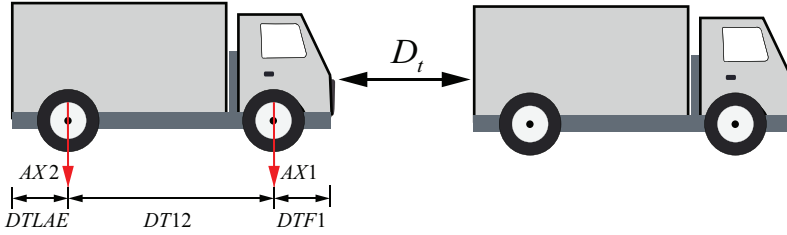
Figure 3.5: Traffic variables

The inter-vehicle distance is used to simulate the traffic variables that define the traffic passing through the SFT. This is done through a copula-based model. A detailed description of this process is presented in Chapter 4.

II

Bi-variate models for SFT loads

4

Simulating traffic loads

To this day, no SFT has been constructed yet. One of the key reasons is that not enough is known about the structural reliability of this structure. This chapter presents a methodology to assess traffic loads and the structural response of a pontoon-type SFT (Fig. 1.1). This methodology proposed an innovative approach to combine copula-based models and structural models to obtain a more realistic structural response of an SFT. The methodology consists of two parts, i) a copula-based model to characterize traffic loads and simulate traffic on an SFT (axle weight, inter-axle distance, and inter-vehicle distance), and ii) a structural model to assess the structural response and derive stresses. The structural model is outside the scope of this dissertation and it is not the main emphasis of this chapter. In this chapter, the focus is on the copula model to simulate traffic loads. For further information on the structural model, see [3].

This chapter is organized as follows: Section 4.1 provides a brief introduction to this study. This is followed by a description of the methodology to perform traffic simulations (Section 4.2). Next, in Section 4.3 the processing of the traffic data is presented. Section 4.4 shows the results of the copula-based model and frequency curves of the resulting bending moments and shear forces. These results are further discussed in Section 4.5. The chapter closes with the conclusions and areas of future work (Section 4.6).

4.1 Introduction

A submerged floating tunnel is situated in a marine environment and, thus is subjected to different loads (Table 1.1), for example, environmental loads, operational loads, deformation loads, and accidental loads [90]. In this chapter, the focus is on the relation between traffic loads and a pontoon-type SFT's resistance to leakage due to cross-sectional failure. Therefore, attention is on failure due to bending caused by traffic. Other loads and failure mechanisms are beyond the scope of this study.

The methodology uses WIM data (Weigh-in-Motion data) from large trucks (heavier than 3.5 tons) to simulate traffic in the tunnel. This data set includes measurements for ve-

hicle type, lane, speed, vehicle length and weight, axle weight, and inter-axle distance. In this thesis, WIM data from The Netherlands is used because similar data was not available in the region. The WIM data was retrieved from the National Highway A12 in Woerden, The Netherlands (For more details see Chapter 3.3 and [97]).

The traffic load varies over the structure in terms of magnitude, occurrence, and position. In a pontoon-type SFT, the weight loads are larger than the buoyancy load of the structure and the traffic loads act in the same vertical downward direction as the resulting forces of the permanent loads. Thus, the traffic loads will add to the resulting forces caused by the permanent and buoyancy loads. An SFT must have sufficient reserve capacity to carry the traffic load [100].

The methodology presented in this chapter consists of i) simulating the traffic passing through the SFT using a copula-based model applied to WIM data and ii) performing a reliability analysis on the bending moments obtained from the structural model. More details of this methodology are presented in the following sections.

A similar approach was developed by [101] to investigate bridges under traffic and earthquake loads. Whereas [102] employed empirical copulas to characterize WIM data to assess the load effect of heavy trucks on bridges.

Due to the unique characteristics of submerged floating tunnels, there is limited empirical data available on their performance and behavior. Thus, evaluating the safety of these structures is challenging. The flexibility of the copula-based methodology presented herein permits investigating many SFT designs (tethered or supported by underwater piers) and understanding the dependence relationship that may exist between traffic variables. It is important to note that while correlation measures the linear relationship between variables, dependence encompasses all types of relationships, including non-linear ones, which copulas are capable of modeling. Copulas also make it possible to create synthetic data that captures the statistical characteristics of the observed traffic data. This methodology can be extended and applied to other relevant variables, including environmental loads like waves and currents, among others. Such flexibility is key in cases where there is limited or incomplete data. In this way, engineers, researchers, and decision-makers can make informed decisions regarding the design, operation, and safety of these structures.

4
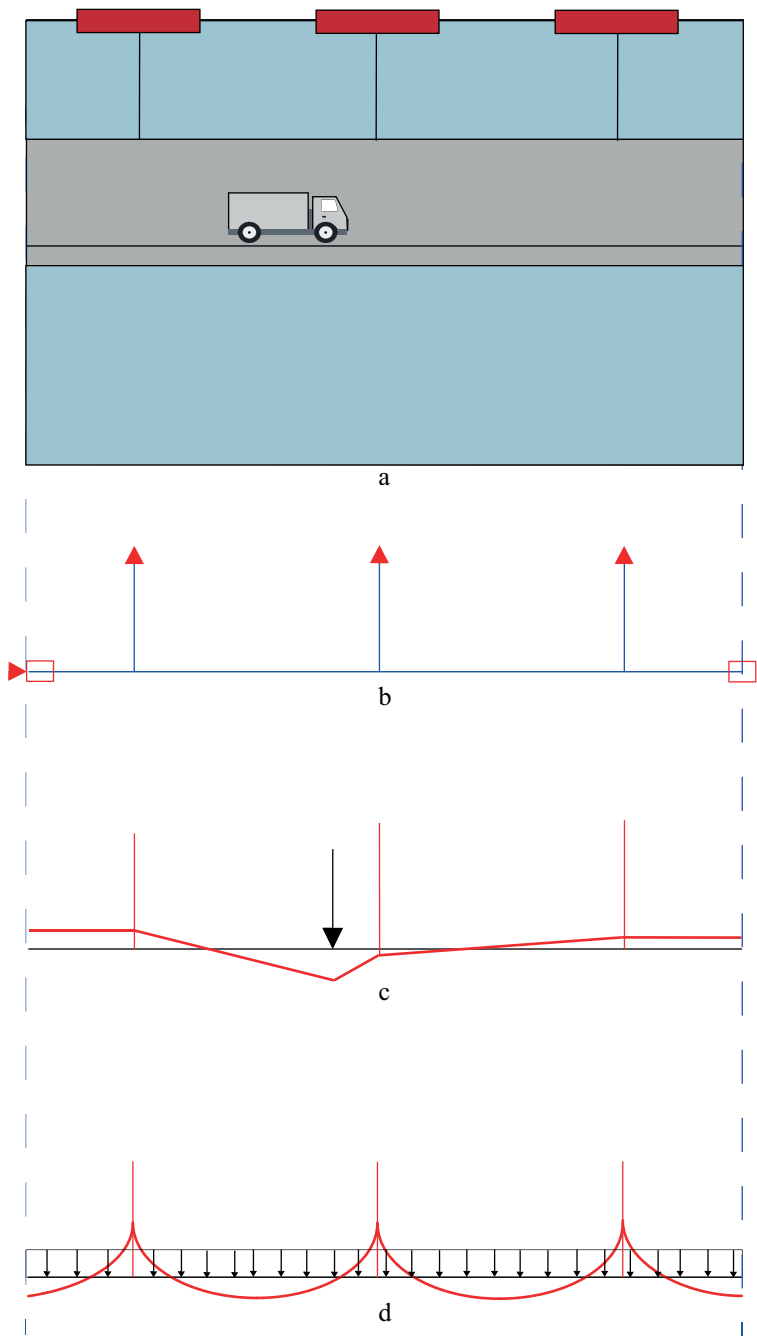
Figure 4.1: From top to bottom: (a) SFT scheme, (b) Structural system, (c) Bending moments due to a unit force load, (d) Bending moments due to buoyancy weight ratio (BWR) load.

4.2 Modeling Approach

4.2.1 General Overview

In this section, the methodology to perform a reliability analysis of an SFT using a combination of copula-based models and structural FEM models is presented. The reliability analysis is conducted by the definition of the Limit State Function. An SFT structure is a buoyant structure where leakage will cause an unbalance of the structure and could initiate a progressive collapse. The limit state function is based on leakage caused by bending moments as a result of traffic loads. Other failure modes or the influence of other loading variables are considered beyond the scope of this research. The following steps make up the methodology used in this work (Fig. 4.3):

- First, simulation of traffic passing through the SFT is carried out by using a copula-based model that characterizes the distance between vehicles (also known as inter-vehicle distance. Fig. 3.5).

- The simulation of traffic is carried out for a determined "period of time" based on an average number of vehicles per unit of time (i.e. one year). The result is a "train" of vehicles that includes the number of axles, axle weights, inter-axle distances, and inter-vehicle distances (Fig. 4.2).
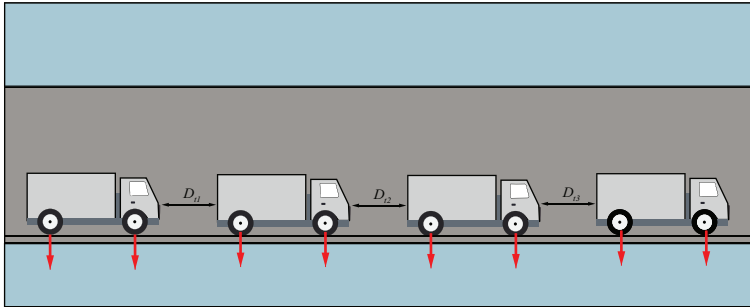
Figure 4.2: Train of vehicles. D_{ti} refers to inter-vehicle distances [m].

- Then, the resulting time series of traffic is used as input in a FEM model, based on the Direct Stiffness Method (DSM) and the Differential Equation Method (DEM), to test its effect on the structure of the SFT in terms of cross-section results, like bending moments, shear forces, and displacements.

- From the bending moments, a stress distribution is derived to validate the compression zone of the section.

- Finally, a reliability assessment is performed on the limit state (leakage failure mechanism due to bending moments in the longitudinal direction). Findings on the assessment can lead to adjustment or optimization of the water-tightness of the SFT section.

The specifics of the structural model are not covered in this study; only the resulting bending moments and shear forces are discussed in the context of the SFT's reliability.
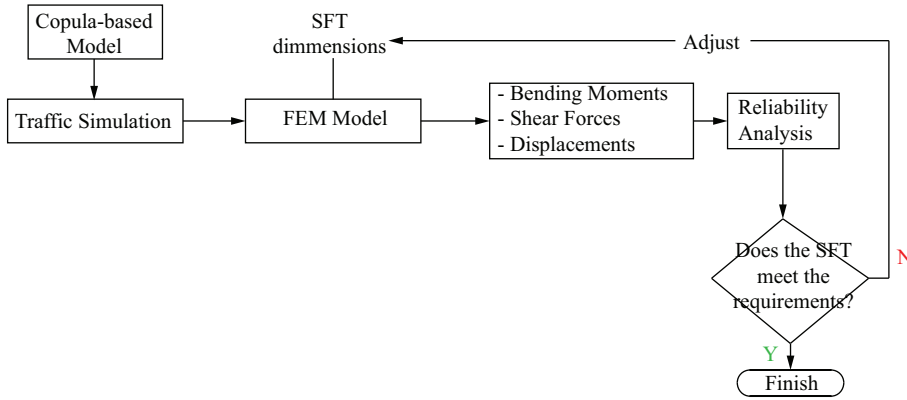
Figure 4.3: Modeling overview flowchart.

4.2.2 Modeling traffic

As mentioned in the previous section, a copula-based model is developed to simulate the traffic passing through the submerged floating tunnel. Copula-based models are important in simulating the distance between vehicles because they allow more accurate simulations of daily and hourly traffic patterns that are valuable for transportation planning. For example, to estimate the maximum traffic capacity in the tunnel. Other applications of these models can be used to analyze potential safety hazards, identify critical areas prone to congestion or accidents on highways, and plan effective strategies to mitigate such risks.

The traffic load passing through the tunnel is defined by four main variables (Fig. 3.5), i) Axle weight ($AX1, AX2$), ii) inter-axle distance, ($DTF1, DT12, DTLAE$) iii) inter-vehicle distance (D_t) and, iv) the number of axles per vehicle. For characterizing traffic variables, copulas are used to model the auto-correlation among inter-vehicle distances (D_t). The distinction between inside and outside congestion hours is also considered for this analysis. For a sequence of inter-vehicular distance, the formulation in Eq. 2.12 is used to simulate values for the distance between vehicles. The graphical representation of this process is presented in Fig.4.4.

$$\ldots \qquad D_{t-1} \longrightarrow D_t \longrightarrow D_{t+1} \qquad \ldots$$
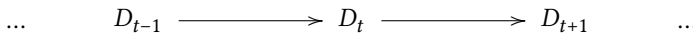
Figure 4.4: Graphical representation of the process for inter-vehicle distance.

This model has been proposed before in [103] and [104] for traffic loads modeling in bridge reliability and for modeling time series of hydrological variables in [41]. The VineCopula package [105] implemented in R (language for statistical computing) [95] is used to choose an appropriate copula model, estimate its parameters, and produce simulations. Copulas including Gaussian, Gumbel, Clayton, t, Joe, BB1, BB6, BB7, and BB8 are included in the package, along with their respective rotated versions. The copula families

were chosen using Akaike's information criteria, and the parameters were estimated using pseudo maximum likelihood (AIC).

To simulate traffic over the SFT, an algorithm was developed. This algorithm's primary objective is to preserve the proportion (number) of cars per traffic scenario (congestion and free flow. Section 4.3) and vehicle category while capturing the daily characteristics of different traffic scenarios. This is crucial because the number of vehicles and the inter-vehicle distance are two factors that have an important influence on congestion and free flow hours. The simulation consists of 4 main steps, i) simulating the number of vehicles (per day, lane, traffic scenario, and vehicle category), ii) simulation of inter-vehicle distances (D_t) using a copula-based model (per traffic scenario), iii) random sampling of axle weights and respective inter-axle distances from a vehicle database (VH) and, iv) combining the results from the previous steps to form a "train" of vehicles.

The algorithm starts by loading the required variables and the fitted copulas corresponding to each traffic scenario. The simulation is performed daily, where the number of vehicles per lane is randomly sampled from its corresponding empirical cumulative distribution function (ecdf). Then, the number of vehicles per traffic scenario and category is obtained by multiplying the total number of vehicles per lane by its corresponding vehicle proportion. This operation is carried out until the desired number of days to simulate is reached.

Next, for each traffic type, the simulation of inter-vehicle distances is executed from its corresponding fitted copula. And, since the vehicle category proportion per traffic type is known, the random extraction of axle weights and inter-axle distances from the VH data set is carried out.

Finally, the inter-vehicle distances (D_t), axle-weights, and inter-axle distances are put together in a vector to form a "train" of vehicles (Fig. 3.5) that is used as input for the structural model. A simplified flowchart of the traffic simulation algorithm is presented in Fig. 4.5.
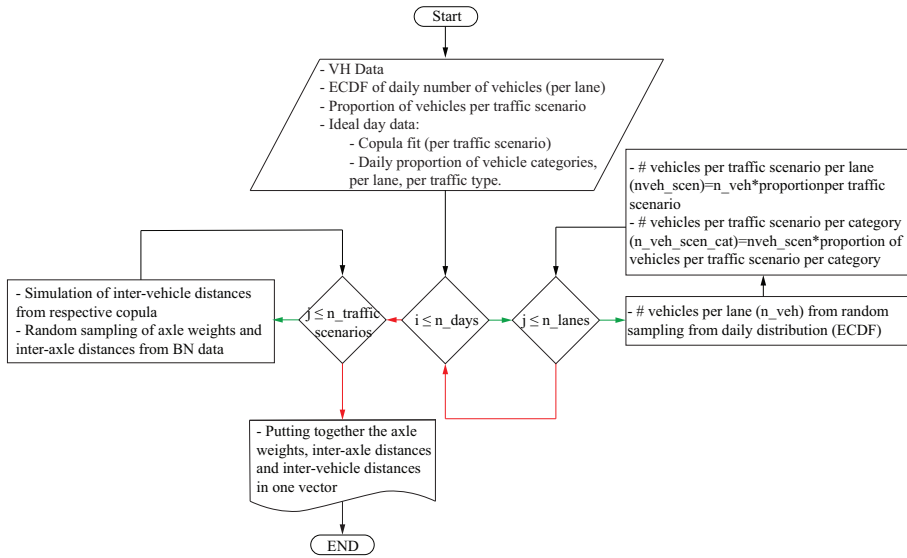
Figure 4.5: Traffic simulation algorithm.

4.3 Processing traffic data

In this section, the relationship between the WIM data set, the VH data sets, and the copula-based model is explained. This link is depicted in Fig. 4.6 and is discussed in the following sections.
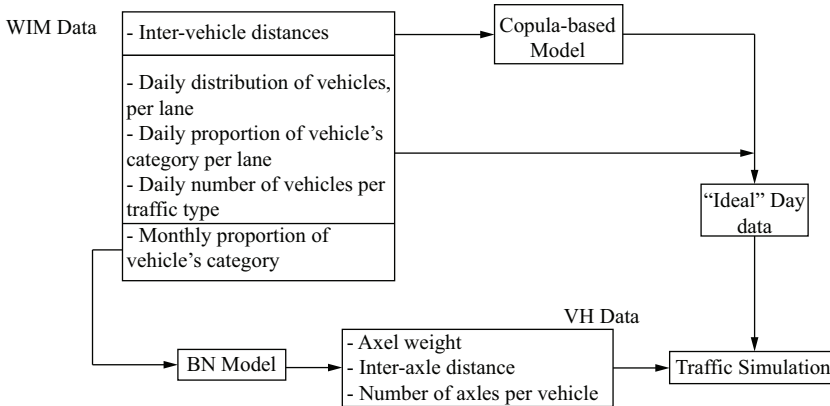
Figure 4.6: Data Overview for simulation of traffic.

Regarding WIM data, weekends and national holidays were excluded from the analysis. The remaining days are considered as "regular" days and were analyzed in three different time scales, hourly, daily, and monthly.

4.3.1 Hourly Analysis

Histograms were used to illustrate the data set so that it could be examined on an hourly time frame. This makes it possible to discern periods of congestion (when there are more vehicles) and periods of free flow (when the number of vehicles is lower). The data were divided into three groups: i) free flow before congestion hour (Free Flow A), ii) congestion hour, and iii) free flow after congestion hour (Free Flow B). See Fig. 4.7 for April 4th. Resulting in six different traffic scenarios: 3 groups for 2 lanes, namely, C_L2, C_L3, F_L2_A, F_L2_B, F_L3_A, and F_L3_B. The definition of this nomenclature is presented in Table 4.1
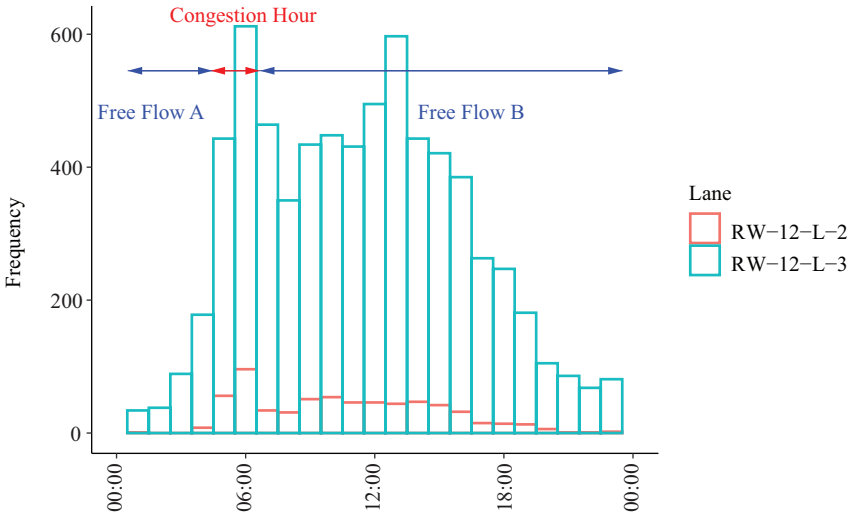
Figure 4.7: Hourly classification of traffic of WIM data [97]. April 4th, 2013.

Nomenclature	Traffic type and lane
C_L2	Congestion lane 2
C_L3	Congestion lane 3
F_L2_A	Free flow A lane 2
F_L2_B	Free flow B lane 2
F_L3_A	Free flow A lane 3
F_L3_B	Free flow B lane 3

Table 4.1: Nomenclature for hourly classification of traffic.

For these six traffic scenarios, the corresponding inter-vehicle distances $\{D_t\}$ are obtained as shown in Eq. 4.1 [97].

$$D_t = S_{t-1} * (i_t - i_{t-1}) \tag{4.1}$$

Where,

- D_t: Inter-vehicle distance at discrete time t [km].

- S_{t-1}: Vehicle's speed at time $t - 1$ [km/h]. It is assumed that the vehicle travels at a constant speed.

- i: Discrete-time indices of the variable of interest (Not calendar time) [h].

4.3.2 Daily Analysis

On a daily scale, two variables are analyzed, i) the daily distribution of vehicles per lane, and ii) the daily amount of vehicles per category per traffic scenario. Empirical cumulative distribution functions (ecdfs) are constructed to describe the daily volume of traffic at lanes 2 and 3 over the course of the month. This is done in order to understand the daily variation in vehicle numbers on normal-condition days. Because there are not many days with normal conditions, these ecdfs were not fitted to parametric distribution functions. Fig. 4.7 shows that the number of vehicles in lane 2 is much smaller than in lane 3 at any time of the day. The average daily number of vehicles for lanes 2 and 3 is approximately 460 and 5150 vehicles respectively.

4.3.3 Creating the "ideal" day

One single day was selected to represent the entire month for calculating the daily amount of vehicles per traffic scenario. This decision was made by comparing data from each day under normal conditions, considering factors such as the daily vehicle count and the existence of measurement errors. Errors are defined as instances where the gap between two consecutive vehicles exceeds 10 hours; these data points were deleted from the data set. The chosen day, April 10th, had the highest vehicle count and the fewest measurement errors. Thus, the number or percentage of vehicles per traffic scenario was determined based on data from this selected day (refer to Appendix A.2). Using this percentage, the estimation of vehicles per category and per traffic scenario is conducted based on the daily vehicle count. Appendix A.1 provides definitions for the vehicle categories.

In summary, an ideal day is defined by combining i) the daily amount of vehicles per category and traffic type and, ii) the fitted copulas characterizing D_t per traffic type. This ideal day is a representation of the entire month and is the basis of the traffic simulation algorithm.

The inter-vehicle distances (D_t) of all traffic scenarios (of every normal-condition day) were fitted to bi-variate copulas. This process characterizes the dependence of the inter-vehicle distance and its lagged version (D_t, D_{t+1}). As a result, the auto-correlation of this variable is obtained.

Following a similar approach as for the number of vehicles, the copula that characterizes the ideal day was selected by comparing the fitted copulas (and their parameters) of every normal-condition day among the 6 traffic scenarios. The criteria for choosing an appropriate copula include:

- The selected copula is the best fit for most of the normal-condition days of a given traffic scenario.

- The Spearman's rank correlation coefficient obtained from the simulated data (generated by the fitted copula) is similar to the coefficient computed from the observations.

As a result, each traffic scenario is characterized by different copulas, each one of them belonging to different days of the month (Section 4.4.1).

4.3.4 Monthly Analysis

In this section, the number of vehicles per category and its corresponding proportion (%) in relation to the monthly number of vehicles were computed. The monthly proportion of vehicles is very similar to the daily proportion. This classification was applied to the entire data set with no distinction between lanes.

The monthly proportion (Appendix A.3) is used as input for the BN model developed by [98] (Fig. 4.6). This model keeps the same vehicle proportion as the input while generating a data set (VH) of vehicle characteristics for each category. In other words, the BN model gives information about the vehicles' number of axles, axle weights, and inter-axle distances based on their category. For a complete overview of the BN model, the reader is referred to [98]. In this study, the VH data set contains 300.000 passing vehicles characterized by the category proportion presented in Appendix A.3.

4.4 Results

4.4.1 Copula-based model for inter-vehicle distances

As mentioned in section 4.3, traffic is characterized by six different traffic scenarios (Table 4.1). By combining the fitted copulas of each traffic scenario with the selected daily proportion of vehicles, an " ideal-day" data set is formed. This data set is the basis for the simulation of traffic through the SFT.

Table 4.2 presents the copulas that were selected for each scenario and their corresponding parameters (See Table 4.1 for nomenclature). Note that copulas from different days characterize each one of the traffic scenarios. The VineCopula package in R (language for statistical computing), developed by [105] was used to fit the copulas to the data sets (Section 4.2.2). The parameters were estimated by pseudo maximum likelihood and the copula families were selected based on Akaike's Information Criterion (AIC).

Scenario	Copula	Day	Parameters
C_L2	Gaussian	25	ρ =0.148
C_L3	Frank	10	θ =-0.304
F_L2_A	Joe	17	θ =1.519
F_L2_B	BB8	17	θ_1 =1.717,θ_2 =0.900
F_L3_A	Gumbel	17	θ =1.137
F_L3_B	Joe	11	θ =1.160

Table 4.2: Selection of copula and corresponding parameters for each scenario.

Table 4.3 shows the Spearman's correlation value for the observations (D_t, D_{t+1}). Note that the correlation values are relatively low, especially for C_L2 and C_L3. Nevertheless, the selected copulas are able to capture well the characteristics of the inter-vehicle distance for the simulation of traffic.

For the case of C_L3, Spearman's correlation coefficient is negative. This means that the inter-vehicle distance at time t increases the inter-vehicle distance at time $t + 1$ de-

	Correlation
C_L2	0.103
C_L3	-0.093
F_L2_A	0.414
F_L3_A	0.289
F_L2_B	0.054
F_L3_B	0.10

Table 4.3: Spearman's Rho correlation value for observations of traffic scenarios.

creases or vice versa. Physically, this means that when vehicles are far apart there is a tendency for them to reduce the distance between them. The vehicles are attempting to close gaps or catch up with faster-moving traffic. In such situations, higher traffic loads are expected. Similarly, a positive correlation means that the inter-vehicle distance behind a vehicle increases as the distance behind it also increases. In other words, when inter-vehicle distances are already large they tend to increase further. This behavior is expected during free-flow hours due to the presence of fewer vehicles.

Fig. 4.8 shows the simulated inter-vehicle distances together with the observations for each traffic type. The data is presented as standard normal, this means that both the simulated inter-vehicle distances and the observed data have been transformed to follow a standard normal distribution $N(0, 1)$ (a mean of 0 and a standard deviation of 1). This transformation does not alter the dependence structure between D_t and D_{t+1}. Thus, the margins are standardized but the dependence structure between the variables is preserved. The plots from both simulations and observations are very similar. Notice that the observations for congestion traffic scenarios (Fig. 4.8a-4.8b) are clustered mostly in the center with their shape resembling a circle. Although the plots for the free flow scenarios (Fig. 4.8c-4.8f) are clustered in the center, they present a slight asymmetry in the upper right corner of the plots. Nevertheless, the dependence structure of these copulas does not show great asymmetry, and the correlation values of the observations and simulations are very similar to each other despite being relatively small. This is confirmed by the results presented in Appendix A.4.

Modeling inter-vehicle distances can capture the behavior of the dependence structure of inter-vehicle distance and provides insight into the behavior of drivers and how they adjust their spacing under specific situations. The resulting simulated traffic series has an extent of 1 year (365 days) and it represents traffic under weekday conditions since weekends and national holidays were ignored in the analysis. This time series is used as input for the structural model.

4

(a) C_L2

(b) C_L3

(c) F_L2_A

(d) F_L2_B

(e) F_L3_A

(f) F_L3_B
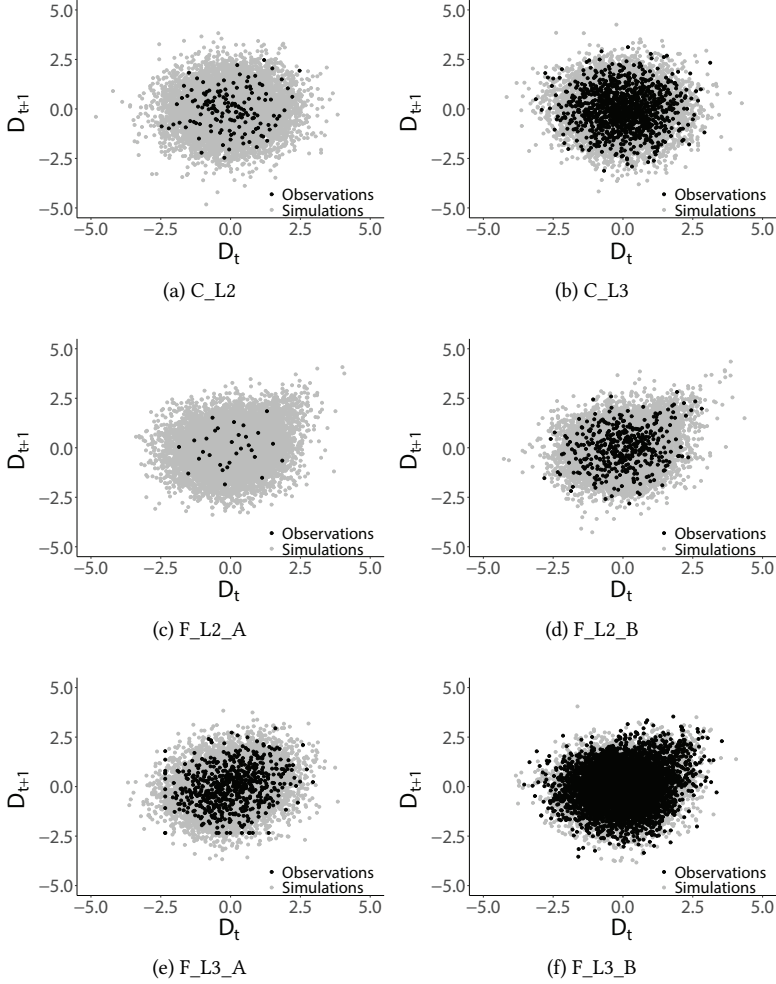
Figure 4.8: Observations and simulations for inter-vehicle distances (D_i,D_{i+1}) for all traffic scenarios from (a) Gaussian Copula, (b) Frank Copula, (c) Joe Copula, (d) BB8 Copula, (e) Gumbel Copula and (f) Joe Copula; parameters are estimated via maximum likelihood. The data is presented in standard normal units.

4.4.2 Structural model: An overview

In this section, a general summary of the structural model is provided. For a detailed description of this model and its respective equations, the reader is directed to [3].

For this particular chapter, the SFT is modeled as a monolithic structure with equal spans and symmetric supports, with a total length of 600 m. It is loaded with traffic loads representing the axle weights of vehicles driving through the structure (Fig. 4.2), meaning that the axle loads can be positioned anywhere on the SFT. For this reason, a grid size of 1m is defined throughout the structure resulting in a total of 600 individual positions along the entire SFT. A unified axle load is used to calculate individual influence on the

system's cross-section results (bending moments, shear forces).

In this chapter, leakage of the SFT is considered as the limit state function. The superposition principle is used to gather the results of a single-point load, resulting in 600 individual unit load cases. The cross-sectional results for each situation are combined with the response caused by the Buoyancy Weight Ratio (BWR). The BWR load is a constant over the length of the system, and the resulting distributed force (BWR) has a downward direction that coincides with the traffic loading (Fig. 4.1).

The axle loads and their corresponding inter-vehicle distance are treated as a long train of axle loads, with each axle load having a different magnitude. Sub-trains (smaller portions of the train of axle loads) can be derived by moving the 600 m model over the train of vehicles. The resulting envelopes of the bending moments and shear forces (M_{max}, V_{max}) are found from the cross-section results and displacements for each sub-train. If the traffic model generates a longer data set, different distributions for the envelopes are found.

4.4.3 Reliability Analysis

In this section, the focus is on the reliability analysis of the SFT using the resulting bending moments (M_{max}) and shear forces (V_{max}) from the structural model.

The probability of failure (P_F) of the SFT was tested for bending failure of the tube in the longitudinal direction (leakage of the SFT) and is defined in Eq.4.2:

$$P_F = Z = P(M_{max} > M_{cap}) \tag{4.2}$$

Where M_{max} is the maximum bending moment from the structural model and M_{cap} is the bending moment capacity derived from a given SFT design (Table 4.4). It is considered failure when the maximum bending moment exceeds the moment capacity M_{cap} because such scenarios could lead to leakage of the SFT. These limit values are directly dependent on the asymmetric post-tensioning design.

Item	Center of span	Tether location
# Axial tendons	9	17
# Asymmetric tendons	5	4
Spread angle [degrees]	125	94
M_{cap} [MNm]	108.4	-141.6
M_{BWR} [MNm]	42.0	-84.0
M_{tr} [MNm]	66.4	-57.6

Table 4.4: Post tension specification and capacity

Where M_{BWR} and M_{tr} are the bending moments due to the buoyancy weight ratio and traffic respectively. In this study, the reliability analysis focuses on fitting the resulting daily bending moments and shear forces to theoretical probability distribution functions. From which their corresponding annual maximum frequency curves are derived. For a given SFT design, the limit bending moments are found. Consequently, the probabilities of exceeding these limit values are found through the annual maximum frequency curves.

The structural analysis was performed for different buoyancy-weight ratio (BWR) values ranging from 1.1 to 1.5. The relationship between the permanent loads and the buoyancy load is described as the Buoyancy Weight Ratio (BWR) and can be influenced by changing the ballast of the structure. The resulting distributed force (BWR load) has a downward direction that coincides with the traffic loading. For simplicity, the BWR is considered constant over the length of the system. From a design point of view, a BWR close to 1.0 is the most economical. The BWR ratio results in a distributed load. By application of a lower BWR, the spans used in the structure can be larger. If larger spans can be used, fewer supporting pontoons are needed. Although other elements such as loading or stability requirements might cause the need for a larger BWR, these are considered beyond the scope of this study.

4.4.4 Frequency Curves

The resulting daily values of bending moments (M_{max}) and shear forces (V_{max}) obtained from the structural model [3] were fitted to probability distribution functions. The results are shown in Table 4.5.

BWR	M_{max} [MNm]	V_{max} [MN]
0	Gamma	Lognormal
1.1	G.E.V. [1]	G.E.V.
1.2	G.E.V.	G.E.V.
1.3	G.E.V.	G.E.V.
1.4	G.E.V.	G.E.V.
1.5	G.E.V.	G.E.V.

Table 4.5: Distribution Fitting for bending moments and shear forces.

BWR	M_{max} [MNm]			V_{max} [MN]		
	Shape	Scale	Location	Shape	Scale	Location
0	25.88	0.95	-	-0.15*	0.22*	-
1.1	-0.17	4.50	106.60	-0.09	0.17	3.32
1.2	-0.17	4.50	176.64	-0.09	0.17	5.42
1.3	-0.17	4.50	235.91	-0.09	0.17	7.20
1.4	-0.17	4.50	286.71	-0.09	0.17	8.72
1.5	-0.17	4.50	330.74	-0.09	0.17	10.05

Table 4.6: Parameters of the fitted distributions. *For the Lognormal distribution, the parameters are mean and standard deviation

The criteria for selecting an appropriate probability distribution function was made based on maximum likelihood estimation (MLE) and by visual inspection. Table 4.6 presents the parameters of the fitted distributions.

---

[1]Generalized Extreme Value Distribution

The corresponding annual maxima frequency curves for the bending moments and shear forces for a BWR of 1.1 are shown in Fig. 4.9. From these plots is possible to determine the return period (or probability of exceedance) of particular values for bending moments and shear forces. The corresponding M_{max}, M_{min}, V_{max}, and V_{min} values for different return periods (or probability of exceedance) and BWR magnitudes are depicted in Table 4.7. The results appear to be sensitive to the choice of BWR. As the BWR increases, the values for the maximum bending moments and maximum shear forces also increase. This highlights the importance of the choice of BWR when designing an SFT.
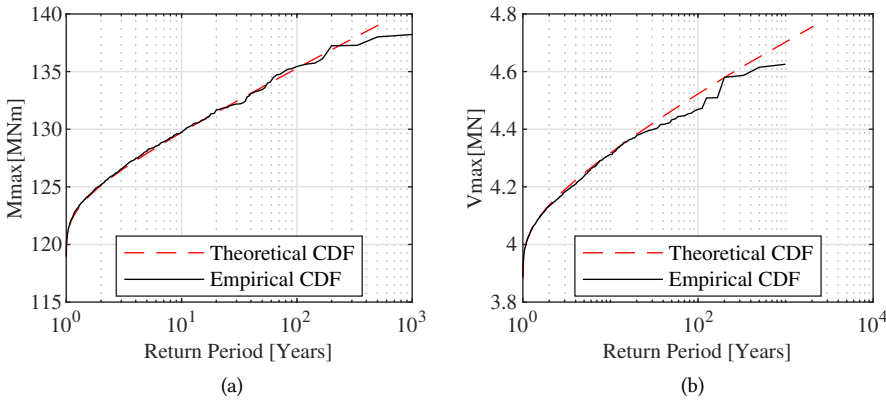
Figure 4.9: Frequency curves for (a) $M_{Max}[MNm]$ and (b) $V_{Max}[MN]$ for a 1.1 BWR

BWR	Variable	Return Period & P_F						
		5	10	20	50	100	200	500
		0.2	0.1	0.05	0.02	0.01	0.005	0.002
0		43	43	44	44	44	44	44
1.1		128	130	132	134	136	140	142
1.2	M_{max}	198	200	201	204	205	207	208
1.3	[MNm]	257	259	261	262	264	265	266
1.4		308	310	312	313	314	316	319
1.5		352	354	356	358	359	360	364
0		2	2	2	2	2	2	2
1.1		4	4	4	4	4	5	5
1.2	V_{max}	6	6	7	7	7	7	7
1.3	[MN]	8	8	8	8	8	8	8
1.4		10	10	10	10	10	10	10
1.5		11	11	11	11	11	11	11

Table 4.7: Extreme values of M_{max}, and V_{max} for different return periods and a BWRs

For the particular SFT design presented in Table 4.4, the corresponding values of M_{cap} at the center of the span and tether location are respectively 108.4 MNm and -141.6 MNm. If we place these values at the frequency curves corresponding to bending moments for

a BWR of 1.1, their respective return periods are 139 and 439 years. This corresponds to probabilities of failure of 0.01 and 0.005.

4.5 Discussion

The inter-vehicle model methodology presented in this study combines uni-variate and multi-variate models (copulas). This not only allows the simulation of the inter-vehicle distance but also models the number of vehicles per lane per day and their classification according to the different vehicle categories (Appendix A.1). Each vehicle category is defined by its axle weight and inter-axle distance. The selection of each one of the passing vehicles is random. In this way, it is possible to obtain a "train" of vehicles that is closer to reality. One of the main advantages of this model is its flexibility. The model can be used for any number of vehicle categories, lanes, and traffic scenarios. In this case study, the model was developed on the basis of one single "ideal day", nevertheless, the inter-vehicle model can be extended to encompass specific daily conditions (weekends and holidays) or seasonal conditions.

In the setup presented in this article, the geometry of the cross-section and the span length are arbitrary choices. Larger BWR values lead to higher bending moments and shear forces as shown in Table 4.7. This can influence other design decisions such as shorter spans or larger tether sections that could affect the stability of the system. In this study, the resulting bending moments and shear forces were computed for different BWR values. However, a BWR of 1.1 was chosen for further analysis. In any case, a design should be optimized for different circumstances. Possibilities to consider are (but not limited to):

- Using larger BWR values. This will lead to larger bending moments and shear forces. Consequently, other requirements for pontoons, tether systems and foundations will be affected. However, a higher BWR could contribute to the stability of the system. Moreover, a longitudinal variation of the BWR might be applicable depending on local situations or specific designs.

- Although the SFT design presented in this study consists of a single tubular tube, the proposed methodology is applicable to different designs of SFT (double tubes or different cross-section geometries as presented in [106]).

4.6 Conclusions

In this study, a methodology to study the reliability of a pontoon-type SFT is presented. Considering that this structure has not been built yet, the variables of interest must be characterized as close to reality as possible. For the purpose of this study, traffic loading is the variable of interest. The methodology focuses on the simulation of traffic using a copula-based model. The reliability of the structure is investigated under the failure mechanism of leakage due to the bending of the SFT tube in the longitudinal direction.

From the original data set (WIM), several characteristics were extracted. Namely, i) the inter-vehicle distance, ii) the daily proportion of vehicles per lane, per category, and per traffic type, and iii) the monthly proportion of vehicles. The first is used as input for the copula-based model, the second is used to create an "ideal" traffic day, and the third

is used to create a large data set of vehicles per category. All of these were combined to finally simulate traffic flowing through the SFT.

The results from the copula model showed that the selected copulas are able to characterize the inter-vehicle distance. Although the correlation of the inter-vehicle distance from the WIM data set is relatively small, the probabilistic model provides a great advantage: with just over a month of measurements it was possible to simulate a total of 1 year of data. Although longer data sets can be produced. The combination of the inter-vehicle copula model and random sampling from the VH data set (which provides the vehicle's characteristics) resulted in one vector that characterizes daily traffic at the SFT. This vector was used as input for the structural model.

Results from the structural model provided the maximum and minimum bending moments and shear forces under the traffic loading for different BWR values. From these results, the annual distribution of these variables was obtained and, consequently, their extreme values for several return periods. The values of M_{cap} at the center of the span and at the tether location were obtained. These values define the limit state function for failure due to the bending of the tube in the longitudinal direction (Section 4.4.3). In other words, failure could only occur if the resulting bending moments from the envelopes are larger than M_{cap}. The return periods for both M_{cap} of 108.4 MNm and -141.6 MNm, are 139 and 439 years at the center of the span and tether location respectively. Their corresponding probabilities of failure are 0.01 and 0.005. These probabilities can be considered very high when compared to international safety standards. For example, a structure with an RC3 reliability level (β=4.3) has an estimated probability of failure equal to 8.5 × 10^{-6} [107] assuming that the lifetime of the structure is 50 years. In the case of an SFT, the consequences of failure are much more severe compared to regular buildings. For this reason, bending moments with larger return periods are needed. In such a case, design changes, such as different BWRs could be appropriate.

Therefore, the combination of probabilistic modeling with structural analysis offers the possibility to study the design choices of this structure. This study shows an effective way to use probabilistic modeling through copulas to simulate traffic and to study their effect on the structure. This methodology offers great flexibility to test the reliability of the SFT considering other loading variables. For example, external environmental variables such as waves, currents, and their simultaneous action on an SFT. Moreover, this methodology is not restricted to being used only on an SFT. It can be applied to other civil structures where the data is scarce.

5

Simulating metocean data

There are uncertainties related to the environmental variables relevant to the construction and operation of an SFT. Wave and current data will be considered for this study. In this chapter, a joint probability distribution analysis is proposed to characterize waves and currents and their dependence. This analysis was carried out using a copula-based model. In this way, the design conditions for the SFT can be modeled more realistically. Copula-based models capture the linear or non-linear behavior of the data because they model dependence structures separately from the marginal distributions. For example, using Archimedean copulas, tail dependence can be modeled, essential for capturing extreme non-linear behavior. The results are several synthetic time series of hourly values and extreme values of all the variables involved.

This chapter is structured as follows: a brief introduction is presented in Section 5.1. The probabilistic model for hourly and extreme values is described in Section 5.2. The findings of this research are detailed in section 5.4, followed by the main conclusions and recommendations (Section 5.5).

5.1 Introduction

In civil engineering, waterway crossings are one of the most challenging structures. In the last few decades, the traffic demand and growing development of cities have increased the necessity of longer waterways that require new and more advanced technologies. One structure has already been proposed to give a solution to this problem: The construction of a submerged floating tunnel (SFT).

However, an SFT has not been built yet, mainly due to the lack of experimental data and knowledge about its actual behavior. In this study, we focus on the simulation of metocean loads that could act on the SFT. This is the first step in estimating the reliability of an SFT aimed to be located at the Qiongzhou strait. The methodology presented in this study considers the combined action of metocean loads acting on the SFT, these are waves and

currents. It is essential to study waves and currents in the context of submerged floating tunnels to optimize their design, ensure their structural integrity, and address safety and operational concerns. This information can aid engineers in creating solutions for constructing and operating SFTs in various marine environments. A copula-based approach is proposed to characterize 3-hourly values of metocean variables (waves and currents). The resulting synthetic simulations represent hourly conditions and extreme events. This study shows how copulas are used as a powerful probabilistic tool to characterize these loads and to generate a synthetic time series (of a thousand years) of the variables under investigation. The results of this study can be incorporated into risk or reliability analyses for an SFT.

5.2 Modeling approach

As mentioned in Chapter 3, wave data are classified into two sets: wind waves (WW) and total swells (TS) whereas currents (C) are classified into currents at 1m and 15m below the water surface. The variables of interest are paired together to form five groups for analysis: Wind waves, total swell, wind waves-currents, and total swell-currents (WW, TS, WWC, TSC, and C). See Table 5.1. In this study, we follow the same nomenclature as in Table 3.2.

Each pair in the second column of Table 3.2 is modeled with a copula. Group WW and TS are divided into two pairs while groups WWC, TSC, and C have one pair of variables each. In group WW, the first pair $(X_t^{(1)}, X_t^{(2)})$ aims to model the dependence relationship between wave height and wave period. The second pair within this group focuses on the order 1 auto-correlation of wave height $(X_t^{(1)}, X_{t+1}^{(1)})$. Group TS is analogous to group WW. For groups WWC and TSC, the focus is on the dependence relationship between wave height (wind waves and total swell respectively) and current velocity at 1m below the water surface $(Z_t^{(1)})$. Finally, group C focuses on the dependence between current velocities at 1m and 15m below the surface $(Z_t^{(2)})$.

| Group | Variables | Approach | |
		ID	POT
-Wind waves (WW)	$(X_t^{(1)}, X_t^{(2)})$	*	*
	$(X_t^{(1)}, X_{t+1}^{(1)})$	*	
-Total swell (TS)	$(Y_t^{(1)}, Y_t^{(2)})$	*	*
	$(Y_t^{(1)}, Y_{t+1}^{(1)})$	*	
-Wind waves & Currents (WWC)	$(X_t^{(1)}, Z_t^{(1)})$	*	*
-Total swell & Currents (TSC)	$(Y_t^{(1)}, Z_t^{(1)})$	*	*
-Currents (C)	$(Z_t^{(1)}, Z_t^{(2)})$	*	*

Table 5.1: Datasets groups for analysis

The five groups are processed under two different approaches of wave's long-term statistics: i) The initial-distribution approach (ID) and ii) the peak-over-threshold approach

(POT). The ID approach considers all observations, conserving the continuity of the data, while the latter consists of modeling the excess values over a high level (or threshold) within a time series [108]. The main challenges in a POT approach are i) making sure that the extracted values are independent of the original time series, and ii) choosing appropriate threshold values [109]. The application of POT models is very popular in hydrology, for example, for the estimation of floods [110].

The choice of threshold is defined by a graphical approach, specifically, by parameter stability plots. With this approach, the selection of the shape and scale parameters are defined at the lowest value where the plots are approximately constant [111]. For more details about ID and POT approaches refer to [112]. Table 5.1 shows the data pairs that were processed with an ID or POT approach.

5.3 Simulating waves and currents

In order to select the copula model, estimate its parameters, and simulate data, the VineCopula package [105] in R [95] (language for statistical computing) was used. The parameters are estimated by pseudo maximum likelihood and the copula families were selected based on Akaike's information criterion.

For the case of ID data, the analysis also includes the computation of the auto-correlation of the variables (Table 5.1). This procedure was applied to wave height and current velocity to characterize their hourly fluctuation, enabling the generation of a more realistic synthetic time series.

Eq.2.12 is applied to simulate values for significant wave height). Hourly values of wave period ($X^{(2)}$) are generated from the copula $C_\theta(F(x_t^{(1)}), G(x_t^{(2)}))$ where G is the distribution of hourly wave period and θ summarizes the dependence between hourly wave height and wave period.

Finally, for current velocities at 1m ($Z^{(1)}$), the formulation in Eq.2.12 is used to characterize the time series given wave height observations ($X^{(1)}$) and current velocity at 15m depth ($Z^{(2)}$) given velocities at 1m depth. The graphical representation of this process is presented in Fig.5.1. The analogous process is applied for total swell.
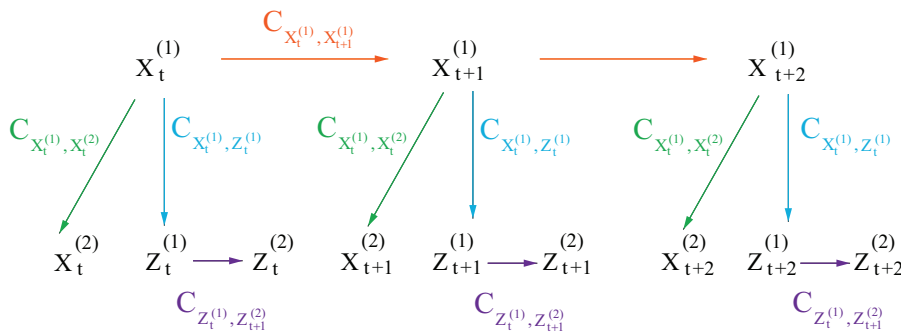
Figure 5.1: Process for wind waves. ID data

A similar process to that used for ID data was used for POT data. The distinction is

that each of the values of wave height in the time series is generated randomly from the extreme-value marginal distribution (Thus, no arrows between $X_t^{(1)}$ and $X_{t+1}^{(1)}$). Simulations of the remaining variables are obtained in the same way as the continuous synthetic time series. This process is illustrated in Fig.5.2.
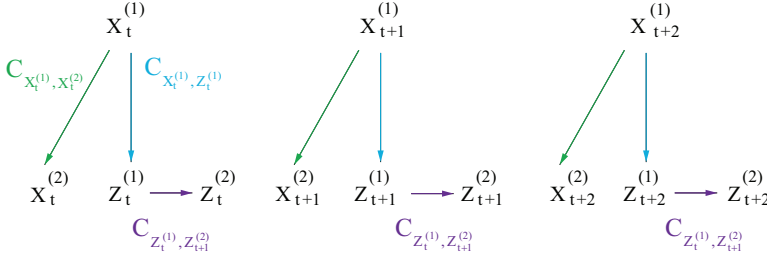
Figure 5.2: Process for wind waves. POT data

5

In summary, the simulation process consists of following the approaches represented in Fig. 5.1 and Fig. 5.2 to generate larger time series of i) 3-hourly wave height, wave period, and current velocities, and ii) extreme values of wave height, wave period and current velocities. Each simulated "year" is 184 days long because only the wet season is being modeled. The synthetic time series spans a thousand years.

5.4 Results

The data is analyzed for the entire strait and is divided into 9 grid points that cover the strait from left to right (Figure 3.4). Moreover, the analysis of the data is limited to the wet season which spans from May 1st to October 31st in the region of the Qiangzhou Strait. Fig. 5.3 shows a scatter plot of wind wave data (significant wave height $X^{(1)}$ and wave period $X^{(2)}$) at grid point 4. The figure displays a second data cluster (at $X^{(2)} \sim 4m$) as well as a few data points that might qualify as outliers. However, to keep continuity in the time series, the ID data was not further divided into different wave climates, nor outliers were removed.

The analysis of the joint distribution of waves and currents usually involves an additional variable: the mean direction. In this study, the data is not conditioned to a predominant wave and current direction. Figure 5.4 illustrates wave and current roses for the grid points situated at the Qiongzhou Strait. A wave or current rose is a graphical representation of the distribution of wave and current directions. It consists of a circular diagram segmented to represent specific compass directions, such as north, northeast, east, etc. ID data (Left column in Fig. 5.4) shows that waves have a wide range of directions during the wet season, while currents are mostly directed towards the southwest and northeast. For POT data (Fig.5.4 right column), currents have the same direction as ID data, and waves are predominantly directed towards the southwest. Conditioning the analysis on wave/current direction is recommended for further studies.

During the wet season, there are strong serial correlations for the wave height as well
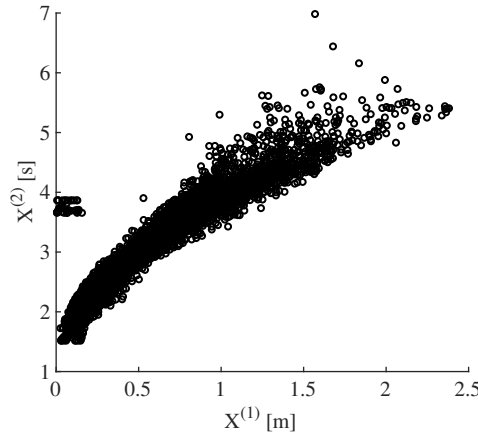
Figure 5.3: Scatter plot of group WW. ID data. Grid point 4.

5

as the wave period time series. The serial correlation for wind waves at grid point 4 is depicted in Fig.5.5 in terms of Spearman's rank correlation coefficient. See how correlation values decline with increasing hour intervals, reaching 0.1 after roughly 60 hours. Overall, the serial correlation of all the variables in this study appears to be pretty comparable. Nevertheless, rather than steadily declining, the serial correlation for grid point 4 oscillates up and down. This variation is periodic, in the order of 24h, which could be due to the effect of the tidal cycle at the strait. The grid points outside of the strait do not present this periodic fluctuation. It is then clear that the effect of the tidal cycle becomes more relevant at the strait. However, in this study, the effect of the tidal cycle is not considered for further analysis.

5.4.1 Univariate Fitting

To choose the probability distribution that might most accurately characterize the data sets, the empirical wave and current distributions were compared to several theoretical univariate distributions. However, not all variables could be fitted to theoretical distributions since distribution candidates did not provide a reliable fit. For such cases, the empirical distribution was chosen instead. For example, Fig.5.6a shows the difference between the empirical cdf (cumulative distribution function) and the theoretical distributions, especially at larger values. This can be evidenced further in the corresponding Q-Q (Quantile-Quantile) plot (Fig. 5.6b). The reference line in the Q-Q plot represents the expected distribution, for the case of Fig. 5.6b, that is a G. Pareto distribution. This reference line indicates how the data points would look like if they would perfectly follow such distribution. Table 5.2 to 5.4 show a summary of the best fit for each variable at each grid point (Grid points are depicted in Fig. 3.4).

(a)   (b)

(c)   (d)

(e)   (f)

(g)   (h)
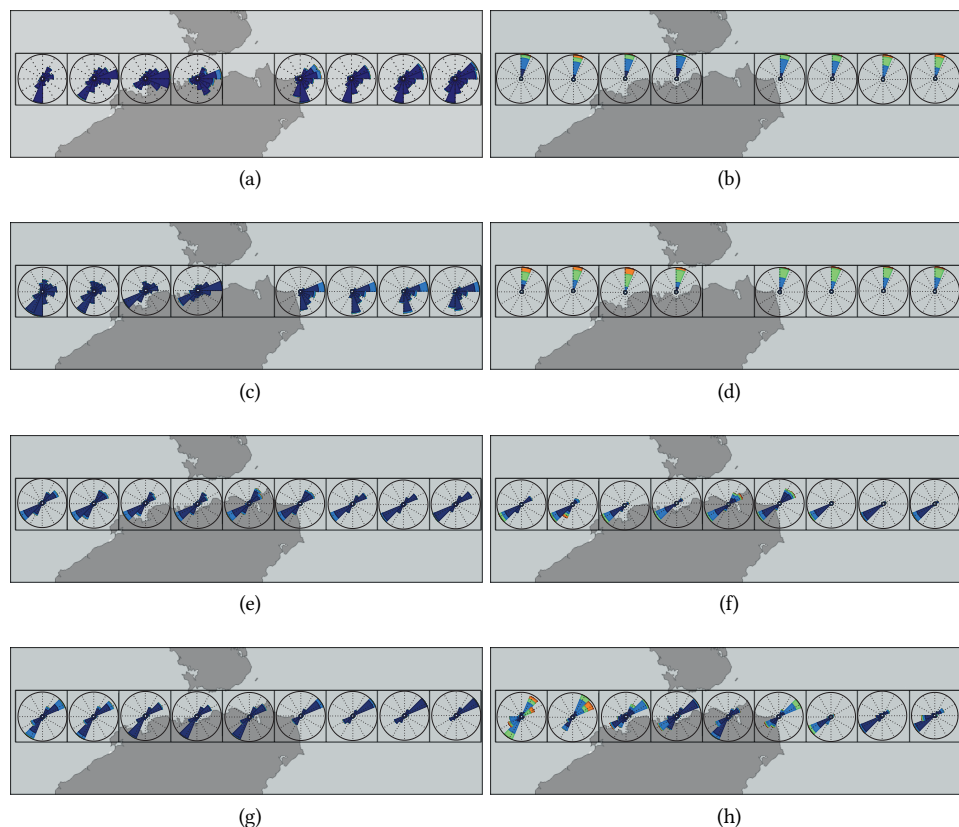
Figure 5.4: Wave and current roses for ID data (left column) and POT data (right column) at the grid points of the Qiongzhou Strait: (a), (b) Wind waves wave height ($X^{(1)}$), (c), (d) Total swell Wave height ($Y^{(1)}$), (e), (f) Currents at 1m ($Z^{(1)}$) and (g), (h) Currents at 15m ($Z^{(2)}$).

5.4.2 Copula fitting

The paired data (Table 5.1) was fitted to copulas using the VineCopula R package. A total of 12 data pairs were compared to several theoretical copulas and finally fitted to the ones that described best their dependence. The results of this process are presented in Table 5.5 (ID data) and Table 5.6 (POT data), with the latter also including the respective number of extreme values identified. The copula's parameters were estimated through maximum likelihood and the selection of copula families was based on Akaike's information criterion.

Next, a total of a thousand wet seasons were simulated for all the variables of interest. The selected copulas generated synthetic data sets that were able to capture the main features of the dependence structure between the variables. An example of a visual comparison between the observations and the simulated points is presented in Fig. 5.7. Table 5.7 and Table 5.8 presents Spearman's rank correlation coefficients from the observations and simulations.
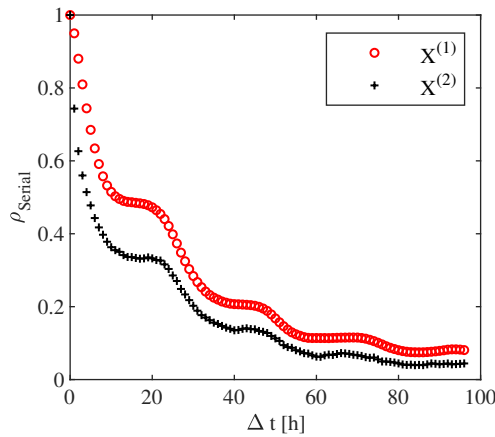
Figure 5.5: Serial correlation for wind waves. ID data. Grid point 4.

Gridpoint	Wind Waves		Total Swell	
	ID	POT	ID	POT
1 to 4	Gamma	Empirical	GEV[1]	Empirical
6 to 9	Gamma	Empirical	GEV	G. Pareto[2]

Table 5.2: Univariate fitting for significant wave height.

Overall, ID data (Fig. 5.7) have a higher degree of dependence than POT data (Fig. 5.8). ID data shows a strong positive dependence between wave variables (Fig. 5.7), being stronger for the pairs $X_t^{(1)}, X_{t+1}^{(1)}$ & $Y_t^{(1)}, Y_{t+1}^{(1)}$. While the correlation between current velocity and wave height pairs, $X_t^{(1)}, Z_t^{(1)}$ & $Y_t^{(1)}, Z_t^{(1)}$ is low, being approximately 0.13. The correlation between current velocity at different depths is low for both ID and POT data ($Z_t^{(1)}, Z_t^{(2)}$ & $Z^{(1)}, Z^{(2)}$).

[1]GEV: Generalized extreme value distribution
[2]G. Pareto: Generalized Pareto distribution

Gridpoint	Wind Waves		Total swell	
	ID	POT	ID	POT
1,3,4	GEV	Empirical	GEV	Empirical
2, 6-9	LogNormal	Empirical	GEV	Empirical

Table 5.3: Univariate fitting for mean wave period.

Gridpoint	1m depth		15m depth	
	ID	POT	ID	POT
1 to 6	Gamma	Empirical	Weibull	Empirical
7 to 9	Weibull	Empirical	Weibull	Empirical

Table 5.4: Univariate fitting for current velocity.

5

(a)   (b)
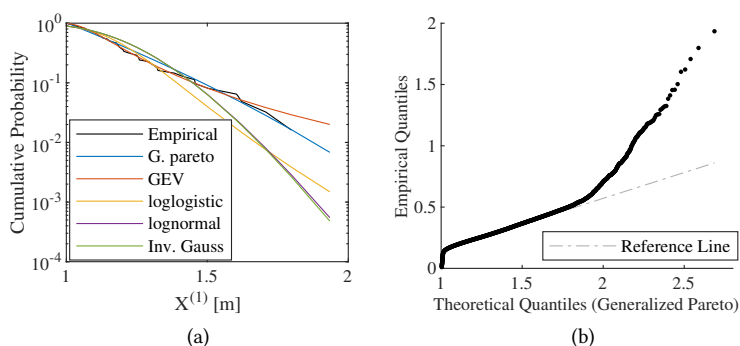
Figure 5.6: CDF (a) and QQ (b) plots for significant wave height for total swell (POT data. Grid point 4)

Copula	Family	Parameters
$C_{X_t^{(1)}, X_{t+1}^{(1)}}$	Joe	θ=9.7411
$C_{X_t^{(1)}, X_t^{(2)}}$	t	ρ= 0.9178 , ν=2
$C_{Y_t^{(1)}, Y_{t+1}^{(1)}}$	t	ρ= 0.9473 , ν=2
$C_{Y_t^{(1)}, Y_t^{(2)}}$	BB6	θ_1=1.0839 , θ_2=1.4174
$C_{Z_t^{(1)}, Z_t^{(2)}}$	Gauss	ρ=0.1461
$C_{X_t^{(1)}, Z_t^{(1)}}$	BB8	θ_1=1.1793 , θ_2=0.9965
$C_{Y_t^{(1)}, Z_t^{(1)}}$	BB8	θ_1=1.1045 , θ_2=0.9953

Table 5.5: Copula families and parameters for grid point 4. ID data.

Copula	Family	Parameters	Num. observations
$C_{X^{(1)},X^{(2)}}$	Frank	$\theta=4.9228$	205
$C_{Y^{(1)},Y^{(2)}}$	Joe	$\theta=1.2949$	62
$C_{Z^{(1)},Z^{(2)}}$	Gaussian	$\rho=0.2939$	234
$C_{X^{(1)},Z^{(1)}}$	Frank	$\theta=1.0901$	205
$C_{Y^{(1)},Z^{(1)}}$	Frank	$\theta=0.9463$	62

Table 5.6: Copula families, parameters, and number of identified extreme values for grid point 4. POT data.

Copula	Observations	Simulations
$C_{X_t^{(1)},X_{t+1}^{(1)}}$	0.94	0.95
$C_{X_t^{(1)},X_t^{(2)}}$	0.69	0.89
$C_{Y_t^{(1)},Y_{t+1}^{(1)}}$	0.89	0.93
$C_{Y_t^{(1)},Y_t^{(2)}}$	0.48	0.47
$C_{Z_t^{(1)},Z_t^{(2)}}$	0.14	0.14
$C_{X_t^{(1)},Z_t^{(1)}}$	0.14	0.13
$C_{Y_t^{(1)},Z_t^{(1)}}$	0.07	0.08

Table 5.7: Spearman's rank correlation for observations and simulations. ID data. Point 4

Copula	Observations	Simulations
$C_{X^{(1)},X^{(2)}}$	0.63	0.64
$C_{Y^{(1)},Y^{(2)}}$	0.12	0.21
$C_{Z^{(1)},Z^{(2)}}$	0.25	0.28
$C_{X^{(1)},Z^{(1)}}$	0.17	0.18
$C_{Y^{(1)},Z^{(1)}}$	0.13	0.16

Table 5.8: Spearman's rank correlation for observations and simulations. POT data. Point 4.

It is evident from Fig. 5.7b that the data has outliers. However, they were not removed from the sample to maintain the continuity of ID data. On the other hand, these points might indicate the presence of different wave climates in the area. To test this hypothesis, these points would need to be separated and analyzed in different clusters but this process is out of the scope of this study.
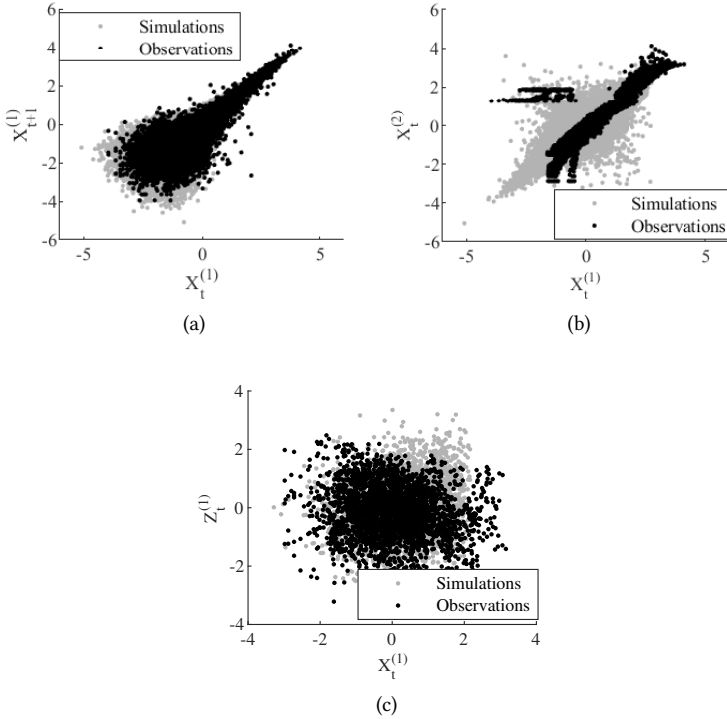
Figure 5.7: Data vs. simulated points from copulas (Table 5.5).WW-ID data. Point 4.

Finally, the data sets were converted into their real units by using the inverse of their corresponding marginal distribution and then were plotted together with the observations. Fig. 5.9 illustrates the results of the ID approach for wind waves. The figure shows the average of the observations and the simulations over a period of 100 years, along with the corresponding 95% confidence interval for the simulations. In general, the simulations are visually very similar to the observations, however, ID current velocity fluctuates much more than their corresponding observations. This is not the case for POT's current data. To improve ID current data, a vine-copula model could be implemented. This model could include the serial correlation of both current velocities to generate the synthetic time series. In other words, adding a copula conditionalized on the serial correlation of $Z^{(1)}$ and $Z^{(2)}$, for example, $C_{(X_{t+1}^{(1)}, Z_{t+1}^{(1)})|Z_t^{(1)}}$ and $C_{(Z_{t+1}^{(1)}, Z_{t+1}^{(2)})|Z_t^{(2)}}$.
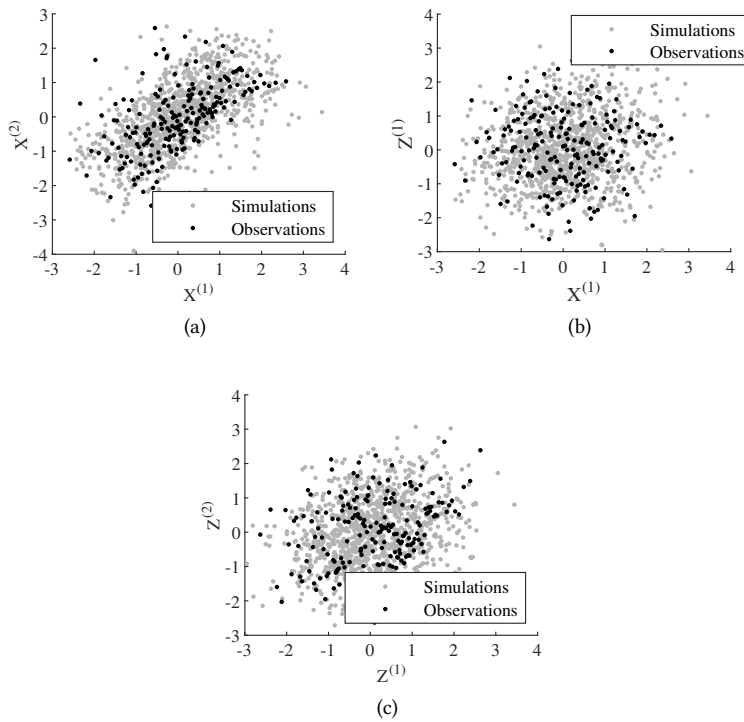
Figure 5.8: Data vs. simulated points from copulas (Table 5.6).WW-POT data. Point 4.

5
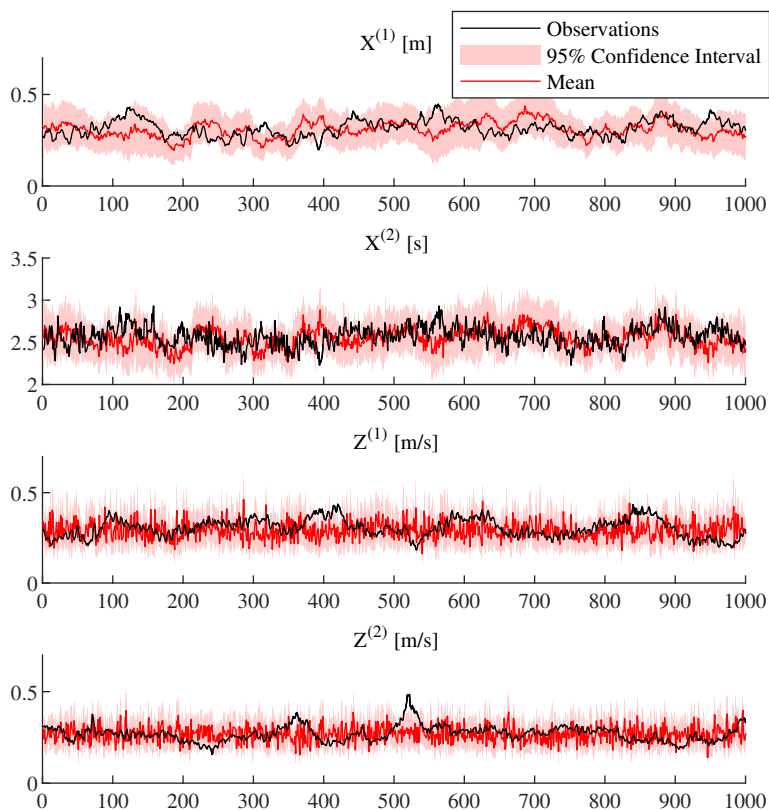
Figure 5.9: Simulated time series of wave height $X^{(1)}$, wave period $X^{(2)}$ and current velocities $Z^{(1)},Z^{(2)}$. ID approach wind waves

5.5 Conclusions

This chapter presented a copula methodology to create a synthetic time series of wave height, wave period (Wind waves and total swell), and current velocities (At 1m and 15m depth) at the Qiongzhou Strait in China. To perform such a task, the VineCopula R package was used.

The univariate fitting of the POT data did not provide a reliable fit to theoretical distributions, which resulted in using the empirical distribution for all the variables. This does not allow extrapolation to larger values and therefore limits the study of extremes in the region, which is key to determining the reliability of the SFT. For this reason, future research should involve fitting extreme data to multi-modal distributions or other complex models.

To develop the copula-model approach, some simplifications were made. ID wave height data ($X^{(1)}$) was not clustered and analyzed in different wave climates because it was important to preserve continuity. Moreover, the influence of the tidal cycle on the variables was not investigated in this study, this factor can be included as part of an expanded vine-copula model. Nevertheless, the copula model was able to capture the main features of the dependence between the variables resulting in a synthetic time series similar to the observations in the area, evidenced by the correlation coefficients between the observed and the simulated values. This characterization could be used to estimate the reliability of the SFT under daily conditions (ID data) and extreme conditions (POT data).

In summary, this chapter demonstrates how modeling the dependence between the variables that represent the loads can be used to determine the joint probability of ID data and extreme data. Once a copula model has been fitted to the data it is possible to calculate the joint probability of the loads. This involves determining the probability of one variable given the other. This enables the assessment of the likelihood of specific load combinations which is valuable for decision-making and SFT design.

5

III

Multivariate models for risk and reliability analysis of an SFT

6

Vine-Copulas for waves, currents, and hydrodynamic forces

As mentioned in previous chapters, an effect that should be further investigated for the design and construction of an SFT is the simultaneous action of waves and currents and their resulting hydrodynamic forces. For this study, we propose vine-copula models because they offer great flexibility and take into account complex relationships by capturing different possible dependencies between pairs of variables. The analysis between metocean variables and their corresponding resulting forces is further expanded to study nine different SFT configurations of different diameters and submergence depths. The results show that larger Froude-Krylov forces are obtained for SFT configurations that place the SFT closer to the water surface.

This chapter is organized as follows: Section 6.1 provides a brief introduction to the application of vines on metocean loads for an SFT. This is followed by a description of the modeling approach that combines extreme value analysis with vines (Section 6.2). Section 6.3 presents the results of the univariate and multivariate analysis. The procedure to estimate the hydrodynamic forces is shown in Section 6.4 followed by a discussion of the findings 6.5. The chapter closes with the conclusions and areas of future work (Section 6.6).

6.1 Introduction

Many preliminary designs and feasibility studies have been proposed worldwide as possible locations to build an SFT [6–11]. One of these locations is the Qiongzhou Strait in China (Fig. 3.1). This narrow ocean passage is very dynamic and characterized by complex physical processes and it is frequently affected by tropical cyclones [88]. These extreme events can jeopardize the construction and operation of an SFT in this location. Usually, when designing structures, extreme values of environmental loads are assumed

to be independent. However, probabilistic models such as vine-copulas take into account the dependence relationship between variables, providing, in this way a more realistic characterization of the environment surrounding the SFT.

Vine-copulas are graphical multivariate models that use bivariate copulas as building blocks to capture more complex dependence structures (Chapter 2.4). There are uncertainties related to the metocean variables (and their combined action) relevant to the construction and operation of an SFT. In general, the dependence between these variables is not taken into account. In this study, therefore, we present a vine-copula approach to characterize the joint action of wind waves, swell waves, currents, and their resulting forces acting on the SFT at the Qiongzhou Strait. Wind waves are generated by local winds that blow over the water surface, while swells are waves that have traveled out of their area of origin [87]. Wind and swell waves are characterized by their significant wave height and mean wave period. Currents are characterized by the velocity at two levels from the water surface (1m and 15m). All these variables are considered in this study.

6.2 Modeling Approach

The methodology presented in this study consists of i) an univariate extreme value analysis (EVA), and ii) a multivariate analysis (Vine-copula modeling).

6.2.1 Extreme Value Analysis

An extreme value analysis (EVA) is applied to the metocean (wave and currents) data sets. For this purpose, a peak over threshold (POT) approach is used. Selecting the appropriate thresholds follows the same graphical approach used in Chapter 5.2.

In this study, an additional step is added after the threshold has been established to extract the extreme values. The data is divided into "clusters of exceedance" that are determined as follows [113]:

- The first exceedance in the data set initiates the first cluster.

- The first observation below the threshold ends the current cluster.

- The next exceedance initiates a new cluster. This is repeated throughout the entire data set (the clusters are represented as grey areas in Fig. 6.1).

Next, the maximum value within each cluster is extracted forming an extreme value time series. This process is called "declustering", where only the highest (peak) observations within the clusters are retained [96].

In this study, the values of significant wave height, wave period, and current velocity are further classified into dominant and concomitant variables. A dominant variable is the one selected as the most relevant variable for the analysis, while the concomitant variables are the ones that remain. The POT approach presented previously is applied to the selected dominant variable. The concomitant variables are those whose clusters are not defined by their own thresholds, instead, the dominant variable defines their clusters. Fig. 6.1 shows an example of the POT selection process. Note that only the cluster maxima are extracted. The gray areas indicate the clusters that correspond to the dominant variable and how
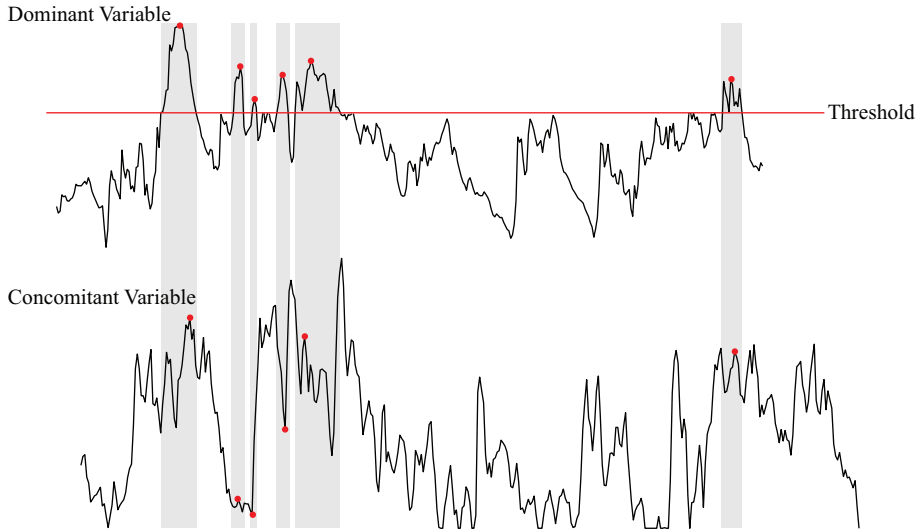
Figure 6.1: Peak over threshold methodology.

they are applied to the concomitant variables. For both the dominant and concomitant variables, the extreme time series are formed by the maximum values in each cluster.

The significant wave height for swell waves is selected as the dominant variable, while all the remaining variables are considered concomitant variables. For this study, the clusters are considered storms and their peaks are the maximum recorded value of the significant wave height of each storm (cluster). Thus, the purpose of applying this approach is to ensure that the extreme values of all the variables correspond to the same storms (depicted as red dots in Fig. 6.1).

The extracted extreme values are assumed to follow a Generalized Pareto distribution with parameters k (shape),σ (scale), and θ (threshold). The values corresponding to the concomitant variables are fitted to theoretical distribution functions. The selection of theoretical distribution is based on Akaike's Information Criterion (AIC) and by visual inspection of the cumulative distributions (CDFs).

To compute the return periods of the extreme values obtained from the POT approach, it is necessary to include the rate of occurrence of the clusters [96, 114]. Thus, the probability of exceeding a certain value of, for example, $Y^{(1)}$, in a specified return period is given by [115]:

$$1 - F(Y^{(1)}) = 1/(\lambda * T_R) \tag{6.1}$$

Where,

- 1-$F(Y^{(1)})$ is the probability of exceedance.

- λ is the yearly cluster rate.

- T_R is the return period in years.

The yearly cluster rate is defined as the average number of storms per year (number of clusters per year). In section 6.3, further details on the application of extreme value analysis and their respective return periods is provided.

6.2.2 Vines

Copulas can be powerful tools to characterize multivariate distributions. However, their application in n-dimensional cases ($n \geq 3$) can be challenging as there are no straightforward copula extensions for such circumstances. Nevertheless, Vine-copulas are an appropriate option to characterize the dependence between more than two variables. Vines offer great flexibility in capturing complex dependence structures compared to copulas. Multiple bi-variate copulas are used as building blocks to construct a vine, this allows for more realistic modeling of the variables involved. For theory on copulas and vine-copulas, see Chapter 2.

When using vine-copulas, selecting the best regular vine to characterize a data set can be a difficult task. This is because the number of regular vines increases substantially given the number of nodes n in the model (Eq. 2.13-Chapter 2).

Currently, there are two approaches for selecting the best vine for a given data set. i) In [116] the vine model is chosen by selecting the first tree, followed by iteratively selecting vines for the subsequent trees, ii) the vine model is selected by comparing the fit of all possible vines. The latter is based on the work of [57], where the exact number of vines possible is estimated given that the first tree is known. Resulting in a catalog that classifies regular vines according to their graphical structure [56].

In this study, both methodologies were applied to find a vine to characterize the data sets. The fit is assessed with likelihood-based measures such as Akaike's Information Criterion (AIC), the Bayesian Information Criterion (BIC), and the negative log Likelihood (NLogL). For this study, the focus is on the AIC [58] coefficient.

6.3 Results

This section presents the results of the extreme value analysis and the multivariate analysis (vines). Seven of the nine grid points presented in Figure 3.4 are considered for univariate analysis (grid points 1-4 and 7-9). This is to investigate the possible similarities or differences in data at the different areas along the Qiangzhou strait and the area just outside of it. The multivariate analysis is only applied to grid point 4 because this area is proposed for the SFT's central line (Fig. 3.2).

The focus is on Qiongzhou Strait's wave and current data sets, more specifically on wave height, wave period, and current velocity that spans 19 years approximately. The data includes wind-sea waves (WW) and total swell (TS) data, with current velocity data classified into two sets: 1 meter and 15 meters below the water surface.

6.3.1 Univariate Analysis

The approach used for the univariate analysis consists in extracting the extreme values of a dominant variable based on a given threshold (Peak over threshold approach in section 6.2.1). The total amount of observations that surpassed the given threshold is equal to 30 (approximately 2 extreme events per year in a period of 19 years). Although only the

threshold of the dominant variable (significant wave height of swell waves, $Y^{(1)}$) is used for the E.V.A, Table 6.1 presents the resulting thresholds of each variable at each grid point.

Grid Point	Wave height and period (WW)		Wave height and period (TS)		Currents at 1m and 15m	
	$X^{(1)}$ [m]	$X^{(2)}$ [s]	$Y^{(1)}$ [m]	$Y^{(2)}$ [s]	$Z^{(1)}$ [m/s]	$Z^{(2)}$ [m/s]
1	4	5.3	1.5	5.3	0.61	0.76
2	3.2	4.7	1.3	5.4	0.65	0.85
3	2.3	4.4	1.3	5.9	0.65	1.03
4	1.6	5	1.4	7.8	0.75	0.88
7	3.8	6.1	2.1	7.4	0.8	0.95
8	3.7	6.4	2.5	7	0.76	0.48
9	4.1	6.3	2.7	7.3	0.76	0.51

Table 6.1: Threshold Values. WW: Wind waves, TS: total swell.

The extracted data sets were fitted to theoretical probability distribution functions. This was done for all grid points with available data at the strait (1-4 and 7-9). Table 6.2 shows the selected theoretical probability distribution functions and their respective parameters at grid point 4. The results from the other grid points (1-3 and 7-9) are similar to the ones shown in Table 6.2. All the theoretical distributions were selected according to the smallest Akaike's information criteria (AIC) and by visual inspection of the CDFs (cumulative distribution functions) and their respective Q-Q plots. An example is presented in Fig 6.2 for the fitting of significant wave height (wind waves) to a Generalized Pareto distribution at grid point 4.

Variable	Distribution	Parameters
$X^{(1)}$	Generalized Pareto	$(k,\sigma,\theta) = (-0.80, 2.33, -1.78 \times 10^{-15})$
$X^{(2)}$	Inverse Gaussian	$(\mu, \lambda) = (5.01, 68.42)$
$Y^{(1)}$	Generalized Pareto	$(k,\sigma,\theta) = (0.59, 0.09, 1.40)$
$Y^{(2)}$	Inverse Gaussian	$(\mu, \lambda) = (9.91, 881.22)$
$Z^{(1)}$	Generalized Pareto	$(k,\sigma,\mu) = (-0.24, 0.43, 0.07)$
$Z^{(2)}$	Generalized Pareto	$(k,\sigma,\theta) = (-0.21, 0.40, 0.07)$

Table 6.2: Univariate fitting of extreme values when $Y^{(1)}$ is the dominant variable. Grid point 4.

6.3.2 Multivariate Analysis

Regular vines (R-vines) are used to characterize the joint dependence of the variables of interest where $Y^{(1)}$ (significant wave height corresponding to swell waves) is the dominant variable. In total, 6 variables are considered (wind and swell wave variables: $X^{(1)}$, $X^{(2)}$, $Y^{(1)}, Y^{(2)}$, and current velocities $Z^{(1)}, Z^{(2)}$). Thus, the R-vine has 6 nodes. Because the SFT's central line is proposed to pass across grid point 4, we focus on the data set corresponding to that area.

Two strategies are explored to find the best vine fit of the multivariate joint distribution, a) a six-node regular vine proposed by the VineCopula package in R [54, 105] (language for statistical computing) and b) the vine with the lowest AIC (Akaike information criterion) value from fitting all possible vines of 6 nodes. The AIC value is a measure of the relative
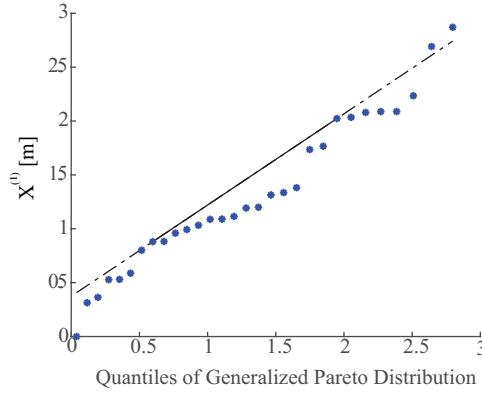
Figure 6.2: QQ plot of univariate fitting for significant wave height of wind waves [m] ($X^{(1)}$)

quality of a statistical model for a given set of data [117]. The regular vine matrices for all regular vines on 6 nodes were found with the algorithms proposed in [57] these matrices are presented in [56]. For simplicity, the proposals are referred to as Proposal A and Proposal B respectively. Figure 6.3 depicts a graphical representation of the first tree of both proposals.

Proposal A is obtained through the VineCopula package in R [105]. The package implements an algorithm where the trees of the vine are selected in such a way that the chosen pairs model the strongest pairwise dependencies [54]. Proposal B is the vine with the lowest AIC value from fitting the data set to all the possible vine structures available when the number of variables of nodes is equal to 6. This results in a total of 23040 vines to be fitted to the data. This is because the number of possible vines for a given number of nodes n is defined by Eq. 2.13 presented in [55]. In this case, proposal B is defined as a T13 R-Vine.
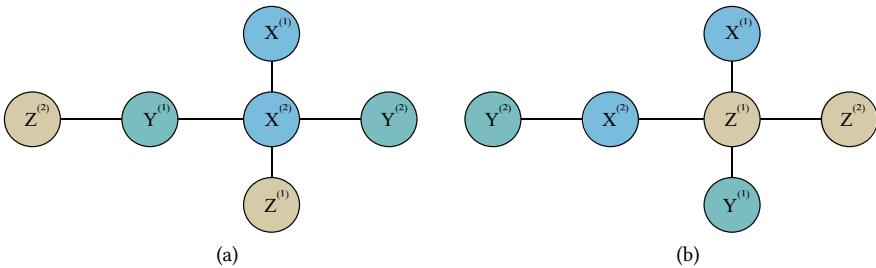
Figure 6.3: Vine proposals: (a) VineCopula package's, (b) Vine with lowest AIC value. Resulting from fitting all possible vines of 6 nodes.

Once Proposal B is defined, it is compared to Proposal A. The AIC value was used for this purpose ($AIC_A = -136.61$, $AIC_B = -140.75$). According to [118, 119], the suitability of a model should be analyzed by rescaling the AIC values to:

Copula	Family	Parameters	Spearman's correlation
$C_{Z^{(2)},Y^{(1)}}$	Joe (180˚)	$\theta = 1.94$	0.51
$C_{Y^{(1)},X^{(2)}}$	Clayton (180˚)	$\theta = 1.40$	0.60
$C_{X^{(2)},Z^{(1)}}$	Gaussian	$\theta = 0.76$	0.76
$C_{X^{(2)},X^{(1)}}$	Frank	$\theta = 21.26$	0.96
$C_{X^{(2)},Y^{(2)}}$	Joe	$\theta = 2.57$	0.66
$C_{Z^{(2)},X^{(2)}|Y^{(1)}}$	Clayton (180˚)	$\theta = 0.20$	0.14
$C_{Y^{(1)},Z^{(1)}|X^{(2)}}$	Clayton (90˚)	$\theta = -1.03$	-0.51
$C_{Z^{(1)},X^{(2)}|X^{(2)}}$	Joe (90˚)	$\theta = -1.39$	-0.28
$C_{X^{(1)},Y^{(2)}|X^{(2)}}$	t	$\rho = 0.03, \nu = 2.00$	0.03
$C_{Z^{(2)},Z^{(1)}|Y^{(1)},X^{(2)}}$	Gaussian	$\theta = -0.26$	-0.26
$C_{Y^{(1)},X^{(2)}|Z^{(1)},X^{(2)}}$	Gaussian	$\theta = -0.01$	-0.01
$C_{Z^{(1)},Y^{(2)}|X^{(1)},X^{(2)}}$	Joe (180˚)	$\theta = 1.22$	0.17
$C_{Z^{(2)},X^{(1)}|Y^{(1)},Z^{(1)},X^{(2)}}$	Clayton	$\theta = 0.16$	0.11
$C_{Y^{(1)},Y^{(2)}|Z^{(1)},X^{(1)},X^{(2)}}$	Gumbel	$\theta = 1.26$	0.32
$C_{Z^{(2)},Y^{(2)}|Y^{(1)},Z^{(1)},X^{(1)},X^{(2)}}$	Joe (180˚)	$\theta = 1.10$	0.08

Table 6.3: Copula families and parameters obtained from the VineCopula R package (Proposal A).

6

$$\Delta_i = AIC_i - AIC_{min} \tag{6.2}$$

where AIC_{min} is the minimum of the different AIC_i values. In this way, the best model has $\Delta = 0$ and the rest of the vine models have positive values. The larger the Δ_i, the less suitable the fitted model i. [119] suggest a simple rule of thumb for assessing the suitability of the fitted models: Models where Δ_i is in the 2–7 range have some support and should rarely be dismissed and implausible models are $\Delta_i > 14$.

Consequently, $\Delta_A = 4.14$ and $\Delta_B = 0$. Thus, both models are suitable for characterizing the data. However, we chose the model with the lowest AIC value. Figure 6.4 presents the empirical cumulative distribution function (ECDF) of the AIC values for the 23040 vine models, with a vertical dashed line indicating the AIC value corresponding to Proposal A. The figure suggests that Proposal A's AIC is relatively low compared to most other vine models, implying it is among the better-fitting models. However, as mentioned previously, proposal A does not have the lowest AIC value. The copula families and respective parameters for proposals A and B are presented in Table 6.3 and Table 6.4 respectively.

A total of 15 unique bivariate copulas were estimated to quantify the selected proposal and are presented in Table 6.4. Each of these copulas was selected by fitting the copula data to several copula families (For details about the copula families, refer to [105]). The AIC value was used as the criteria for copula selection and the parameters of the copulas were obtained by maximum likelihood. These copulas are able to capture the dependence structure of the variables of interest. Fig. 6.5a depicts the observations of all the variables as a scatter matrix plot. All the variables are positively correlated except the pair $\{Z^{(1)}, Z^{(2)}\}$.
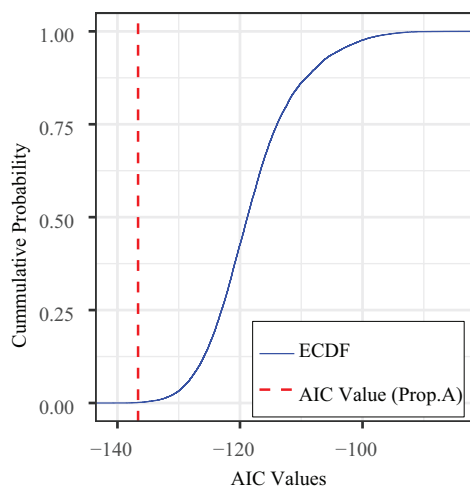
Figure 6.4: Empirical cumulative distribution function of the AIC values from the fitted 23040 vine for proposal A. Vertical Line corresponds to the AIC of proposal A

Copula	Family	Parameters	Spearman's correlation
$C_{Z^{(2)},Z^{(1)}}$	Frank	$\theta = -0.18$	0.03
$C_{Z^{(1)},Y^{(1)}}$	Joe	$\theta = 1.37$	0.27
$C_{Z^{(1)},X^{(2)}}$	Gaussian	$\theta = 0.76$	0.76
$C_{X^{(2)},Y^{(2)}}$	Joe	$\theta = 2.57$	0.66
$C_{Z^{(1)},X^{(1)}}$	Gumbel	$\theta = 1.97$	0.7
$C_{Z^{(2)},Y^{(1)}|Z^{(1)}}$	Clayton	$\theta = 1.22$	0.56
$C_{Y^{(1)},X^{(2)}|Z^{(1)}}$	Frank	$\theta = 7.04$	0.77
$C_{Z^{(1)},Y^{(2)}|X^{(2)}}$	Clayton	$\theta = 0.24$	0.17
$C_{Y^{(1)},X^{(1)}|Z^{(1)}}$	t	$\rho = 0.66, \nu = 30$	0.66
$C_{Z^{(2)},X^{(2)}|Y^{(1)},Z^{(1)}}$	Joe	$\theta = 1.40$	0.29
$C_{Y^{(1)},Y^{(2)}|Z^{(1)},X^{(2)}}$	Frank	$\theta = 2.73$	0.43
$C_{Z^{(2)},X^{(1)}|Y^{(1)},Z^{(1)}}$	Joe	$\theta = 1.31$	0.23
$C_{Z^{(2)},Y^{(2)}|Y^{(1)},Z^{(1)},X^{(2)}}$	Gaussian	$\theta = -0.09$	-0.08
$C_{X^{(2)},X^{(1)}|Z^{(2)},Y^{(1)},Z^{(1)}}$	Frank	$\theta = 11.85$	0.89
$C_{Y^{(2)},X^{(1)}|X^{(2)},Z^{(2)},Y^{(1)},Z^{(1)}}$	t	$\rho = 0.10, \nu = 2.58$	0.10

Table 6.4: Copula families, parameters and Spearman's correlation coefficients for vine proposal B.

Notice that the pair $\{X^{(1)}, X^{(2)}\}$ is highly correlated, thus, their respective observations are distributed closer to the main diagonal.

After fitting the data to the vine-copula model, 300 simulations were produced. Fig. 6.5a and Fig. 6.5b depict the scatter matrix plots for both the observations and the sim-
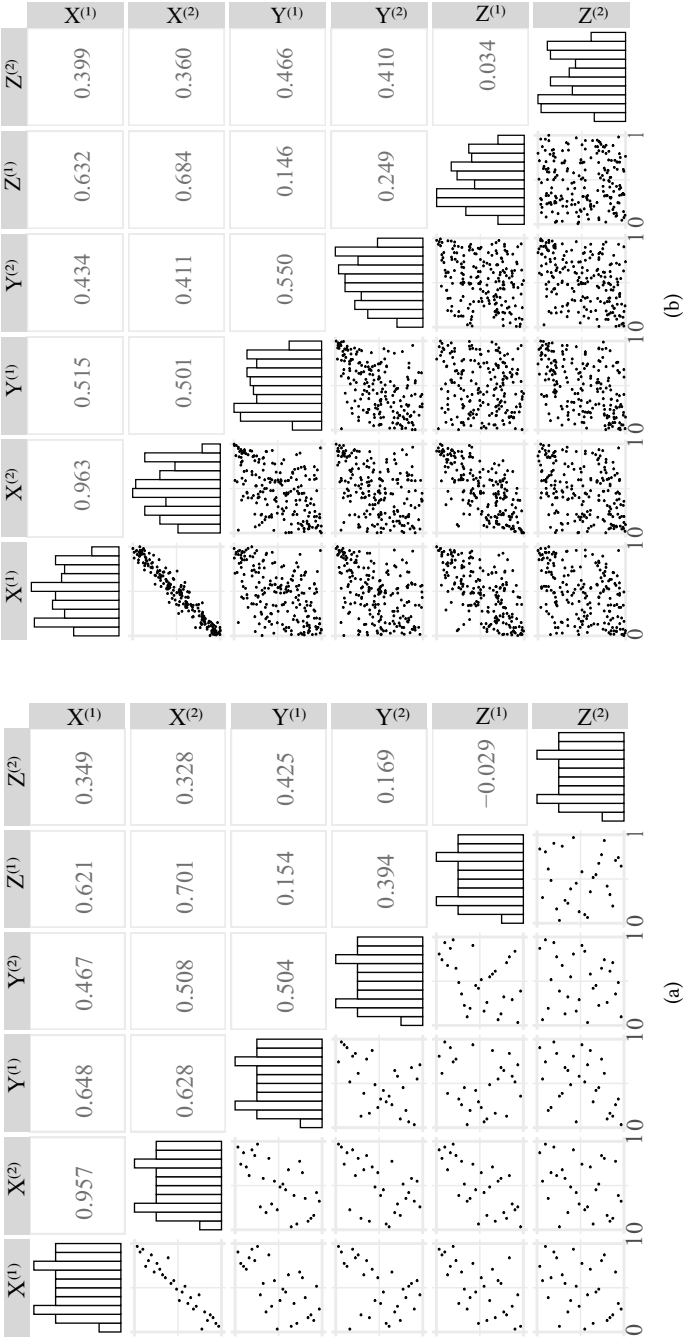
Figure 6.5: Scatter matrix plot of (a) observations and (b) simulations (Proposal B) for metocean variables in [0,1] margins.

ulations of each variable in $[0,1]$ margins. These plots display the pairwise relationships between the variables in the data set and provide a comprehensive view of the correlations and scatter patterns between the variables. Certainly, larger samples can be simulated from the vine model. However, in this study, the number of simulations was restricted to 300 because of computational feasibility (Section 6.4). The scatter plots from the simulations are very similar to the observations presented in Fig. 6.5a. This is confirmed by the correlation values in both figures. However, there are some differences. At the pair $\{X^{(2)}, Y^{(1)}\}$, the correlation from the simulations is slightly lower (0.50) than the observations (0.63). Similar results can be shown for the pairs $\{X^{(2)}, Y^{(2)}\}$ and $\{Z^{(1)}, Y^{(2)}\}$. While for the pair $\{Z^{(1)}, Z^{(2)}\}$, the model estimates a correlation of 0.03 while the observations have a correlation of -0.03.

In summary, the proposed vine copula model provides a good characterization of the joint distribution of the metocean variables. This is confirmed by examining the scatter plots between the data and the simulations and the shared similarities between them. Also, by comparing the Spearman's rho from the simulations it is shown that this dependence measure aligns well with the observed values.

The resulting simulations were transformed from the $[0,1]$ margins to their original space (real units) by applying the inverse of their respective marginal distribution functions (Table 6.2).

6.4 Estimating the hydrodynamic forces acting on an SFT

As shown in the previous section, vine-copula models provide a good representation of the multivariate dependence between metocean variables. Thus, enabling the simulation of longer and more reliable data sets that can support the estimation of extreme loads. This is particularly important when data is scarce as in the case of the Qiongzhou Strait. In Fig. 6.5a it is shown that the number of observations is limited to a total of 30 points (this represents an average of 2 extreme events per year within a period of 19 years). In cases where the reliability of a structure under extreme conditions is investigated, larger amounts of data are preferred. Therefore, the vine-copula model presented in the previous section is used to simulate three hundred values of each variable. This data set is used as a base for a new vine-copula model: Froude-Krylov (FK) vine-copula model (Section 6.4.2) that aims to characterize the combined action of metocean variables acting on an SFT and their resulting hydrodynamic forces.

The hydrodynamic forces acting on the SFT (introduced by the combined action of waves and currents) are estimated using the Froude-Krylov (FK) equation [16] (Section 6.4.1. Eq. 6.3 and 6.4). This equation provides a reasonable approximation of the hydrodynamic forces acting on the SFT (f_y, f_z) in terms of a simple expression and also computes a new estimation of wave heights due to the presence of currents ($X_c^{(1)}$ or $Y_c^{(1)}$). Input metocean variables of this equation are the significant wave height, wave period, and current velocity. Other input variables are related to the SFT configuration (Fig. 6.6), such as the diameter of the SFT (D), submergence depth (h), and the distance from the center of the SFT to the seafloor (z). A more detailed description of this equation can be found in Section 6.4.1.

A total of 9 SFT configurations are evaluated based on different combinations of D, h,
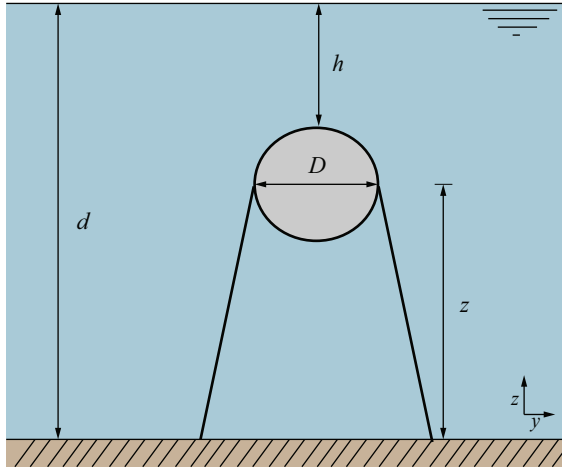
Figure 6.6: Reference scheme

and z. These configurations are depicted in Table 6.5. The SFT studied in this study is aimed to be constructed at the Qiongzhou Strait. The corresponding total water depth (d) at this particular location ranges between 40 and 120m. For the remainder of this study, the total water depth is assumed constant and equal to 120 m. Furthermore, the SFT is simplified as a submerged horizontal cylinder with no tethers or pontoons.

Config.	D [m]	h [m]	z [m]
1	20	20	90
2	20	30	80
3	20	40	70
4	25	20	87.5
5	25	30	77.5
6	25	40	67.5
7	30	20	85
8	30	30	75
9	30	40	65

Table 6.5: SFT Configurations.

In this study, two wave systems and current velocities at different depths are studied, where $Y^{(1)}$ (significant wave height of swell waves) is the dominant variable. To compute the resulting FK forces, the variables of only one wave system (swell) and one current velocity (15m from the water surface) are used as input. In other words, the simulations of $Y^{(1)}, Y^{(2)}$, and $Z^{(2)}$ together with their respective resulting hydrodynamic forces and new estimation of wave height due to the presence of currents (f_y, f_z, and $Y_c^{(2)}$) are the nodes of the FK vine-copula model (Section 6.4.2).

6.4.1 Froude-Krylov (FK) force

The Froude-Krylov (FK) force is the force that acts on an ideal water cylinder that has the same radius as the tunnel and is located at the same depth. It is assumed that the pressure field is not affected by the presence of the tunnel and can be determined from the incident wave potential by itself [120]. The horizontal and vertical components of the Froude-Krylov force per unit length (kN/m) are estimated as follows [121]:

$$f_y = \Phi \pi R^2 a_y \tag{6.3}$$

$$f_z = \Phi \pi R^2 a_z \tag{6.4}$$

Where a_y and a_z are given by:

$$a_y(y, z, t) = g\frac{H}{2}k_c\frac{cosh(k_c z)}{cosh(k_c d)}sin(k_c y - \omega t) \tag{6.5}$$

$$a_z(y, z, t) = -g\frac{H}{2}k_c\frac{sinh(k_c z)}{sinh(k_c d)}cos(k_c y - \omega t) \tag{6.6}$$

Where Φ is the density of ocean water (1030 [kg/m^3]), R is the radius of the SFT in [m], H is the wave height in [m] ($X^{(1)}$ or $Y^{(1)}$), g is the acceleration of gravity equal to 9.81 [m/s^2], k_c is the wave number that depends also on the current velocity in [rad/m], z is the distance from the center of the SFT to the seafloor (Fig. 6.6), and ω is the angular frequency [rad/s]. In this section, H is used as a general term to depict wave height that can be either from wind waves or total swell. As mentioned in the previous section, total swell is selected as the wave system of interest.

It is assumed that waves and currents travel in the same direction. The resulting variables from the FK approach and its nomenclature are depicted in Table 6.6.

Result Variables	Standard Name	This article
FK component (y-direction)	f_y	f_y
FK component (z-direction)	f_z	f_z
New significant wave height (due to the presence of currents)	H_c	$X_c^{(1)}$, $Y_c^{(1)}$
Wave number (due to the presence of currents)	k_c	k_c

Table 6.6: Name and description of resulting variables from the FK approach.

6.4.2 FK vine-copula model

The FK vine model considers as input the simulations of swell waves, current velocity at 15m from the surface from the previous vine model, and their respective FK variables (computed as in Section 6.4.1). The purpose of the FK vine model is to analyze the resulting forces from swell waves and currents for the 9 SFT configurations presented in Table. 6.5. Thus, there are 9 different variations of the FK vine model (where the metocean variables remain the same but the magnitude of the forces change given each SFT configuration). The univariate fit for the FK variables was also performed for the 9 configurations. The fitted probability distribution for f_y and f_z is a t-location scale distribution (for all 9 SFT configurations). Meanwhile, $Y_c^{(2)}$, was fitted to a generalized extreme value distribution (G.E.V) with parameters $\mu, \sigma, k = 0.24, 0.09, 1.40$ respectively. The parameters for f_y and f_z are presented in Table 6.7.

Config.	f_y t-location scale $[\mu,\sigma,\nu]$	f_z t-location scale $[\mu,\sigma,\nu]$
1	$[26.79,1.83,1.45]$	$[26.74,1.77,1.44]$
2	$[18.08,2.53,2.16]$	$[18.02,2.46,2.16]$
3	$[12.17,2.57,2.59]$	$[12.07,2.47,2.63]$
4	$[37.95,3.24,1.64]$	$[37.86,3.15,1.62]$
5	$[25.60,4.04,2.29]$	$[25.48,3.91,2.30]$
6	$[17.23,3.94,2.67]$	$[17.06,3.77,2.73]$
7	$[49.55, 5.15,1.83]$	$[49.41,4.99,1.82]$
8	$[33.39,5.87,2.40]$	$[33.21,5.67,2.42]$
9	$[22.48,5.54,2.74]$	$[22.22,5.28,2.81]$

Table 6.7: Parameters of the GEV distributions for f_y and f_z.

In Table 6.7, the parameters for f_y and f_z are very similar. Thus, from this point forward, the analysis is focused only on f_y. The vine proposal for the FK model corresponds to a T10-type regular vine (Fig. 6.7) and is the same for the 9 SFT configurations. The vine model proposal was obtained by fitting the data to all possible vines when n=6 (23040 vines), similar as in Section 6.3.2. The process of fitting 23040 vines for different 9 scenarios is computationally expensive (in the order of magnitude of several days) in a regular laptop computer (Processor: Intel(R) Core(TM) i7-8650U CPU @ 1.90GHz 2.11 GHz and RAM of 8GB). Thus, a total of 207360 vines were fitted.

From the selected vine model (Fig. 6.7), a total of 500 thousand simulations were produced for each variable and for each of the 9 SFT configurations. Fig. 6.8a and Fig. 6.8b show the matrix correlation plot of the input variables and the resulting simulations from the FK vine model. The plots correspond to the SFT configuration 2 ($D = 20m$ $h = 30m$).

For the pairs $\{f_y, Y^{(1)}\}$, $\{f_z, Y^{(1)}\}$, and $\{Y^{(1)}, Y_c^{(1)}\}$, the correlation values between the data and the simulations are very similar. However, the shape of the scatter plots differs slightly. For the pairs $\{Z^{(2)}, Y_c^{(1)}\}$, $\{f_y, Y_c^{(1)}\}$, and $\{f_z, Y_c^{(1)}\}$, the correlation values from the simulations are slightly higher than the observations, but the model is able to capture the dependence between pairs that have low correlation values. Notice that in Fig. 6.8a, their
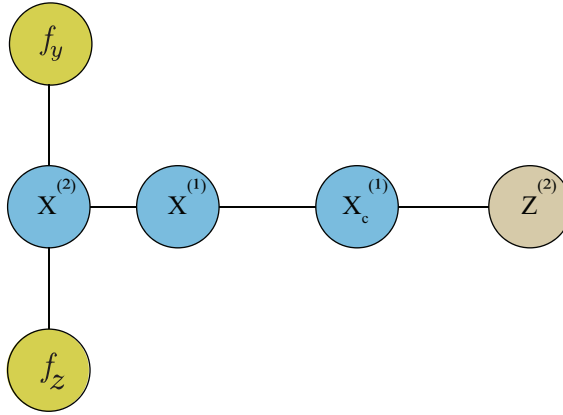
Figure 6.7: Vine for swell wave and currents at 15m from the surface and their resulting hydrodynamic forces.

respective scatter plots have defined sharp edges (suggesting physical limits to these variables), while in Fig. 6.8b the scatter plots those edges are not correctly modeled. Similar results were obtained for the remaining SFT configurations.

Table 6.8 (Columns 4 and 5), shows the correlation values for $\{f_y, Y_c^{(1)}\}$. Overall, the FK vine model is able to capture quite well the dependence between the variables. Additionally, the correlation values appear to decrease for increasing diameter and submergence depths (D and h). For example, when D=20m (Config. 1-3) the correlation value starts at 0.84, and for each increasing submergence depth h, the correlation value decrease to 0.65. The same occurs throughout the remaining SFT configurations. This trend is also present in the correlation values of the simulations. This may be explained because water depth acts as a damping factor for the forces acting on the SFT. Wave energy decreases deeper in the water, therefore the resulting forces for deeper water have smaller correlations with variables at the water's surface.

Conditional distribution of FK variables

The new set of simulations (500 thousand values per variable) from the FK vine (Fig. 6.7) is used to analyze the conditional distributions of the FK variables for the different configurations of the SFT. The focus is on f_y (f_z is not further investigated in this section given its high correlation value with f_y). The conditional analysis is carried out to show how vine copula models can be used to investigate f_y given specific values of wave height, wave period, or current velocities ($Y^{(1)}$, $Y^{(2)}$, and $Z^{(2)}$). In other words, the conditional marginal distribution of f_y is investigated. This distribution focuses on the f_y values under specific conditions of wave height, period, and current velocity.

The first step to obtain the conditionalized distributions of f_y is to define the conditional values of $Y^{(1)}$, $Y^{(2)}$, and $Z^{(2)}$. In this study, the values correspond to their 100-year return period. However, as mentioned in section 6.2.1, in a POT approach, the return period or probability of exceedance is calculated by taking into account the rate of occurrence of the clusters (Eq. 6.1). The yearly cluster rate (λ) is defined as the average number of storms per year and is equal to 1.59. Thus, for a return period of 100 years, the
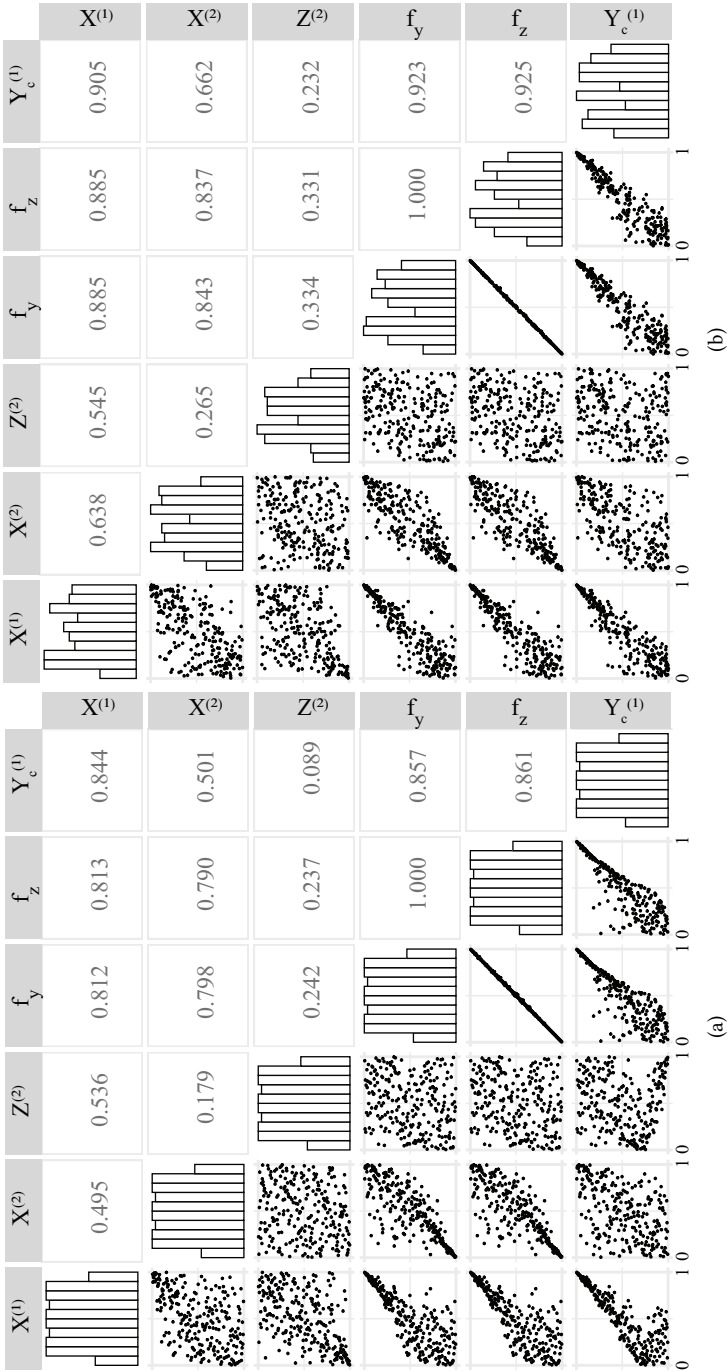
Figure 6.8: Scatter matrix plot of (a) observations and (b) simulations (200 out of 500.000 samples) for SFT configuration #2 of the FK vine model in [0,1] margins.

respective probability of exceedance is 0.006 instead of 0.01 as it would be in an annual maxima analysis (AMA). See section 6.2.1. The conditional values of $Y^{(1)}$, $Y^{(2)}$, and $Z^{(2)}$ that correspond to a 100-year return period are 4.5 [m], 12.8 [s], and 1.3 [m/s] respectively.

The conditional distributions are defined by the values of f_y that occur at the same time when the 100-year values of $Y^{(1)}$, $Y^{(2)}$, and $Z^{(2)}$ are exceeded within the simulations. The number of values that complied with such conditions ranges between 30 and 60 samples for the nine SFT configurations. These conditionalized data are fitted to parametric probability distribution functions and estimations of the variables of interest are drawn for a 100-year return period. This process was performed for all 9 SFT configurations. Table 6.8 shows the resulting design values of the non-conditional distributions (NCD) versus the conditional distributions (CD) for the 9 SFT configurations.

| Config. | D [m] | h[m] | $\{f_y, Y_c^{(1)}\}$ | | f_y [kN/m] | |
			Obs.	Sim.	NCD	CD
1	20	20	0.84	0.82	57	964
2	20	30	0.72	0.71	38	107
3	20	40	0.65	0.65	28	157
4	25	20	0.80	0.79	79	253
5	25	30	0.70	0.69	55	179
6	25	40	0.64	0.64	41	198
7	30	20	0.77	0.76	102	577
8	30	30	0.68	0.67	73	339
9	30	40	0.63	0.63	55	367

Table 6.8: Correlation values of the pair $\{f_y, Y_c^{(1)}\}$ for 9 SFT configurations.

A non-conditional distribution (NCD) also known simply as a marginal distribution describes the probabilities of the variable of interest (f_y) without taking into account any specific constraints or conditions regarding other variables. However, the conditional distribution (CD) provides the probabilities of f_y under specific values of wave height, period, and current velocity. In general, note that in Table 6.8 (Columns 6-7), for configurations with the same diameter, shallower submergence depths are associated with larger forces. For example, out of Config. 1-3 the largest force is found in Config. 1. The same can be noted for Config. 4 and 7. This occurs for both the non-conditional (NCD) and conditional distributions (CD). Moreover, f_y decreases for an increasing submergence depth in cases that share the same diameter. The forces decrease around 50% from a depth of 20m to 40m. For configurations that share the same submergence depth but different diameters (For example Config. 4 and 7), note that for an increasing diameter, the forces are larger (at the non-conditional values in column 6). The largest computed force for both the NCD is found for Config. 7 and for the CD, the largest force is found in Config. 1. That has the biggest diameter (30m) and shallower submergence depth (20m) respectively with 102 and 964 kN/m for the NCD and CD. The smallest forces for both CD and NCD are found in configurations 3 and 2 respectively.

Overall, for all configurations, larger values are obtained for the CD (Column 7 Table 6.8) due to the conditionalization of the forces on high values of wave height, wave period,

and currents. For example, the effect of conditionalizing f_y can be appreciated in Fig. 6.9 where the mean of the distribution changes from 50 to 119 kN/m.

The values from the CD provide insight into the importance of taking into account the dependence between variables when investigating the forces acting on the SFT. Additionally, the case study presented in this study highlights the effect of different combinations of diameters and submergence depths that can be considered for the design of an SFT.
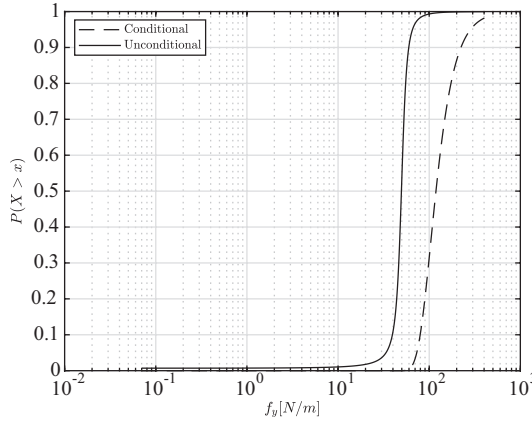
Figure 6.9: Cumulative probability distribution of f_y (Unconditional and conditionalized). Configuration 7.

6.5 Discussion

In engineering, its common practice to define metocean variables as independent from each other. These values usually represent extreme events. In this study, a vine-copula model is presented as a novel methodology to characterize the joint distribution of metocean variables by taking into account the dependence structure between them.

When using vine-copula models, a challenge arises as to choosing the best vine to characterize the variables of interest. As shown in section 6.3.2, software such as the VineCopula R package [105] can help to find the best vine model for a given data set. Such tools can help reduce computational efforts but do not always provide the vine with the lowest AIC value. Another approach is to fit every possible vine of n nodes and use the one with the lowest AIC value.

An additional application is presented as a case study to investigate the forces acting on the SFT. These studies are important for engineers focused on designing the SFT. In this study, the importance of taking into account the dependence between the metocean variables and their respective hydrodynamic forces for different SFT configurations is illustrated. In Table 6.8 we present the non-conditional (NCD) and conditional distribution (CD) of f_y as a direct consequence of conditionalizing the distributions to larger values of $Y^{(1)}$, $Y^{(2)}$, and $Z^{(2)}$. There are significant differences between both distributions. It is also shown which SFT configurations result in the largest forces acting on the structure (Config. 7 and 1 respectively). This information is useful for engineers and decision-makers to make informed choices for the design of the SFT.

In general, the structure is subjected to horizontal and vertical forces. In this study, only the horizontal component of the hydrodynamic force is taken into account. The vertical force depends on the external diameter of the structure and the weight of ballast. For the horizontal component of the hydrodynamic force, both the diameter and the submergence depth are factors that influence its computation. In Table 6.9 we present an estimation of the uplift force (F_u), the weight of the concrete (F_c), the weight of ballast (F_b), and the resultant vertical force (F_R) using the results from the conditional distributions. This was done assuming an SFT's wall thickness of 1.3m for all configurations. The amount of ballast used in the calculations has been determined in such a way that the BWR is always 1.3 to ensure the stability of the structure.

Config.	D [m]	h [m]	f_y (CD) [kN/m]	A_{SFT} [m^2]	A_c [m^2]	F_u [kN/m]	F_c [kN/m]	F_b [kN/m]	BWR	F_R [kN/m]	F_R/f_y
1	20	20	964	314	76	3174	1873	600	1.3	900	0.9
2	20	30	107	314	76	3174	1873	600	1.3	900	8.4
3	20	40	157	314	76	3174	1873	600	1.3	900	5.7
4	25	20	253	491	97	4960	2374	1500	1.3	1391	5.5
5	25	30	179	491	97	4960	2374	1500	1.3	1391	7.8
6	25	40	198	491	97	4960	2374	1500	1.3	1391	7.0
7	30	20	577	707	117	7142	2875	2700	1.3	2009	3.5
8	30	30	339	707	117	7142	2875	2700	1.3	2009	5.9
9	30	40	367	707	117	7142	2875	2700	1.3	2009	5.5

Table 6.9: Buoyancy weight-ratio (BWR) and vertical forces for different SFT configurations. A_{SFT}: Cross-section area of the SFT. A_c: Area of concrete. F_u: Uplift force. F_c: Weight of concrete. F_b: Weight of ballast. BWR: Buoyancy-weight ratio. F_R: Resultant vertical force.

Notice that for an SFT with an external diameter of 20m (Config. 1-3), the resultant vertical force is approximately 900 KN/m (First row of Table 6.9). This horizontal force (f_y 4th column in Table 6.9) is slightly larger than the corresponding vertical force F_R. For the case of an SFT with tethers, this can influence the way the tethers are arranged to avoid large displacements. However, for diameters such as 25m or 30m, the resultant vertical force is 3 to 8 times larger than the horizontal force (Column 12). In such cases, the horizontal force is less likely to cause large displacements in the structure because the resultant vertical force can compensate for it.

The choice of configuration for an SFT depends on many factors. In Table 6.9, it is shown that varying diameters and submergence depths can lead to different estimations of horizontal and vertical forces. At the same time, the thickness of the walls and the amount of ballast are also aspects to take into account. Larger diameters will need more ballast to keep the structure stable.

An optimum design must ensure an acceptable level of safety at the lowest cost possible. In the case of an SFT, a structure that has never been built before, there is a lack of experience in its design and construction. An SFT combines elements of other civil structures such as bridges, tunnels, offshore platforms, and even dike rings [122]. Thus, from a safety perspective, the SFT also combines different aspects like structural safety, risk of flooding, and length effect among others. An SFT is, therefore, a special structure that does not meet the standards set by any other structure and requires its own reliability validation. [122] proposed that this validation can be achieved by combining different approaches described in ISO2394 [123] and JCSS 1999 [124]. The structural design and

design decisions for an SFT could be evaluated by the risk-informed method (also known as the level IV method). In this method, decisions are made based on minimizing the risks and can provide an optimum design by considering the expected consequences in case of failure. However, estimating the consequences and respective safety measures is out of the scope of this study. Nevertheless, it is recommended that the SFT configurations presented previously should be evaluated using the level IV method.

6.6 Conclusions

The methodology presented in this study uses vine-copula models to approximate the stochastic processes that characterize the metocean variables at the Qiongzhou Strait and their resulting hydrodynamic forces acting on different configurations of an SFT.

Specifically, this tool was used to characterize extreme events. Generally, extreme events are rare, thus, having large data sets of extreme events is also rare. Vine-copula models allow insight into the dependence structure of several variables. Thus, this study aims to represent metocean variables as close to reality as possible by considering their dependence structure. A total of 300 samples of wave height and wave periods (for wind waves and swell waves), and current velocities at 1m and 15m depth ($X^{(1)}$, $X^{(2)}$, $Y^{(1)}$, $Y^{(2)}$, $Z^{(1)}$, $Z^{(2)}$) were simulated. These simulations were used as input for a second vine-copula model to study the resulting forces produced by the simultaneous action of the metocean variables for 9 SFT configurations. Then the simulated values for the force f_y were conditionalized on the 100-year values of significant wave height, wave period, and current velocity. The results show that larger forces are obtained when conditional distributions are used instead of considering the non-conditional distribution of the variables. This highlights the importance of dependence between variables when designing an SFT. Finally, we presented an estimation of the expected resultant vertical force and BWR for the 9 SFT configurations given a wall thickness and different amounts of ballast. A brief discussion was presented to illustrate the importance of the ratio between the vertical force F_R and the horizontal force f_y and their impact when choosing a configuration for future design.

This methodology can be extended to different sea states or to take into account the direction of incoming waves and currents. Other variables may be used in addition to those listed in this study. For example, internal waves, tsunami waves, earthquakes, or the traffic passing through the SFT. For the case of a pontoon-type SFT, wind data could be included in the analysis. However, increasing the number of variables n in vine-copula models involves some challenges (as described in Section 2.4). Moreover, the conditional study of the forces acting on the SFT can be extended to investigate other scenarios or other values of wave height, wave period, and currents. Nevertheless, the methodology presented in this study is not restricted to a particular design of an SFT, its flexibility allows to simulate different variables and use it to test any type of civil structure.

The findings of this research demonstrate that a multivariate approach can aid in the design and evaluation of civil structures by considering more realistic extreme events.

7

Bayesian Networks for waves, currents, and hydrodynamic forces

The Qiongzhou Strait in China is a very dynamic region in terms of waves and currents. It is thus of interest to study the forces acting on a hypothetical SFT due to the combined action of these variables. It is crucial to consider the dependence between waves and currents, especially during extreme events. In this chapter, we present a methodology that allows representing the multivariate joint distribution between metocean variables, these are a) wave variables such as significant wave height and period for two wave systems (wind waves and swell waves), b) current velocities at two different depths below the surface (1m and 15m), and c) the forces acting on the SFT due to the combined action of a and b.

In this chapter, we present a BN model that evaluates twelve different configurations of the SFT, with varying submergence depths and diameter sizes. The proposed methodology can be used to provide a realistic estimation of the forces on the SFT by considering the dependence between the variables of interest. Moreover, this methodology can be extended to test different configurations of the SFT and other hydraulic or maritime structures subjected to simultaneous loading. The inference process is less computationally expensive for Bayesian Networks. One of the reasons is the assumption that the joint distribution follows a Gaussian distribution. This allows for faster computations even for high-dimensional problems. However, these models might not be able to capture non-Gaussian or non-linear behaviors in the data. The choice between Bayesian Networks and other probabilistic models such as vine-copulas relies on the nature of the problem, the type of data, and the complexity of the dependencies.

This chapter is organized as follows. First, a brief introduction to this study is presented in Section 7.1. Followed by a description of the modeling approach (Section 7.2). Next, the results for the twelve SFT configurations are discussed in Section 7.3. Finally, Section 7.4

concludes the chapter by presenting the conclusions and identifying the areas for future work.

7.1 Introduction

There are several challenges remaining regarding the design and construction of an SFT due to a lack of data and experience. One topic of interest is the effects of the combined action of metocean variables. Usually, in the design of offshore structures, the simultaneous action of design values is investigated under the assumption of independence [125]. For example, the Norwegian practice assumes that the simultaneous action of the 100-year sea state, the 100-year mean wind speed, and the 10-year current velocity represents the environmental conditions from where the extreme loads and effects can be calculated [125]. In such cases, a probabilistic model that takes into account the dependence between the variables of interest could represent the surrounding environment more realistically.

In this chapter, we use a data set generated by the Vine-Copula model developed by [4] (Chapter 6) as input for the BN model. This data set describes extreme events of significant wave height (defined as the average wave height of the highest one-third of the waves) for wind and swells waves (as the dominant variable) and their corresponding accompanying values of wave period and current velocity (as concomitant variables). The choice of the data set was made due to its larger size compared to the original extreme value data set.

Next, the hydrodynamic forces acting on the SFT (introduced by the combined action of waves and currents) are computed through the Froude-Krylov (FK) equation [16] (Section 6.4.1). The simplicity of this equation provides a reasonable approximation of the hydrodynamic forces acting on the SFT in terms of a simple expression. Finally, both the metocean data set and the resulting forces are used as input to a probabilistic model (Bayesian Networks) that allows the evaluation of the conditional probability of the resulting forces subject to the simultaneous action of the variables mentioned previously. Different SFT configurations (combinations of diameters and submerged depths) were subjected to this approach. Due to the computational efficiency offered by Bayesian Networks, it is possible to investigate more SFT configurations. Thus, 12 SFT configurations are introduced in this chapter while Chapter 6 (which focuses on the application of vine-copulas) investigates 9 configurations.

Bayesian Networks have been widely studied in the literature to analyze the dependence between variables within a system and have been applied to several fields. For example, [126] uses Bayesian Networks to assess the impact of climate change on water quality, while [127] presents a risk analysis for reservoir regulation using BNs. Moreover, BNs have been used to simulate environmental data sets. [69] models monthly regional rainfall using local meteorological drivers in India. Another example is the work developed by [71], where peak storm surges and precipitation are simulated to determine the hydraulic boundary conditions for a low-lying coastal watershed. In [70] a BN model was used to estimate extreme river discharges in Europe. As mentioned in previous chapters, submerged floating tunnels are relatively new and specialized structures. The application of Bayesian Networks to investigate loading scenarios on this structure has not been explored yet due to a lack of specific domain expertise, data availability, and the complexity of the structure.

The aim of this study is to shed light on a probabilistic methodology using continuous

Bayesian networks to study the conditional distribution of the hydrodynamic forces acting on an SFT under the simultaneous action of metocean variables (Section 3.2) for twelve SFT configurations. This methodology can be extended to other and more complex models for describing the relation between metocean variables and testing different shapes, sizes, and elements of the SFT.

7.2 Modeling approach

7.2.1 Overview of the model

The first part of the methodology consists of computing the components of the Froude-Krylov forces acting on the SFT where the 12 SFT configurations (Table 7.1) and the metocean data are used as input. Next, a BN model is constructed to study the resulting conditionalized distribution of the forces based on the simultaneous action of the metocean variables on the SFT (Fig. 7.1). In Bayesian Networks, a conditionalized distribution is the probability distribution of a variable given the value of its parent variables within the network (Section 2.5). This distribution represents the conditional dependence relationships between the variables in the BN.

Config.	D [m]	h [m]	z [m]
1	10	30	85
2	10	40	75
3	10	50	65
4	20	30	80
5	20	40	70
6	20	50	60
7	25	30	77.5
8	25	40	67.5
9	25	50	57.5
10	30	30	75
11	30	40	65
12	30	50	55

Table 7.1: Case scenarios.

The analysis is divided into two main loading scenarios, i) wind waves and currents, and ii) swell waves and currents. In the previous chapter, the dominant variable is the significant wave height of swell waves. For each scenario in this chapter, the respective significant wave height is used as the dominant variable, and the 12 SFT configurations are evaluated. This approach ensures a comprehensive assessment of the loading scenarios under different wave conditions. Each scenario is represented by its own Bayesian Network (BN), specifically BN1 for wind waves and currents, and BN2 for swell waves and currents (Section 7.2.2).

The general SFT configuration scheme is the same as in Chapter 6 (Fig. 6.6), where D is the SFT diameter, h is the submergence depth, and z is the distance from the center of the SFT to the seafloor. The total water depth at the strait (d) is constant and equal to 120

m. For this study, the SFT is simplified as a submerged horizontal cylinder with no tethers or pontoons.

Vine Copula Model
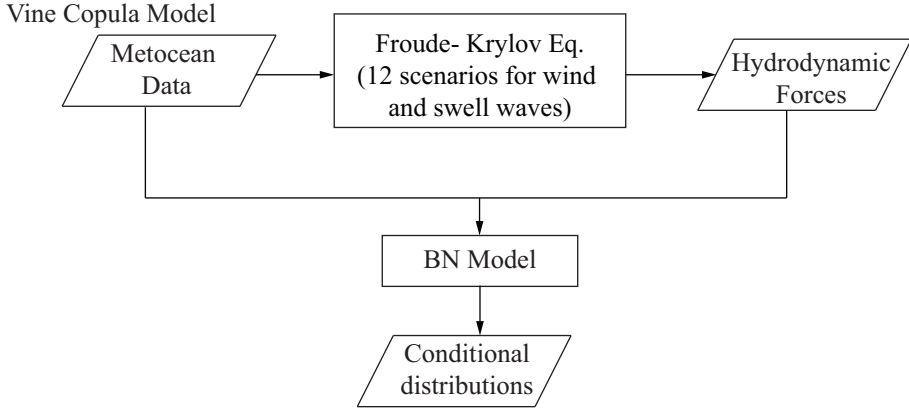
Figure 7.1: Modeling approach

7.2.2 Building the BNs

Two BNs are presented, one for wind waves and currents (BN1) and the other for swell waves and currents (BN2). Regardless of the type of waves, the order of the nodes for both BNs is the same (Fig. 7.2).

To define the arrangement of the nodes, the physical relationship of the nodes needs to be considered. In general, the construction of the BN structure was done by using general knowledge of the variables and their relation with each other. Some relations are expected, for example, significant wave height and wave period, as well as current velocity and wave height. This is proved by their somewhat high correlation values (0.67 and 0.41 respectively). From the FK approach, a new estimation of wave height is derived ($X_c^{(1)}$) (A wave height that results from its interaction with currents). Thus, it makes sense that their parent nodes are the initial significant wave height and current velocity. Finally, the force is computed from the new estimations of wave number and wave height, therefore these variables are defined as parents of the force's nodes.

In Fig. 7.2, the nodes are depicted as histograms with numbers representing the variables' mean and standard deviation. The values on the arcs are the conditional rank correlation coefficients. Each BN consists of 2 main categories, i) input values: wave height and period, and current velocities ($X^{(1)}, X^{(2)}, Y^{(1)}, Y^{(2)}, Z^{(1)}, Z^{(2)}$), and the resulting variables from the FK approach: the force components, the new estimation of the wave height and wave number (f_y, f_z, H_c, k_c).

The BN setup presented in Fig. 7.2 was derived by testing several configurations. The position of the nodes shows their order relative to the force components (f_y and f_z). To estimate the force components given certain conditions (i.e. a specific wave height and period), the BN is updated. This means that the value of the node (or nodes) is defined based on the observations of that particular node.
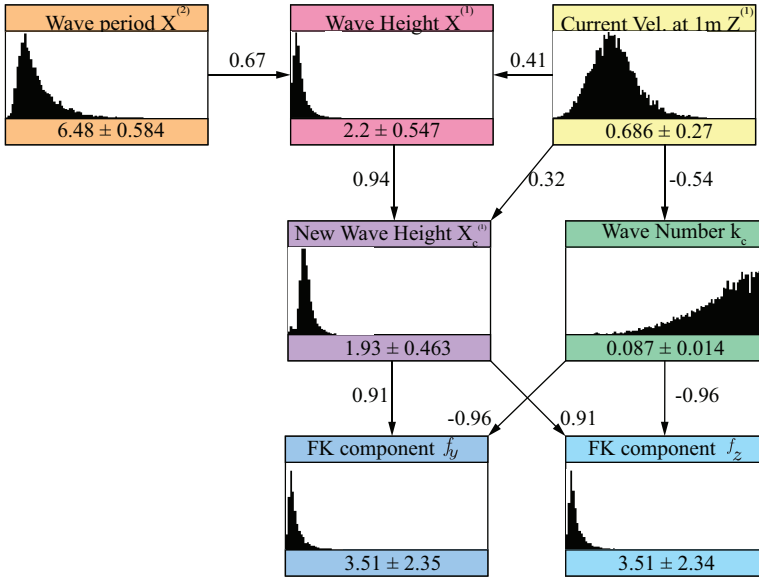
Figure 7.2: Uninet visualization of the Bayesian network (BN1) for metocean variables and Froude-Krylov forces at the Qiongzhou Strait

The BN model was implemented using the MATLAB toolbox for Non-Parametric Bayesian Networks: BANSHEE–A [128] and the Uninet software was used to visualize the model (for more details see [129]).

In this study, it is of interest to conditionalize the BN on values that are out of the range determined by the data. Thus, instead of using the empirical distributions of each node, the data were fitted to univariate theoretical distributions to allow extrapolation to larger values.

Finally, a total of 10.000 samples were generated each time the BN was conditionalized. This was done to estimate the force components for a given environmental condition (different values of wave height, wave period, or current velocities).

7.3 Results

7.3.1 Univariate Fitting

The metocean variables (wave height, wave period, and current velocities) and the 12 SFT configurations were used as input to compute the FK forces acting on the SFT. As a result, we obtain 12 different estimations of the FK force components. Then, the variables were fitted to theoretical univariate distributions.

In the case of the metocean variables, all of them are best described by a Generalized extreme value distribution. The univariate fit for the FK variables (f_y, f_z, H_c, k_c) for both wind waves and swell waves was performed for each of the 12 configurations. The fit for each of the FK variables in each configuration is described by the same distribution. The corresponding fits are shown in Table 7.2.

Variable	Wind Waves	Swell Waves
f_y	Loglogistic	Weibull
f_z	Loglogistic	Weibull
H_c	Loglogistic	Gamma
k_c	G.E.V	Inv. Gaussian

Table 7.2: Univariate fitting for the FK variables

7.3.2 Validation of the Bayesian Network Model

To validate the BNs, the dependence calibration (d-cal) score was computed. This score measures the distance between the empirical rank correlation matrix (ERC), the BN rank correlation matrix (BNRC), and the empirical normal rank correlation matrix (NCR) [128]. If the matrices are equal, the score is equal to 1. If one matrix has a pair of perfectly correlated variables and the other one does not, the score is 0. The score tends to zero as element-wise the bivariate correlations are equal in magnitude but different in sign [130].

Through this diagnostic test, two properties are checked, i) that the joint Gaussian copula is adequate to represent the data, and ii) that the proposed BN is an appropriate model for the saturated graph (i.e. when all the nodes are connected to each other).

The resulting average d-cal score for all twelve scenarios of the BN1 is equal to 0.23, while the d-cal score between BNRC and NRC is equal to 0.003. Similar results were obtained for BN2. Thus, it is found that for both BNs the Gaussian copula does not represent adequately the data, nor this copula is valid for the particular configuration of the BNs presented in this study. This is because the original data comes from a vine-copula model in which a variety of copulas (different from a Gaussian) were used to generate the data set.

However, different d-cal scores may arise if the original observations are used instead but such analysis is out of the scope of this study. The BNs presented herein were still used to analyze the conditional distributions of forces acting on the SFT. This is done in order to show how BNs can be used to study different variables when the dependence between them is taken into account or what can be done if the empirical data were used instead.

Conditional distribution of force components   To simulate the conditional distribution (CD) of the hydrodynamic forces, the BN is updated. This means that the resulting conditionalized distribution is the probability distribution of the force component given specific values of its parent variables (wave height, wave period, and current velocity). This was done for all twelve case scenarios of both BNs in order to compute the design values of the force from the conditional distributions. A conditional distribution represents the conditional dependence relationships between variables in the network.

In this study, we present an example where we conditionalize (or update) the BNs on large values of waves and currents ($X^{(1)}$ = 15 m, $Y^{(1)}$ = 8 m, and $Z^{(1)}$ = 1 m/s). The design values correspond to a probability of 1/100. Table 7.3 presents the design values of f_y obtained from the conditional distribution (CD) and the marginal distribution (MD). The marginal distributions represent the probability of a single variable within the network without considering the values of any other variables.

Config.	BN1 (Wind waves)		BN2 (Swell waves)	
	CD	MD	CD	MD
1	106	12	21	7
2	123	8	20	5
3	59	5	7	4
4	459	38	82	24
5	537	24	81	18
6	346	15	30	14
7	779	53	127	35
8	844	33	125	26
9	656	21	54	20
10	1111	68	182	47
11	543	42	60	36
12	1176	26	97	27

Table 7.3: Design values of f_y [kN/m] corresponding to a probability of exceedance of 0.01 for both BNs.

Table 7.3 shows that the design values obtained from the conditional distributions are significantly larger than the ones from the marginal distribution of f_y. In general, larger diameters and shallower submergence depths (h) lead to stronger forces. Thus, the largest force for BN2 is found in case scenario 10 with f_y = 182 kN/m. However, in BN1 the largest force correspond to case scenario 12 (D = 30 m and h = 50 m) with a f_y = 1167 kN/m. Similar results were obtained for f_z.

Overall, large design values are obtained from the CD as a result of updating the BN. By conditionalizing the BN1 on high values of wave height and currents, the distribution of f_y shifted its mean from 14.5 to 265 kN/m (configuration 10). Fig. 7.3 depicts the effect of conditionalizing the BN and reflects the updated probabilities of f_y when the values of the parent nodes are known. This allows us to investigate the variable's (f_y) behavior given different values of wave height, wave period, and current velocities.

The resulting design values provide insight into the importance of considering the dependence between the variables rather than studying them independently. Moreover, the methodology also highlights the role of each variable when designing an SFT, for example, the design values from BN1 are larger than those from BN2. Thus, in this particular case, wind waves generate larger forces than swell waves.

7
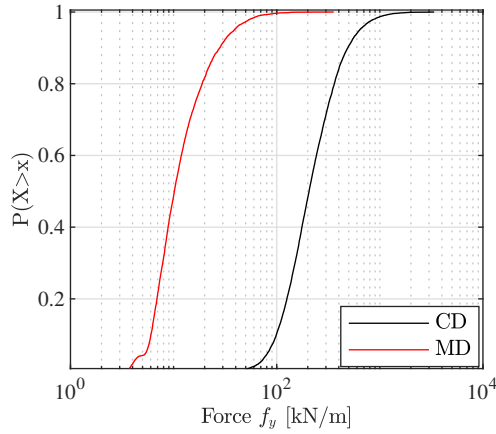
Figure 7.3: Cumulative probability distribution of force: unconditional and conditionalized on 1 node (wave height) case study 10. BN1

7.4 Conclusions

In this study, we present a methodology to study the conditional distribution of the force components acting on an SFT as a result of the simultaneous action of waves and currents. The method focuses on taking into account the complex dependence structure between metocean variables and the resulting forces.

Two Bayesian Networks (BN1 and BN2 for wind and swell waves respectively) were used to characterize the joint dependence of the variables for twelve different configurations of the SFT. The BNs were conditionalized on different values of significant wave height and period for both wind waves and swell waves. The focus is on large values of wave heights and fast current velocities to compute design values for the force components f_y and f_z. The results show that stronger forces are obtained when conditional distributions are used instead of considering the variables as independent. This highlights the importance of dependence between variables when designing an SFT.

The methodology presented in this study can be extended for more complex models (advanced physical models for structural response) and to analyze the SFT (or any of its elements) under different environmental variables. Therefore, this methodology can be used as a reference for other SFT configurations.

8

Discrete Bayesian Networks for Reliability of an SFT

There is a lack of knowledge and experience about the hazards that are most pertinent to a submerged floating tunnel and how they can contribute to the failure of this structure. This chapter aims to provide a methodology to identify and quantify scenarios that can lead to the failure of the SFT by using a discrete Bayesian network (BN) model. The method consists of 1. Identifying the hazards that are relevant for the SFT, 2. Constructing the BN, 3. Quantifying the marginal probabilities of the root nodes, the conditional probability tables (CPTs), and the BN in general, 4. Estimating the conditional probability of failure of the SFT given different combinations of hazard events called scenarios. For the case presented herein, fire and terrorism were found to have the most impact on SFT's failure. Environmental loads with a 500-year return period had less of an impact, raising the risk of failure by 40%.

This chapter is organized as follows: Section 8.1 provides an overview of the discrete BN used in this research. This is followed by a description of the methodology and construction of the BN (section 8.2). Section 8.3 presents the analysis of the results. Finally, the conclusions and areas of future work are addressed in Section 8.4.

8.1 Introduction

Forecasting the failure of an SFT or its elements is critical to developing more complex reliability studies for this type of structure. Analyzing the failure of an SFT over its lifetime can be difficult and requires a multidisciplinary approach. This study aims to provide engineers with a methodology to quantify the probability of failure of the SFT based on predetermined scenarios to assist decisions regarding its design. This makes it possible to support a safe and stable design. Moreover, investigating different scenarios (cases that consider the occurrence or non-occurrence of specific events that could lead to failure) can aid in identifying the primary contributing factors to the failure of the SFT or its elements.

A methodology for assessing the reliability of the SFT using a discrete Bayesian Network (BN) is developed. Bayesian Networks are probabilistic graphical models that consist of random variables, either continuous or discrete, represented by nodes and conditional probabilities between said variables represented as arcs [84]. Bayesian networks may substitute fault trees or event trees in risk and reliability analysis [74]. Fault Tree Analysis (FTA) was first introduced by [66] to facilitate analysis of the launch control system of the intercontinental Minuteman missile at Bell Telephone Laboratories. Nowadays, this methodology is widely employed in a variety of fields including nuclear engineering, aerospace and aviation, telecommunications, chemical and industrial processes, and civil engineering (See for example, [131–136]). However, FTA can have limitations when modeling complex systems [67]. In these circumstances, Bayesian Networks are a suitable option. The edges in a BN represent causal dependencies that make it possible to assess the impact of interventions or changes in variables. The dependencies between the variables are clearly represented which enhances transparency and readability. In this way, it is easier for stakeholders and decision-makers to comprehend and explain safety analyses. Moreover, with BNs is possible to incorporate prior knowledge or experts' opinions through prior distributions. With fault trees, the inclusion of new evidence can be challenging. In cases of complex systems with a large number of variables and dependencies, Bayesian Networks are more computationally efficient than fault trees. The choice of technique is dependent on the type of study, the complexity of the system, and the availability of data. Due to the reasons previously mentioned, a Bayesian Network is a valuable tool to study the safety of a submerged floating tunnel.

Although previous studies have utilized BNs for tunnel risk assessment [137, 138], their application to floating tunnels remains unexplored. In this research, random variables that are of interest for the reliability analysis of an SFT have been grouped into five main categories, i) environmental loads, which refers to waves, currents, water level, wind, and earthquakes, ii) maritime accidents, iii) calamity events, iv) vertical stability factors (related to the equilibrium between the weight and buoyancy of the structure); and v) SFT elements.

The BN model presented in this research is (to the author's knowledge) the first attempt to characterize the variables of interest of an SFT to quantify the conditional probability of failure of the SFT under different scenarios. The scenarios combine the occurrence (or non-occurrence) of specific events. In this study, the focus is on developing a discrete Bayesian Network methodology applied to the SFT to assess its safety and investigate the potential main factors contributing to the failure of this structure.

8.2 Methodology

The methodology is divided into two main parts, a qualitative and a quantitative part (Fig. 8.1). First, the qualitative part aims to establish and classify the basic events (or root nodes) that are relevant to the SFT. For this purpose, brainstorming and preliminary hazard analysis (PHA) are performed to identify the main hazard events for an SFT. Then, the BN is constructed by considering the relationship between the variables involved. Hakkaart et al. [18] presented a proposal for a fault tree that can be used for probabilistic analysis of an SFT. Any fault tree can be transformed into a BN [139] Therefore, the fault tree presented by [18] is the foundation to construct the BN presented in this research. The BN's category

on maritime accidents (section 8.2.2) is based on the work of Uğurlu et al. [140], which presents a fault tree to assess maritime accidents caused by collision and grounding. The procedure for building the BN is described in Section 8.2.1.
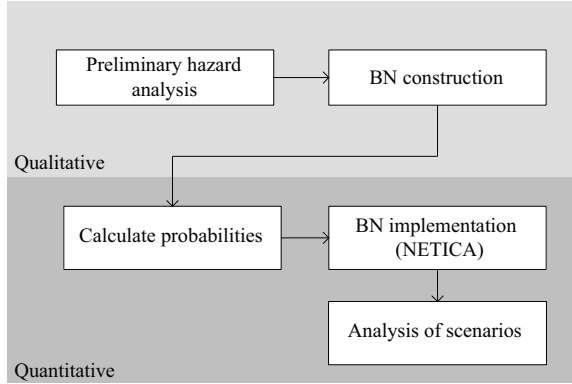
Figure 8.1: Methodology Overview.

For the quantitative analysis, the marginal probabilities and conditional probability tables (CPTs) of the nodes are defined in Section 8.2.2. The BN model is implemented and quantified using the discrete BN software Netica from Norsys Software Corp [141]. Finally, the BN is used to estimate the conditional probability of failure of the SFT under different scenarios that combine the occurrence (or non-occurrence) of certain events. Fig. 8.1 depicts the main parts of the methodology and their respective steps.

8.2.1 Construction of the BN

The proposed BN model is classified into four categories that could contribute to the overall failure of the SFT (Fig. 8.2), namely, (i) maritime accidents (blue), (ii) environmental loads (green), (iii) vertical stability (purple), and (iv) calamities (yellow). In addition, one category takes the SFT's elements into account (orange).

The BN model was constructed by establishing relationships between the nodes. The layout of some categories was based on the work from Uğurlu et al. [140], and Hakkaart et al. [18], namely the sections on maritime accidents and SFT elements respectively. The relationship between the rest of the nodes and categories is based on the author's judgment. The nodes are classified into two types, root nodes that depict the basic events (nodes that have no parents), and functional nodes that depict the intermediate events (nodes that have one or more parents). The target node is the general failure of the SFT (FL on Fig. 8.2). In this chapter, the general failure of the SFT is defined as the collapse of the structure.

The nodes of the discrete BN are expressed in two binary states. The occurrence/failure/exceedance of an event/value and the non-occurrence/failure/exceedance of an event/value (Fig. 8.2). The marginal probabilities of the root nodes were computed using data available at the SFT's particular location [92, 142, 143] or were derived using information from other studies [140, 144–147].

However, it is appropriate to clarify that the main objective of this study is not the computation of the marginal probabilities but to present a methodology that can allow the analysis of different scenarios and their contribution to the general failure of the SFT or any of its elements.

The functional nodes are characterized by conditional probability tables (or CPTs). The CPTs reflect the conditional relationship between the connected nodes, and it is the basis of the BN probability reasoning [148]. The "AND/OR" logic relationship, is usually based on the two-state assumption of an event. For the "AND" gate, the upper-level event only occurs when the basic events occur simultaneously. Regarding the "OR" gate, the upper-level event occurs when any basic event or combination of basic events occurs [148]. This is equivalent to the upper-level event not occurring when none of the basic events occur. In this study, the "OR" logic relationship is used for all the functional nodes. A representation of the CPT of an "OR" functional node with two parents is shown in Fig.8.3.

Once the BN is constructed and the CPTs have been quantified, the safety of the SFT can be assessed to identify the possible main contributors to the failure of a tethered submerged floating tunnel (SFT) and its elements. This was achieved by establishing different scenarios that would consider the occurrence of different combinations of events (section 8.3).

8.2.2 Marginal probabilities and CPTs

Maritime accidents   In this research, ship collisions are referred to as maritime accidents. This BN category is depicted in Fig. 8.2 as blue nodes. The BN configuration is based upon the ship collision fault tree presented in [140]. Maritime accidents are associated with mechanical errors and human errors (related to the ship officer on watch). An overview of these nodes is presented in Table 8.1. In this study, the original fault tree was modified and some of the nodes were excluded to reduce the total number of nodes of the BN. The marginal probabilities of the root nodes were also obtained from [140], and the functional nodes were estimated using the software Netica [141] (assuming an "OR" logical relationship). The marginal distributions of the nodes in this category are defined as the probability of occurrence/failure of a variable and its respective complement (section 8.2.1).

Environmental loads   Wind, earthquakes, and hydraulic loads such as waves, currents, and water levels are all relevant for an SFT and are included in this BN category. The environmental loads are highlighted in green as shown in Fig. 8.2. The marginal distributions of the nodes, except for earthquakes (EL2), are described based on the probability of exceeding each node's 500-year return period value. The marginal distribution of earthquakes is based on their probability of occurrence. The current choice of variables for this particular category is based on reviewing the literature [26, 149–152] and comparing the loads that are relevant for the SFT and similar structures as shown in Table 1.1. Table 8.2 provides a summary of the nodes in this category.

Wind, wave, and current data (nodes EL11 to EL17) were retrieved from ERA5 [92, 142] and the Copernicus Marine Environment Monitoring Service [93] respectively as climate
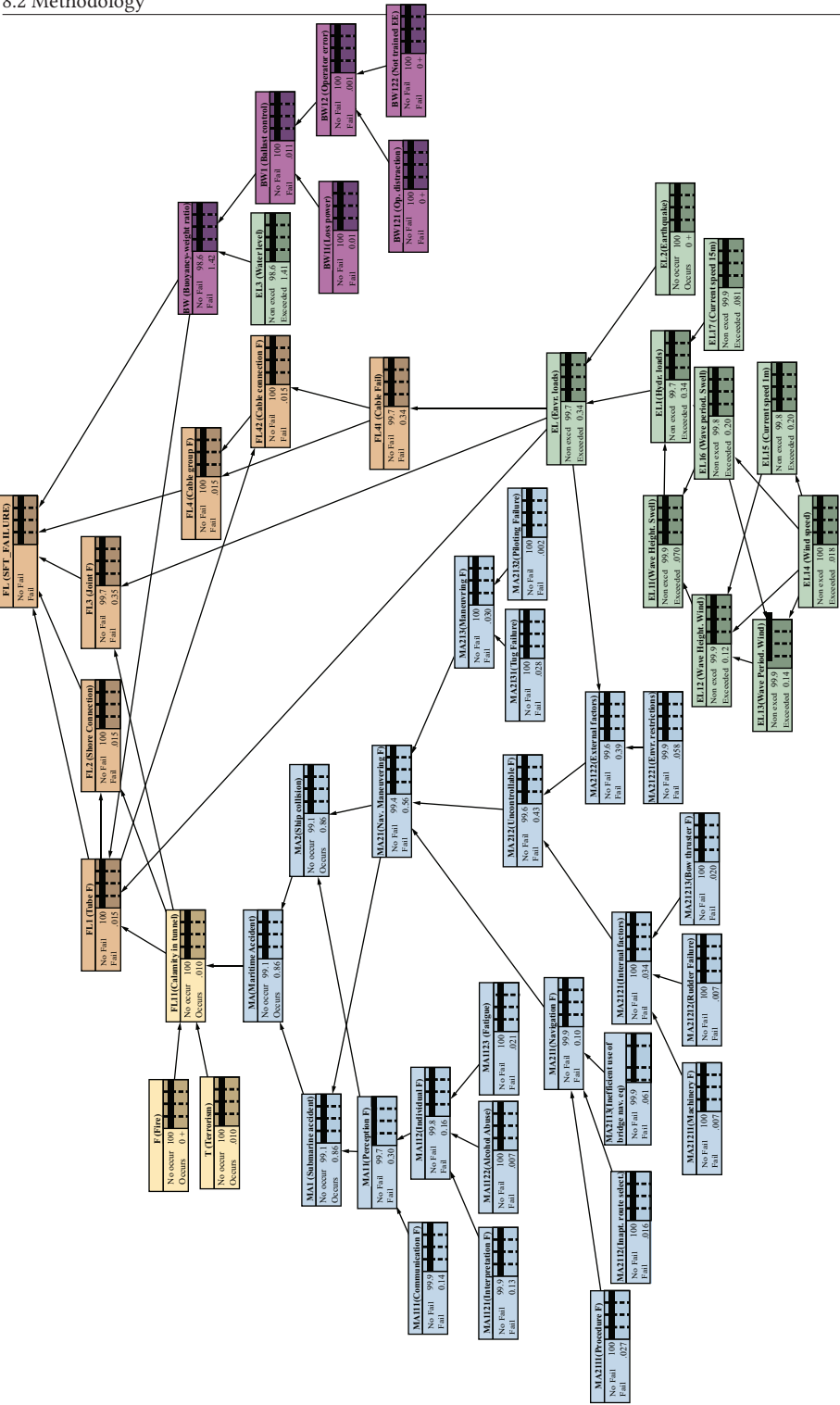
Figure 8.2: SFT Bayesian Network probability distribution (The probabilities are shown in percentages)

8

BW121	BW122	BW12
No fail	No fail	No fail
No fail	Fail	Fail
Fail	No fail	Fail
Fail	Fail	Fail
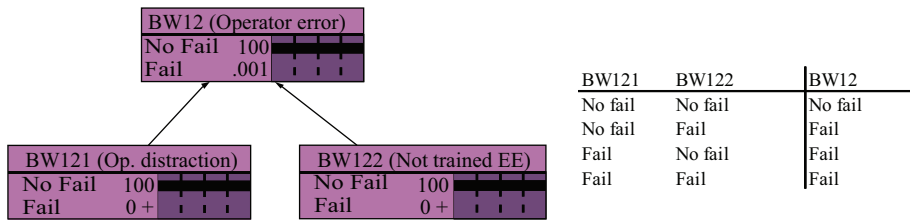
Figure 8.3: Example of a "OR" functional node. Nodes: BW12-Operator error; BW121-Operator distraction; BW122-Not trained employee.

Functional nodes	Code	Root nodes	Code
Maritime accident	MA	Communication failure	MA111
Submarine accident	MA1	Interpretation failure	MA1121
Perception failure	MA11	Alcohol abuse	MA1122
Individual failure	MA112	Fatigue	MA1123
Ship collision	MA2	Procedure failure	MA2111
Navigation maneuvering failure	MA21	Inappropriate route selection	MA2112
Navigation failure	MA211	Inefficient use of bridge navigation equipment	MA2113
Uncontrollable factors	MA212	Machinery failure	MA21211
Internal factors	MA2121	Rudder failure	MA21212
External factors	MA2122	Bow thruster failure	MA21213
Maneuvering failure	MA213	Environmental restrictions	MA21221
		Tug failure	MA2131
		Piloting failure	MA2132

Table 8.1: Nodes: Maritime accidents.

Functional nodes	Code	Root nodes	Code
Environmental loads	EL	Wind speed	EL14
Hydraulic loads	EL1	Current speed 15m	EL17
Significant wave height (swell waves)	EL11	Earthquake	EL2
Significant wave height (wind waves)	EL12	Water level	EL3
Wave period (wind waves)	EL13		
Current speed 1m	EL15		
Wave period (swell waves)	EL16		

Table 8.2: Nodes: Exceedance of loads.

8

reanalysis data with a 3 hourly frequency. This data was used to compute their respective marginal probabilities.

The BN presented in this study is discrete. However, data of waves, currents, and wind (EL11 to EL17) are continuous. Therefore, such data needs to be discretized into two binary states (exceedance and non-exceedance of the loads). In this research, we used the methodology presented in [81] to discretize the data and quantify the corresponding conditional probability tables using continuous BNs. This procedure is further explained in Appendix B and the resulting CPTs are presented in Appendix C.

For earthquakes (EL2), data from [143] was used. This data set consists of a record of

all the earthquakes (larger than 5 Mw magnitude)[1] that occurred in the area surrounding the Qiangzhou Strait between the years -193 and 2022. Although the data shows that there have not been major earthquakes in the area of the Strait, it is important to consider them and to show the implementation of this variable in the analysis of the failure of the SFT and its elements. Thus, a Poisson distribution was used to model the occurrence of earthquakes. This discrete probability distribution function takes into account the frequency of earthquakes in the past to calculate the probability of an earthquake occurring in the future. The Poisson probability mass function on a discrete random variable Q is defined as:

$$f(k;\lambda) = P(Q = k) = \frac{\lambda^k e^{-\lambda}}{k!} \tag{8.1}$$

where $P(Q = k)$ is the probability that an event will occur k times, $\lambda > 0$ is the number of times an event occurs and k is the number of occurrences.

The probability of exceedance for water level (EL3) was retrieved from [147] and this probability is defined as the probability of exceeding its 500-year-return period value, while the probability of non-exceedance is computed as its complement. In [147], a 60-year water level data set (between 1960 and 2019) from the Xiamen tide gauge station located at Gulangyu Island is used to study the extreme water levels related to astronomical tides and storm surges. [147] used a Gumbel distribution to characterize the extreme water level rise. In this research, the focus is on the total water level and we do not make a distinction between water levels related to tides or storms. Additionally, Gulangyu Island and the Qiongzhou Strait have different geographical and topographic characteristics, thus it is likely that the water level conditions differ from one another. Nevertheless, for this study, the water levels at Qiongzhou Strait are assumed the same as at Gulangyu Island.

Vertical stability Including the buoyancy weight ratio (BWR) in the BN allows for assessing its contribution to the failure of the SFT. This category combines nodes related to human error and mechanical errors that could influence the vertical stability of the SFT. There are two nodes on human errors (SFT operators/employees in charge of the vertical stability monitoring system) and they consider distractions by the operators (BW121), and not properly trained employees (BW122). See Table 8.3. The corresponding probability of failure of these nodes was obtained from the study developed by [145] and is equal to 6.00×10^{-6} for both nodes. In the case of loss of power (BW11), the failure rate is equal to 0.0001, assumed as a mechanical error as described in [144]. This category is illustrated in purple in Fig. 8.2, where the marginal distributions are defined by their respective probability of failure/occurrence.

Calamity Events In this category, two calamity events are considered: fire and terrorism (Table 8.4). Because no SFT has been constructed yet, databases for tunnels are used

---

[1]The Mw magnitude is based on the moment magnitude scale and it is a measure of seismic energy (Valid values: 0.0 to 9.9). It provides an estimate of earthquake size that is valid over the complete range of magnitudes. The magnitude scale is logarithmic. An increase of one in magnitude represents a tenfold increase in the recorded wave amplitude. However, the energy release associated with an increase of one in magnitude is not tenfold, but about thirtyfold [143].

Functional nodes	Code	Root nodes	Code
Buoyancy weight ratio	BW	Loss power	BW11
Ballast control	BW1	Operator Distraction	BW121
Operator error	BW12	Not trained employee	BW122

Table 8.3: Nodes: Vertical stability

to estimate calamities in the SFT. For example, fire (F) is described as the probability that a fire event would cause structural damage in the tunnel. This value was obtained from the database presented in [153], which presents a record of accidents in tunnels around the world. For terrorism, the minimum attack probability is 0.0001/building/year for high-density occupancies, monumental or iconic buildings among others [146]. In Fig. 8.2, calamity events are displayed in yellow. The functional node "Calamity in the tunnel" (FL11) is the only node in the entire network that is not described by an "OR" relationship. In this node, the presence of either fire or terrorism can result in a calamity in the tunnel, different from maritime accidents, which do not always lead to calamities in the tunnel.

Functional nodes	Code	Root nodes	Code
Calamity in tunnel	FL11	Fire	F
		Terrorism	T

Table 8.4: Nodes: Calamities.

SFT Elements   This category of nodes of the BN is based on a fault tree presented in [18] and consists of the key components of the SFT (orange nodes in Fig. 8.2). The original fault tree was modified to a tethered SFT. Therefore, pontoon-related elements were neglected. All the nodes in this category are functional nodes (Table 8.5).

Functional nodes	Code
SFT failure	FL
Tube failure	FL1
Shore connection	FL2
Joint failure	FL3
Cable group fail	FL4
Cable fail	FL41
Cable connection fail	FL42

Table 8.5: Nodes: SFT elements.

8.3 Results

Once the layout of the BN is defined and all the nodes have been populated with their corresponding marginal probabilities and CPTs (conditional probability tables), the model is used to study different scenarios. The probability distribution for all the nodes in the

networks is shown in Fig. 8.2. This figure depicts the BN before any nodes are conditionalized and this scenario is referred to as the "base" scenario for the remainder of this study. In this research, the design life of the SFT is assumed equal to 100 years [18].

The lifetime failure probability (FL) of the SFT in the base scenario is 1.5×10^{-4} approximately (Appendix D). As a result, the SFT elements have a failure probability of 0.0035, except the joints (FL3) and cables (FL41), which have a probability of failure of 0.0034. There is a probability of 0.0034 that the environmental loads are exceeded. This is depicted by the functional node EL. Calamities (C) have an occurrence probability of 0.0001, and there is a probability of 0.0142 of failure due to a wrong buoyancy-weight ratio (BW) (Fig. 8.2).

The joint distribution represented by the BN is then updated based on assuming the occurrence of a particular state for a node or set of nodes. For each of those nodes, either their non-occurrence/non-exceedance/non-failure, or occurrence/exceedance/failure is assigned. In other words, the nodes are conditionalized or instantiated. In Netica, the conditionalized nodes appear in gray, and the specific state chosen is assigned 100% probability (in Netica the probabilities are shown in percentages). Fig. 8.4 depicts an example of when node EL is conditionalized on the assumption that the environmental loads are exceeded. The changes that occur due to this conditionalization are displayed in the probability distributions of the other nodes in the BN.
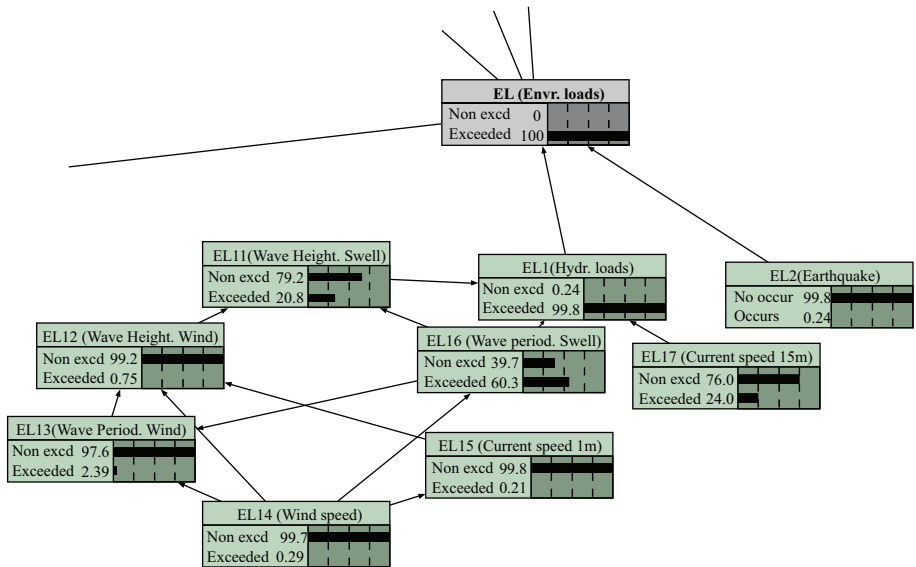
Figure 8.4: Example of scenario when EL is conditionalized on the assumption that the environmental loads are exceeded.

8.3.1 Root nodes

As a first analysis, the BN is conditionalized on each of the root nodes (one at a time). The resulting probability of failure of the SFT was calculated and examined (Table 8.6). Maritime root nodes are not displayed in this table as they did not affect the probability of failure of the SFT. The rate is defined as the ratio between the probability of failure given a specific scenario ($P(SFT_{fail}|scenario)$) and the probability of failure given the base scenario ($P(SFT_{fail}|Base)$).

Conditionalized node	Code	$P(SFT_{fail}|rootnode_{fail})$	Rate[2]
Fire	F	1	6667
Terrorism	T	1	6667
Earthquake	EL2	1.43×10^{-2}	95
Current speed (15m)	EL17	1.43×10^{-2}	95
Loss of power	BW11	3.46×10^{-2}	23
Distraction	BW121	3.46×10^{-2}	23
Not trained employee	BW122	3.46×10^{-2}	23
Water level	EL3	3.46×10^{-2}	23
Wind	EL14	8.8×10^{-4}	6

Table 8.6: Probability of failure of the SFT when the BN is conditioned on one root node at a time. The term $rootnode_{fail}$ stands for exceedance/occurrence/failure of the selected root nodes.

The root nodes with the most influence on the probability of failure of the SFT and its elements are calamity events (Fire and terrorism), with a resulting probability of failure of 1. Followed by the environmental loads. These are earthquakes (EL2) and a current speed at 15m below the water surface (EL17), resulting in the SFT's probability of failure being 95 times its base value. Considering failure at the nodes of vertical stability, the probability of failure of the SFT increases by 23 times its base value (3.46×10^{-2}). Finally, the BN was conditionalized on the assumption that the 500-year return period value of wind is exceeded. In that case, the effect of fast winds on the probability of exceeding the other environmental loads is investigated. The probability of currents at 1m (EL15) exceeding its 500-year return value within the design life of the SFT is 0.033, while the probability of exceedance for periods of wind waves and swells (EL13 and EL16) increases to 0.052 and 0.0507, respectively. In the case of wave height of wind waves (EL12), the probability of exceedance increases from 0.012 to 0.23. This large increase makes sense because wind waves are highly correlated with wind speed. The resulting probability of failure of the SFT is 8.8×10^{-4} which is 6 times its base probability of failure.

8.3.2 Scenarios

In this section, a total of 15 scenarios are considered. Table 8.7 presents a summary of these scenarios and the nodes that were conditionalized for each one of them. Scenarios are defined as a combination of events that lead to a certain probability of occurrence of the target node (SFT failure). For simplicity, the corresponding updated BN figures are not

---

[2]$Rate = \dfrac{P(SFT_{fail}|scenario)}{P(SFT_{fail}|Base)}$

shown. The probability of occurrence/exceedance/failure of each node for the 15 scenarios is displayed in Appendix D.

The scenarios presented in Table 8.7 aim to provide insight into the effects of calamities, environmental loads, and vertical stability on the SFT and its elements. Nevertheless, the BN can be updated to assess as many additional scenarios as engineers and decision-makers would render necessary.

Scenario	Conditionalized nodes	Code	Node_{Nofail}	Node_{fail}	$P(SFT_{fail}\|scenario)$	Rate[2]
Base	-	-	-	-	1.50×10^{-4}	-
1	Exceedance loads	EL	1	0	0	0
	Water level	EL3	1	0		
	Calamity	FL11	1	0		
2	Exceedance loads	EL	1	0	1.00×10^{-4}	0.67
	Water level	EL3	1	0		
3	Exceedance loads	EL	0	1	2.10×10^{-4}	1.4
	Water level	EL3	1	0		
4	Wave period (Wind)	EL13	0	1	1.70×10^{-3}	11
	Wind speed	EL14	0	1		
	Current speed (1m)	EL15	0	1		
5	Wind speed	EL14	0	1	8.80×10^{-4}	6
6	Wave period (Swells)	EL16	0	1	1.40×10^{-2}	93
7	Exceedance loads	EL	0	1	1.40×10^{-2}	93
8	Calamity	FL11	0	1	1	6667
9	Marine accident	MA	0	1	5.60×10^{-3}	37
10	Buoyancy-Weight ratio	BW	0	1	3.50×10^{-3}	23
11	Buoyancy-Weight ratio	BW	1	0	1.00×10^{-4}	0.67
12	Tube failure	FL1	0	1	1	6667
13	Tube failure	FL1	1	0	0	0
14	Joint failure	FL3	0	1	4.27×10^{-2}	285
15	Joint failure	FL3	1	0	0	0

Table 8.7: Scenarios. The terms Node_{Nofail} and Node_{fail} stand for the non-exceedance/non-occurrence/non-failure and the exceedance/occurrence/failure of the selected nodes.

8

In scenario 1, the environmental loads (EL), water level (EL3), and calamities (FL11) are assumed as non-exceeded/non-occurred. In other words, no load has been exceeded and there are no calamities in the tunnel. According to this scenario, there are no significant threats to the SFT. The SFT and its elements, therefore, have a probability of failure of zero. However, it is key to keep in mind that zero-risk situations cannot always be ensured in real life. Similar distributions are found for wave height and period for swells (EL11 and EL16), current velocities at 15m (EL17), and earthquakes (EL2). See Appendix D.

In scenario 2 (Table 8.7), the BN is conditionalized on the assumption that the environmental loads (EL) and the water level (EL3) are not exceeding their respective thresholds (section 8.2.2). As a result, the SFT and its elements' probability of failure is 1×10^{-4}. This is equivalent to a 33% decrease in the base probability of failure (1.5×10^{-4}). For the third scenario, all the environmental loads except the water level are exceeded, and their effects are examined. The SFT (FL) base probability of failure increases by 40%, which is equivalent to 2.1×10^{-4}. The SFT elements (FL1, FL2, FL4, and FL42) all yield the same value, except for the joints (FL3) and cables (FL41), whose respective probabilities of failure rise

to 1. The probability of failure for the buoyancy-weight ratio (BW) drops from 0.00142 to 0.00011 (Appendix D).

We evaluate the implications of exceeding loads for scenarios 4, 5, and 6. The nodes of wave period of wind waves (EL13), wind speed (EL14), and current speed at 1m (EL15) are modified in scenario 4 to surpass their respective loads. As a result, the probability of exceedance of the environmental loads (EL) is 0.112, and the probability of failure of the SFT (FL) is 0.0017 as well for its elements. This probability is 11 times its base value (1.5×10^{-4}). In scenario 5, wind speed (EL14) is exceeded. Although wind might not directly affect a tethered SFT, we use it to study its influence on wave height and wave period. The probability of exceedance for the environmental loads (EL) is now updated to 0.055. This represents an increase of 16 times its base value (3.40×10^{-3}). The resulting probability of failure of the SFT increases to 8.8×10^{-4} (6 times its corresponding base distribution).

In scenario 6, the 500-year return period value of wave period of swells (EL16) is exceeded. The probability of exceedance of the environmental loads (EL) rises to 1. This increases the probability of maritime accidents by 1 (due to its connection to node MA2122-External factors that is linked to maritime accidents) and the probability that the SFT will fail by 0.0143.

In scenario 7, the model is conditionalized on the exceedance of node EL (environmental loads) as shown in Fig. 8.4. The probability of failure of the SFT (FL) increases to 1.43×10^{-2} which is 93 times the SFT's base probability of failure. The same holds for all SFT elements, except for the joints (FL3) and cables (FL41), which have a probability of failure of 1 (see Appendix D). The changes in the probability distribution of the parent nodes are also studied. For instance, the probability of experiencing fast winds rises to 2.95×10^{-3}, which is 16 times higher than its base probability (1.8×10^{-4}). Refer to Fig. 8.4. A significant increase is noticed in the probability of exceeding significant wave height (EL11) and period (EL16) of swells with 0.21 and 0.60 respectively.

It is crucial to research the impact of calamities on any tunnel, especially on an SFT. In the previous section, the effects of conditionalizing the BN on fire and terrorism were evaluated. In scenario 8, the node calamity (FL11) is assigned to occur. Therefore, if a calamity were to occur, there is a probability of 0.20, 0.99, and 0.0086 that it may be caused by fire (F), terrorism (T), or maritime accidents (MA), respectively (Appendix D). This finding can help the development of appropriate countermeasures that, if successfully applied, could reduce such probabilities. For the SFT elements (FL1–FL4), the resulting likelihood of the SFT failing is 1. This is to be expected as events that have a low probability of occurring frequently represent increased risk.

Then, we focus on the effect of maritime accidents (MA) on the safety of the SFT (scenario 9). The resulting probability of failure of the SFT is 37 times its base probability and is equal to 0.0056, as well for its elements except for the joints and cables (FL3 and FL41) which have a probability of failure of 0.391 (Appendix D). Changes are noticed on the nodes that precede maritime accidents (MA). Piloting failure (MA2132), navigation failure (MA21), interpretation failure (MA1121), and bow thruster failure (MA21213) with corresponding probabilities of occurrence of 0.0026, 0.653, 0.155, and 0.0236 (Appendix D). Additionally, the environmental loads (EL) have a probability of exceedance of 0.391 which is 115 times higher than its base value (Fig. 8.2). This provides insight into the primary causes of maritime accidents. This subject will not be covered in this study because it is

further discussed in [140].

The effects of vertical stability or the buoyancy-weight ratio (BW) on the SFT are the main focus of scenarios 10 and 11. According to Table 8.7, when the buoyancy-weight ratio fails, the SFT and its elements' failure probabilities rise to 3.5×10^{-3} when compared to the base scenario. High water levels also play a significant role in the failure of the BW, increasing its exceedance probability from 0.0114 to 0.992 (Appendix D). The probability of distraction by an operator (BW121) and not having a properly trained employee (BW122) increased to 4.20×10^{-4} which is 70 times higher than their respective base probabilities (6×10^{-6}). This highlights the importance of having adequate staff to monitor the vertical stability of the SFT. On the other side, the probability of failure of the SFT (FL) is 0.001 when the buoyancy-weight-ratio (BW) does not fail, representing a 33% decrease in the SFT's base probability of failure.

In scenarios 12, 13, 14, and 15 (Table 8.7), the focus is on the behavior of the parent nodes. The analysis is focused on identifying the nodes that may contribute the most to the failure of the tube (FL1) and joints (FL3). In scenario 9, it is assumed that the SFT's tube (FL1) fails. The distributions of the remaining SFT elements change significantly, with a probability of failure of 1. The probability of occurrence for calamities increases to 0.677 with terrorism (T) accounting for most of that probability (Appendix D). The probability of failure of the buoyancy-weight ratio (BW) is 0.332, of which the main contributor is water level (EL3) with 0.33. Similar numbers are found for the environmental loads (EL) with a probability of failure of 0.325 of which the main contributor is the hydraulic loads (EL1) with a probability of 0.324 (Appendix D). However, the probability of failure for the joints and cables falls to values near zero when there is no tube failure (scenario 13).

When failure at the joints (FL3) is examined (scenarios 14 and 15). The probability of failure of the SFT and its elements (tube, shore connection, and cables) increases to 0.042. Where the main contributor is the environmental loads (EL) with a probability of exceedance of 0.971, the wave height (EL11) and wave period of swells (EL16) have the highest probabilities of exceedance with 0.202 and 0.586 respectively (Appendix D). These findings suggest that wave height and period for swells (EL11 and EL16) should be considered when formulating strategies to reduce the risk of failure of the SFT and its elements. The probability distributions on the vertical stability nodes remain unchanged. Calamities (FL11) have a resulting probability of failure of 0.028. Its main parent contributor is maritime accidents (MA) with 0.971. If the joints (FL3) do not fail, the SFT and its components have a probability of failure of close to zero.

In summary, for the particular SFT case presented in this research and the scenarios examined, calamities (fire and terrorism) were discovered to have a significant impact on the failure of the SFT and its elements. This is followed by scenarios where the environmental loads are exceeded or when one of the SFT's elements has failed (scenarios 12 and 14). This is an unwanted scenario as it could lead to a progressive collapse of the system. Therefore, it's crucial to contemplate repair strategies to guarantee that the SFT won't collapse under the failure of a single element. Consult Appendix D to view the resulting occurrence/exceedance/failure probabilities of the nodes in the BN for all 15 scenarios.

8

8.4 Conclusions

The main objective of this study is to provide engineers with a discrete Bayesian Network methodology to assess the safety of the SFT and investigate the potential main contributors to the failure of this structure and its elements. This was achieved by conditionalizing the BN on different scenarios that would consider the occurrence of different events or combinations of events (section 8.3).

The links depicted in the network (Fig. 8.2) serve as a model that characterizes the scenarios that might be relevant for the SFT. One of the main advantages of Bayesian Networks is that the model allows the user to apply their knowledge of the world to determine causal influences. In this way, the resulting graph is a compressed representation of the system. The BN used in this study was built under this logic.

Without taking structural deterioration and maintenance strategies into account, the base failure probability of the SFT over its lifetime is 1.5×10^{-4} (Fig. 8.2). In this research, the base scenario is when the BN is not conditionalized on any node. The root nodes related to calamities (Table 8.4) are the dominant factors towards the failure of the SFT and its elements (section 8.3). This contribution is higher for fire (F) and terrorism (T) because if either of those scenarios occurred, the probability of failure of the SFT would be 1 (Table 8.6). Less significant effects are seen concerning environmental loads, earthquakes (EL2), and current velocity at 15m below the water surface (EL17). However, they should not be ignored. On the other hand, when exceeding loads and calamities do not occur, the probability of failure of the SFT reduces significantly (close to zero). It is important to take into account that the BN does not yet include policies or countermeasures to reduce the risk of any of the scenarios presented in this research. Some examples of risk-reducing measures include the i) development of a proper emergency response plan that combines evacuation procedures, communication protocols, and coordination with authorities, ii) implementation of automated monitoring and early warning systems in case structural abnormalities, leaks or extreme loads are detected, iii) installation of clear signs and proper lighting inside the tunnel to prevent accidents and to ensure visibility during emergencies, iv) implementation of fire safety measures such as fire detection systems, proper ventilation (a key aspect in tunnel design), and fire-resistant materials, among others. The design of the tunnel should also include a detailed plan for regular inspections and maintenance to ensure the safety of the structure during its design life. Specific risk-reducing measures may vary depending on the location, design, and intended use of the SFT.

Bayesian Networks are flexible models that can be used as a viable alternative when little is known about a system. When modeling dependencies in a structure, Bayesian Networks have significant advantages over conventional risk analysis techniques like fault trees (FTs). While FTs can become confusing and difficult to handle when dependencies are incorporated, BNs can effectively depict complicated probabilistic relationships between random variables [67]. Another benefit is that any model can be extended thanks to the flexibility provided by BNs. This is a crucial factor to take into account in the specific situation of the SFT since it allows for the addition of new information as it becomes available.

The main limitation of this research is the lack of information, hence, the BN described here was modified for this particular situation. For instance, water level data (EL3) were obtained from the vicinity of Gulangyu Island, China [147] because water level data at the

Qiongzhou Strait were not accessible. However, as mentioned previously, BNs can be updated once new information is known. The main objective of this study is to demonstrate the applicability of BNs in assessing the probability of failure of the SFT rather than the retrieval of data for each of the nodes in the BN. The methodology described in this research can be utilized as an alternative to assist engineers and decision-makers in planning and designing the SFT to prevent substantial structural damage, injuries, or loss of lives.

Future work should include the implementation of a BN that includes risk-reducing measures, evacuation plans, and maintenance strategies that may lower the likelihood of failure of the SFT. Moreover, detailed BNs that focus on specific failure modes or hazard events such as fire, terrorism, vehicle or maritime collision, leakage, etc. would ensure a more precise assessment of the failure of the SFT and its elements. This could be achieved by adding information about the structural design of the SFT and the durability of its materials.

8

IV

Epilogue

9

Conclusions and Recommendations

This chapter concludes the dissertation by readdressing the research objectives in Section 1.4 and summarizes the most important findings. Furthermore, to offer insights and potential avenues for future research, recommendations arising from the research findings and limitations are also explored.

9.1 Conclusions

Submerged floating tunnels (SFTs) are a promising solution for a wide variety of waterway crossings. However, their design, construction, and operation require careful consideration of site-specific conditions. Factors such as extreme environmental conditions, geological features, operational requirements, and potential element failures must be addressed. Probabilistic models can help to study the likelihood of extreme loads and failures, capturing the complex dependencies between loading conditions, and offering a comprehensive understanding of potential risks and failure modes. This information can be used to assist engineers and decision-makers in planning and designing stable SFT designs. Thus, this dissertation sought to:

Investigate and develop probabilistic-based models to quantify the probability of failure of a SFT during operation under different loading conditions and hazard scenarios.

This objective was met by exploring bi-variate and multivariate probabilistic models like copulas, vine-copulas, and Bayesian Networks. Chapter 4 describes traffic flow using copulas, while Chapter 5 analyzes pairwise dependencies among waves and currents. Multivariate analyses in Chapters 7 and 6 examine the relationship between waves, currents, and their resulting hydrodynamic forces using continuous Bayesian Networks and vine-copula models respectively. Additionally, Chapter 8 investigates hazard scenarios and their impact on SFT failure probability. effectively capturing relevant dependencies. The main findings from the research objectives outlined in the introduction (Section 1.2) are given below.

9

Objective 1: Identify methods that can properly characterize the dependence among metocean variables, traffic loads, and hazard scenarios relevant to submerged floating tunnels

The analysis in Chapter 4 demonstrates that copulas can be used to characterize the autocorrelation in inter-vehicle distance. Correlation coefficients of 0.103 and -0.093 were identified for congestion traffic scenarios in both lanes (C_L2 and C_L3), and are described by Gaussian and Frank copulas respectively. Free-flow traffic scenarios exhibit correlations ranging from 0.054 to 0.414 and are described by Gumbel, BB8, and Joe Copulas, signaling upper tail dependence in free-flow traffic scenarios. Despite varying correlation values and tail dependencies, the traffic scenarios were well represented by the fitted copula models due to their flexibility to accommodate wide dependence ranges. Refer to Table 4.2 for the copula parameters.

In Chapter 5, the investigation focused on understanding the dependence between waves and currents in the Qiangzhou Strait during the wet season. Two perspectives were considered: the entire dataset, and extreme values. In both approaches, the correlations and fitted copula models remained consistent throughout all grid points within the strait suggesting similar metocean conditions along the Qiongzhou Strait and its immediate vicinity.

Autocorrelation values for wave height were notably high for wind and swell waves (0.94 and 0.89). Wave height and period showed moderately strong dependence, with a correlation of 0.69 for wind waves and 0.48 for swells. The correlations between current velocities and wave height exhibited lower values such as 0.14 and 0.07. Examining extreme values revealed shifts in correlations. a notable 75% decrease in correlation was observed between wave height and period of swells. However, the correlation for extreme current velocities increased to 0.25, while the correlation between significant wave height of swell waves and current velocity at 1m increased to 0.13.

Copula selection was crucial to characterize wave height autocorrelation. Joe and t copulas were chosen for wind and swell waves, respectively. BB6 copulas were selected to model upper tail dependence for wave height and period dependence in swells. Gaussian copulas described the relationship between current velocities, while BB8 copulas described the correlation between current velocity at 1m and wave height for both wind waves and swells (Table 5.5). Extreme values were best described by a Frank copula for wind waves and a Joe copula for swell waves (Table 5.6). These selections, based on the copula with the lowest Akaike's information criteria (AIC) a measure of goodness of fit (GOF), were validated through data variability analysis and correlation comparisons with simulated datasets (Tables 5.7 and 5.8).

Chapters 7 and 6 present multivariate analyses focusing on extreme values of six variables (wave height, wave period, current velocity, and resulting hydrodynamic forces) and various SFT configurations encompassing a variety of submergence depths and tube diameters. Chapter 8 investigates the reliability of SFTs under different hazard scenarios.

The statistical method used in this dissertation for the identification of extreme values is peak over threshold (POT), where the wave period of swell waves is chosen as the dominant variable. Thus, all the values that exceed its selected threshold are considered extreme events. The other variables are thought of as concomitant variables. These are

the values that accompany the dominant variable's extreme values. The concept of return period cannot be directly applied to concomitant variables in the same way it is to the dominant variable. In such situations, the return period relies on the conditional probability distribution function of variables given that a specific condition is met (Section 2.2). These conditional events are chosen depending on the matter under consideration.

In Chapter 7, a Bayesian Network is applied to characterize the dependence between extreme values of waves (wind and swell), currents, and their resulting hydrodynamic force components. It was found that the proposed configuration of this BN does not represent adequately the data nor that the Gaussian copula is a suitable choice to characterize these variables. Nevertheless, the results presented in Chapter 7 showed stronger forces are obtained when conditional distributions are used instead of considering the variables as independent. For designers, accounting dependence allows the opportunity to develop more robust designs by understanding how variables change under specific conditions and their potential impact on SFT performance.

Chapter 6 introduces a vine-copula model, showing its applicability in characterizing extreme values of significant wave height, wave period, current velocities, and their resulting hydrodynamic forces at the Qiangzhou Strait. The fitted copulas, including Joe, Gumbel, Clayton, and t copulas, are able to capture the interdependence among variables, particularly tail dependence (refer to Figures 6.5 and 6.8). However, limitations were observed in capturing asymmetries between hydrodynamic forces and significant wave height. These copulas serve as the building blocks of the vine-copula models discussed in Chapter 6, but they can also be used independently for studying bivariate and conditional distributions. For a larger number of variables, the quantity of vine-copula models expands significantly, as discussed in Section 2.4 (Eq. 2.13). This poses a challenge when computational resources are limited. In this study, 23040 vine models were fitted for each of the 9 SFT configurations, totaling 207360 vines. The goal was to identify the vine model with the lowest Akaike Criteria (AIC), serving as a measure of goodness of fit (GOF).

Chapter 8 presents a Bayesian Network with 51 nodes used to understand the effect of a variety of hazard scenarios on the failure probability of the SFT. In this dissertation, it is shown that the application of BNs has a significant advantage: the incorporation of user knowledge to determine causal influences, resulting in a solid representation of the system. This model proves to have powerful advantages when compared to Fault Trees (FTs). While FTs may face limitations when modeling complex systems. For example, in FTs, basic events are considered independent from each other unless they are caused by a common cause failure, or that FTs do not inherently account for uncertainty in the variables of the system. BNs emerge as a suitable and flexible alternative for assessing the safety of SFTs while offering adaptability, essential for high-dimensional and dynamic scenarios like SFTs. Objective 3 (below) addresses the probability of failure of the SFT under various hazard scenarios.

Computational efficiency played an important role in selecting the models presented herein. Moreover, the asymmetries in the bivariate distributions are an important characteristic of the data that we aimed to preserve. For this reason, copulas, and vine-copulas prove to effectively capture complex multivariate dependencies and generate synthetic data that exhibits similar dependence relationships as the observed data.

The approaches discussed in this dissertation produced large amounts of data that

could be useful to other researchers. All significant outputs were made available to the public as a result. Data from Chapters 4-6 are accessible at 4TU.ResearchData.

Objective 2: Formulate a methodology to evaluate different SFT configurations to assist decision-making

In Chapters 6 and 7, a methodology is developed to evaluate various Submerged Floating Tunnel (SFT) configurations, considering different combinations of tube diameter and submergence depth. The aim is to offer valuable insights to aid decision-making in the design and construction of these unique structures. An important contribution of this methodology is the integration of multivariate probability models with the analysis of specific SFT configurations outlined for the Qiangzhou Strait. Further details are provided below:

- In Chapters 6 and 7, vine-copula and BN models were applied to investigate the dependence relationship between wave height, wave period, current velocities, and hydrodynamic forces (Froude-Krylov FK forces) (Section 6.4.1). The FK force is the force that acts on an ideal water cylinder that has the same radius and is located at the same depth as the SFT. This framework is not fixed to the use of the Froude-Krylov forces but its flexibility allows the use of other equations to compute the hydrodynamic forces on SFTs.

- In Chapter 6, 500k simulations per variable were generated from the Froude-Krylov (FK) vine model (Fig. 6.7). These simulations were used to investigate the conditional distributions of horizontal force component, f_y, across 9 SFT configurations. The distribution of f_y was conditionalized on specific values of wave height (4.5m), period (12.8 s), and current velocity (1.3 m/s). Among the proposed SFT configurations, The largest horizontal force was found in configuration 1 (D = 20m, h = 20m) and 7 (D = 30m h = 20m).

- The analysis in Chapter 6 also considers the resulting vertical force F_R, and the ratio between the horizontal force and the vertical force, denoted as F_R/f_y. Despite configuration 1 showing the largest hydrodynamic force f_y, it was found that this configuration exhibits the smallest F_R/f_y ratio. Therefore, it is less likely that this configuration could lead to large displacements in the structure, as the resultant vertical force has the potential to compensate for it (Table 6.9).

- The BN model proposed in Chapter 7, was used to simulate the conditional distributions (CD) of the horizontal FK force component (f_y), considering specific values of wave height, wave period, and current velocity for 12 SFT configurations with varying diameters, D, and submergence depths, h. This analysis was carried out with two BNs, one for wind waves (BN1) and the other for swell waves (BN2). Out of the 12 configurations presented in this chapter, the largest force within BN1 is found in configuration 12 (D = 30m, h = 30m). Within the BN2 model, the largest force is found in configuration 10 (D = 30m, h = 50m). As a result, different wave systems can impact the design choices of SFTs.

This methodology contributes to advancing the state-of-the-art in submerged floating tunnel studies. It provides a structured framework for evaluating various SFT configurations by allowing researchers and engineers to explore different design options and their potential implications. The integration of multivariate probability models enables a deeper understanding of the complex interactions between variables. This not only enhances the accuracy of predictions but also supports informed decision-making in the design and construction phases.

Objective 3: Compare different hazard scenarios and identify the main contributors to the failure of the SFT in the specific case presented in this thesis

Through a comprehensive analysis of various hazard scenarios (Chapter 8), this dissertation identified critical factors that could contribute to the potential failure of a submerged floating tunnel (SFT). These contributors, considered for the specific context of this dissertation, range from extreme metocean events to human-induced errors and calamities.

Utilizing a discrete Bayesian network conditionalized on various nodes (variables), the resulting causal inferences were explored. The base failure probability of the SFT over its lifetime (100 years) was determined to be 1.5×10^{-4}. Notably, nodes related to calamities such as fire and terrorism emerged as dominant factors, closely followed by extreme environmental loads and human errors.

Nonetheless, it is key to acknowledge that the model presented in this dissertation does not incorporate risk-reducing measures, evacuation plans, or maintenance strategies. The absence of these elements in the analysis implies that the current estimation of the probability of failure under different scenarios might vary.

9.2 Recommendations for future work

In this section, a series of suggestions are presented concerning the utilization of probabilistic approaches within the realm of submerged floating tunnels. The methodologies presented in this dissertation play an important role in assessing the intricate interactions of uncertainties pertinent to SFTs. These recommendations aim to propose potential avenues for additional research, exploration, or enhancement of the insights conveyed in this dissertation.

The following paragraphs encapsulate the main recommendations formulated within this dissertation, categorized across various themes:

About data:

- Prioritize the integration of experimental data to validate probabilistic models. For instance, contrasting hydrodynamic forces measured in laboratory experiments with those simulated by probabilistic models. This validation process is essential to enhance the reliability of models, ensuring accurate predictions of hydrodynamic forces, structural integrity, and overall SFT performance. The absence of experimental data constrained the possibility of conducting validation with probabilistic models within the scope of this dissertation.

9

- Extend the investigation to encompass additional influencing factors on SFTs, such as storm surges, tsunamis, tide variations, and real-time buoyancy-weight ratio changes. These aspects, not considered in this dissertation due to lack of data, merit thorough exploration for a comprehensive analysis.

About SFTs

- A topic for future research is the assessment of SFT reliability by introducing additional critical limit states (compromised buoyancy due to leakage or damage, water ingress, operational failures, etc) and coupling them with more sophisticated structural analysis techniques. Specifically, evaluate potential failure scenarios involving tethers, foundations, and cross-sections both individually and in combinations.

- Future research on the effect of persistent loadings, such as the constant action of waves, not necessarily extreme, has the potential to provide deeper insights into stress, fatigue, deformation, and the long-term structural health of SFTs.

- Extend the application of the methodologies discussed in this dissertation to SFTs in diverse regions beyond the Qiangzhou Strait. Validate these methods in regions with varying traffic and environmental variables to ensure their applicability and effectiveness in different contexts.

- Apply the methodologies presented here to assess the reliability of SFTs and compare them with reliability index targets of the structures (i.e. bridges, tunnels, offshore platforms, etc.). This integration enhances objectivity, strengthening the robustness of SFT projects and ensuring their long-term success.

- The estimation of consequences and their corresponding safety measures, while not within the scope of this study, is recommended for further consideration. The SFT configurations previously presented should be subjected to evaluations that may integrate principles of economic analysis under uncertainty.

About vine-copulas

9

- Explore higher-dimensional vine-copula models in the context of SFTs to handle more than the six variables investigated in this dissertation. Including water level, wind speed, water temperature, tides, etc., and their resulting hydrodynamic forces. This research avenue would enhance the understanding of the dependence and tail asymmetries between metocean loadings and forcings on SFTs in the Qiangzhou Strait and other potential SFT locations. However, as noted in Chapter 6, higher dimensionality can increase computational demands, especially if the vine-copula model is selected based on the lowest Akaike criteria, leading to fitting all possible vine models given the number of nodes. Nonetheless, algorithms like those developed by [54] would assist in efficiently selecting a vine copula model.

About BNs

- Future research should be directed toward integrating hydrodynamic models and Bayesian Networks. For instance, attention should be given to the inherent variations in tides and water levels resulting from the specific geographical location of the Submerged Floating Tunnel (SFT) within the Qiongzhou Strait.

- Regarding the Bayesian Network presented in Chapter 8, it is advised to collaborate with experts specializing in fields such as structural dynamics, and hydrodynamics. These collaborations play a crucial role in identifying key variables contributing to failures. Based on their expertise and knowledge, experts' judgment can provide important guidance on the main contributors.

- Future efforts should focus on developing a more comprehensive discrete Bayesian Network (BN) that incorporates safety measures, evacuation plans, and maintenance strategies adapted to submerged floating tunnels. These enhancements are anticipated to contribute to a decreased probability of SFT failures.

9

Appendix

A

Vehicle characterization

A.1 Vehicle categories

Item	Class	Code											
1	B2	B11	B2										
2	B3	B111	B12	B3									
3	O3	O3											
4	O4	O4											
5	O5	O5											
6	O6	O6											
7	O8	O8											
8	O9	O9											
9	O10	O=											
10	O11	O>											
11	R5	R11111	R1112	R1211	R122								
12	R6	R111111	R11112	R11121	R1113	R11211	R1122	R12111					
		R1212	R123	R1311	R132								
13	R7	R1111111	R111112	R111121	R11113	R111211	R11122	R112111					
		R124	R13111	R133	R2221	R223	R11311	R1123					
		R1132	R115	R121111	R12112	R1213	R12211	R1222					
		R11212	R11221										
14	R8	R11111111	R1111112	R1111121	R111113	R111122	R1112111	R111212	R111221	R11123	R1121111	R112112	R112121
		R11213	R112211	R11222	R1124	R113111	R11312	R11321	R1223	R12311	R1232	R125	R131111	R1313
		R121211	R12122	R1214	R122111	R12212	R12221	R123	R224				
		R13211	R1322	R134	R2123	R2213	R2222	R224					
15	R9	R1112121	R1112211	R11124	R1121121	R112113	R1122111	R112221	R11223	R1125	R1134	R12111111	R1211112
		R1211121	R121113	R1212111	R121212	R121221	R12123	R1221111	R122112	R122121	R12213	R1224	R123111
		R12321	R1233	R126	R1314	R132111	R13221	R1323	R1332	R1341	R135	R1413	R144
		R2214	R2223	R225	R234	R3312	R54						
16	T3	T11O1											
17	T4	T11O1	T11O11	T11O2	T12O1	T21O1	T2O2						
18	T5	T111O11	T11O2	T11O111	T11O12	T11O21	T11O3						
		T12O11	T12O2	T21O11	T21O2	T2O21	T2O3	T3O2					
19	T6	T11O111	T111O12	T111O21	T11O3	T11O1111	T11O112	T11O121	T11O13	T11O211	T11O22	T11O31	T11O4
		T12O111	T12O12	T12O21	T12O3	T21O111	T21O12	T21O21	T21O3	T2O22	T2O4	T3O3	
20	T7	T111O112	T111O121	T111O13	T111O22	T111O31	T111O4	T12O1111	T12O112	T12O121	T12O13	T12O211	T12O22
		T12O31	T12O4	T21O211	T21O22	T21O4	T3O4						
21	V2	V11											
22	V3	V111	V11A1	V12	V21	V3							
23	V4	V1111	V112	V11A11	V11A2	V121	V13	V211	V22	V4			
24	V5	V111A11	V111A2	V11A111	V11A12	V12A11	V12A2	V21A11	V21A2				
25	V6	V1111A11	V1111A2	V111A111	V111A12	V112A11	V112A2	V121A11	V12A111	V12A12	V12A21	V12A3	V13A11
		V13A2	V211A11	V211A2	V21A12	V22A11	V22A2						
26	V7	V1111A111	V1111A12	V1111A3	V112A111	V112A12	V112A21	V112A3	V121A111	V121A12	V121A3	V13A111	V13A12
		V13A21	V13A3	V211A12	V211A3	V22A111	V22A12	V22A21	V22A3	V4A12			

Table A.1: Vehicle categories of WIM observations.
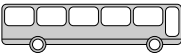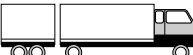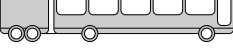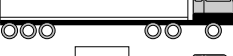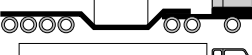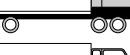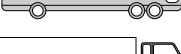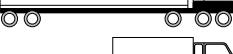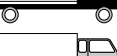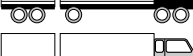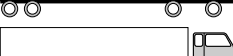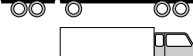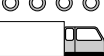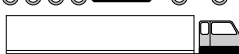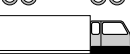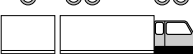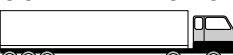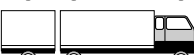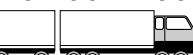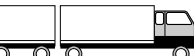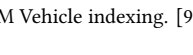
Sub-class	Symbol	Sub-class	Symbol	Sub-class	Symbol
B11		T12O111		V11A2	
B11A1		T12O111		V12	
B11A2		T12O1111		V12A11	
B12		T12O2		V12A12	
B12A1		T12O3		V13	
B12A2		T12O4		V21	
B21		T21O11		V211	
T11O1		V11		V21A2	
T11O11		V111		V21A2	
T11O111		V1111		V22	
T11O1111		V112		V22A1	
T11O2		V11A1		V22A1	
T11O3		V11A1		V22A11	
T11O4		V11A11		V22A12	
T12O1		V11A12			
T12O11		V11A2			

Figure A.1: WIM Vehicle indexing. [97]

A.2 Daily proportion of vehicles' categories

Vehicle Category	C_L2	F_L2_A	F_L2_B	C_L3	F_L3_A	F_L3_B
B2	0.61	5.56	1.65	0.69	0.58	0.39
B3	1.83	0.00	3.31	0.61	0.17	0.33
O3	3.05	1.85	2.13	0.69	0.42	1.11
O4	15.24	3.70	4.96	4.59	1.83	2.66
O5	0.61	1.85	0.71	0.61	0.58	0.20
O8	0.00	0.00	0.00	0.17	0.25	0.09
O9	0.00	0.00	0.00	0.00	0.08	0.00
OT10	0.00	0.00	0.00	0.00	0.00	0.02
OT11	0.00	0.00	0.00	0.00	0.00	0.00
R5	0.00	0.00	0.00	0.00	0.00	0.07
R6	0.00	0.00	0.00	0.17	0.83	0.11
R7	0.00	0.00	0.24	0.26	0.42	0.30
R8	0.00	0.00	0.00	0.26	0.17	0.41
R9	0.00	0.00	0.00	0.09	0.08	0.07
T3	1.83	3.70	2.60	5.37	4.33	4.22
T4	10.98	16.67	14.89	15.34	19.83	18.35
T5	26.83	33.33	37.12	29.29	38.25	36.04
T6	2.44	7.41	2.60	6.07	6.25	6.81
T7	0.61	0.00	0.00	0.26	0.33	0.33
V2	14.63	9.26	15.37	14.99	9.92	12.80
V3	3.66	1.85	1.65	4.51	1.92	4.16
V4	14.02	5.56	5.91	8.23	6.67	6.03
V5	1.83	5.56	4.73	5.37	5.33	3.53
V6	1.22	3.70	1.89	1.65	1.67	1.61
V7	0.61	0.00	0.24	0.61	0.08	0.37

Table A.2: Daily proportion of vehicles' categories. 10th April 2013.

A.3 Monthly proportion of vehicles' categories. April 2013.

Vehicle Category	Proportion [%]
B2	1.014
B3	0.779
O3	1.295
O4	3.116
O5	0.400
O8	0.128
O9	0.026
OT10	0.012
OT11	0.006
R5	0.047
R6	0.216
R7	0.264
R8	0.317
R9	0.054
T3	3.851
T4	17.795
T5	35.481
T6	5.871
T7	0.277
V2	12.801
V3	3.582
V4	6.902
V5	4.005
V6	1.445
V7	0.297

Table A.3: Monthly proportion of vehicles' categories. April 2013.

A.4 Copula Results-April 2013

Day	C_L2	C_L3	F_L2_A	F_L3_A	F_L2_B	F_L3_B
4	Joe	Frank	Joe	BB8	Joe	BB8
5	Gaussian	Gaussian	Clayton	Frank	Joe	Joe
6	t	Frank	Joe	t	Joe	Joe
7	Frank	Frank	Joe	Frank	Joe	BB7
8	Joe	Clayton	Clayton	Clayton	Gaussian	Gumbel
10	Gumbel	Frank	Joe	BB8	Joe	BB7
11	Gaussian	Frank	Joe	BB8	Joe	Joe
12	Gaussian	Joe	Joe	t	Joe	Joe
13	Clayton	Frank	t	BB8	Joe	Joe
14	t	Frank	Joe	Gaussian	Joe	Joe
15	t	Frank	Gaussian	Clayton	Joe	Joe
17	Gaussian	Gaussian	Joe	BB8	Gumbel	BB8
18	Gumbel	Frank	Joe	Frank	Joe	BB8
19	Frank	Frank	t	Clayton	Joe	Joe
20	Gaussian	Frank	Joe	t	Joe	Joe
21	BB7	Frank	BB7	Frank	Joe	BB8
22	t	Clayton	Clayton	Gaussian	Joe	Joe
24	Gaussian	Gaussian	t	BB8	Joe	Joe
25	Gaussian	Clayton	Joe	BB8	Joe	BB8
26	Joe	t	Gaussian	BB8	Joe	BB8
27	t	Frank	Gumbel	BB8	Joe	BB8
28	Joe	Frank	Joe	BB8	Joe	BB8
29	Gaussian	Clayton	Gaussian	Frank	Joe	BB7

Table A.4: Copula fit for inter-vehicle distances per traffic type. April 2013.

Day	C_L2		C_L3		F_L2_A		F_L3_A		F_L2_B		F_L3_B	
	Obs.	Sim.	Obs.	Sim.	Obs.	Sim.	Obs.	Sim.	Obs.	Sim.	Obs.	Sim.
4	0.213	0.091	-0.039	-0.088	0.477	0.584	0.218	0.300	0.149	0.177	0.088	0.113
5	0.084	0.259	-0.010	-0.017	0.535	0.563	0.177	0.170	0.109	0.129	0.097	0.140
6	0.068	-0.014	-0.103	-0.088	0.153	0.312	0.157	0.156	0.140	0.208	0.089	0.186
7	-0.045	0.004	-0.121	-0.160	0.508	0.163	0.265	0.240	0.152	0.186	0.136	0.173
8	0.099	0.231	0.033	-0.022	0.500	0.350	0.116	0.172	0.210	0.060	0.179	0.177
10	0.114	0.048	-0.050	-0.038	0.154	0.857	0.281	0.256	0.131	0.188	0.117	0.171
11	-0.003	-0.037	-0.023	0.007	0.106	0.367	0.245	0.242	0.162	0.218	0.102	0.112
12	-0.021	-0.142	0.004	-0.031	0.486	0.097	0.222	0.177	0.054	0.069	0.090	0.150
13	0.036	0.040	-0.029	-0.046	0.202	0.398	0.245	0.313	0.112	0.294	0.104	0.110
14	0.124	0.303	-0.035	0.023	0.414	0.419	0.190	0.227	0.147	0.226	0.118	0.147
15	-0.333	-0.103	0.065	0.003	0.300	0.400	0.115	0.176	0.154	0.078	0.119	0.165
17	0.133	0.170	-0.019	-0.043	0.365	0.351	0.289	0.290	0.156	0.132	0.099	0.138
18	0.154	0.100	-0.054	-0.068	0.388	-0.159	0.177	0.129	0.086	0.165	0.085	0.114
19	0.259	0.184	-0.086	-0.116	0.060	0.414	0.216	0.222	0.211	0.323	0.086	0.096
20	-0.001	-0.008	-0.009	0.017	0.566	0.712	0.165	0.100	0.121	0.152	0.101	0.136
21	0.148	0.262	-0.093	-0.088	0.307	0.384	0.231	0.256	0.204	0.270	0.086	0.122
22	-0.355	-0.346	0.036	0.079	0.164	0.291	0.059	0.112	0.197	0.067	0.112	0.152
24	0.103	0.107	0.001	-0.045	0.102	-0.278	0.168	0.176	0.106	0.146	0.067	0.123
25	0.115	0.125	0.007	0.059	0.389	0.218	0.139	0.068	0.217	0.296	0.122	0.155
26	0.088	0.007	-0.044	-0.067	0.470	0.517	0.256	0.277	0.161	0.228	0.091	0.150
27	-0.049	-0.147	-0.006	0.013	0.535	0.348	0.284	0.288	0.105	0.220	0.113	0.148
28	0.002	-0.108	-0.055	-0.025	0.558	0.593	0.222	0.240	0.066	0.120	0.092	0.155
29	-0.257	-0.388	0.023	0.047	0.543	0.257	0.053	0.100	0.274	0.325	0.158	0.125

Table A.5: Spearman's correlation coefficient for observations and simulations for inter-vehicle distance. April 2013.

B

Discretization procedure

Discretizing continuous variables can lead to the quantification of large conditional probability tables (CPTs). The hybrid method developed by [81] can aid in reducing this burden by following these steps.

1. Implement a continuous BN where the nodes are quantified as continuous univariate random variables and the arcs as parent-child rank correlations.

2. Sample this structure creating a sample file.

3. Use the sample file to build conditional probability tables for a discretized version of the continuous BN.

In this study, the continuous version of the BN of environmental variables was developed and implemented using the MATLAB toolbox for Non-Parametric Bayesian Networks, BANSHEE-A [128] (Fig. B.1). From this Bayesian network, a large sample of 300,000 simulations was generated. Finally, the conditional probability tables of each node were computed based on their 500-year-return-period values. The resulting conditional probabilities are presented in Appendix C.
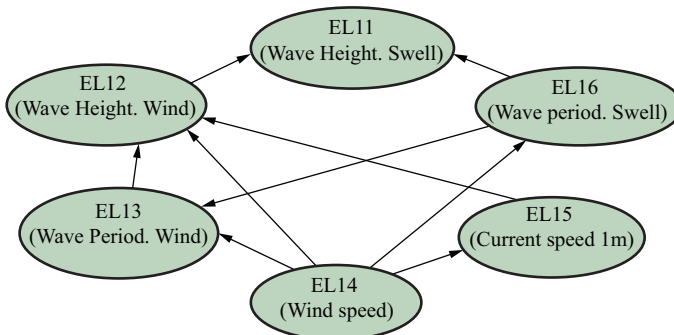
Figure B.1: Continuous BN for environmental variables.

C

CPTs for environmental variables (EL11-EL16)

EL16	EL12	EL11 non-exceedance	exceedance
non-exceedance	non-exceedance	0.999	0.001
non-exceedance	exceedance	0.986	0.014
exceedance	non-exceedance	0.912	0.088
non-exceedance	exceedance	0.875	0.125

Table C.1: CPT for wave height. Swell waves (EL11).

EL14	EL15	EL16	EL12 non-exceedance	exceedance
non-exceedance	non-exceedance	non-exceedance	0.999	0.001
non-exceedance	non-exceedance	exceedance	0.963	0.037
non-exceedance	exceedance	non-exceedance	0.998	0.002
non-exceedance	exceedance	exceedance	0.667	0.333
exceedance	non-exceedance	non-exceedance	0.773	0.227
exceedance	non-exceedance	exceedance	0.528	0.472
exceedance	exceedance	non-exceedance	0.818	0.182
exceedance	exceedance	exceedance	1	0

Table C.2: CPT for wave height. Wind waves (EL12)

		EL13	
EL14	EL16	non-exceedance	exceedance
non-exceedance	non-exceedance	0.999	0.001
non-exceedance	exceedance	0.962	0.038
exceedance	non-exceedance	0.951	0.049
exceedance	exceedance	0.885	0.115

Table C.3: CPT for wave period. Wind waves (EL13)

EL14	
non-exceedance	exceedance
0.997	0.003

Table C.4: CPT for wind speed (EL14)

	EL15	
EL14	non-exceedance	exceedance
non-exceedance	0.998	0.002
exceedance	0.967	0.033

Table C.5: CPT for current speed at 1m below the water surface (EL15)

	EL16	
EL14	non-exceedance	exceedance
non-exceedance	0.998	0.002
exceedance	0.949	0.051

Table C.6: CPT for wave period. Swell waves (EL16)

D

Beliefs

Node	Base	1	2	3	4	5	6	7	8	9	10	11	12	13	14	15
BW	1.42×10^{-2}	1.12×10^{-4}	1.12×10^{-4}	1.42×10^{-2}	1.42×10^{-2}	1.42×10^{-2}	1.12×10^{-4}	1	0	3.32×10^{-1}	1.41×10^{-2}	1.42×10^{-2}	1.42×10^{-2}	1.42×10^{-2}	1.42×10^{-2}	1.42×10^{-2}
BW1	1.12×10^{-4}	1.12×10^{-4}	1.12×10^{-4}	1.12×10^{-4}	1.12×10^{-4}	1.12×10^{-4}	1.12×10^{-4}	7.89×10^{-3}	0	2.62×10^{-1}	1.12×10^{-4}	1.12×10^{-4}	1.12×10^{-4}	1.12×10^{-4}	1.12×10^{-4}	1.12×10^{-4}
BW11	1.00×10^{-4}	1.00×10^{-4}	1.00×10^{-4}	1.00×10^{-4}	1.00×10^{-4}	1.00×10^{-4}	1.00×10^{-4}	7.05×10^{-3}	0	2.34×10^{-3}	9.97×10^{-5}	1.0×10^{-4}	1.00×10^{-4}	1.00×10^{-4}	1.00×10^{-4}	1.00×10^{-4}
BW12	1.20×10^{-5}	1.20×10^{-5}	1.20×10^{-5}	1.20×10^{-5}	1.20×10^{-5}	1.20×10^{-5}	1.20×10^{-5}	8.46×10^{-4}	0	2.81×10^{-4}	1.20×10^{-5}	1.20×10^{-5}	1.20×10^{-5}	1.20×10^{-5}	1.20×10^{-5}	1.20×10^{-5}
BW121	6.00×10^{-6}	6.00×10^{-6}	6.00×10^{-6}	6.00×10^{-6}	6.00×10^{-6}	6.00×10^{-6}	6.00×10^{-6}	4.23×10^{-4}	0	1.40×10^{-4}	5.98×10^{-6}	6.00×10^{-6}	6.00×10^{-6}	6.00×10^{-6}	6.00×10^{-6}	6.00×10^{-6}
BW122	6.00×10^{-6}	6.00×10^{-6}	6.00×10^{-6}	6.00×10^{-6}	6.00×10^{-6}	6.00×10^{-6}	6.00×10^{-6}	4.23×10^{-4}	0	1.40×10^{-4}	5.98×10^{-6}	6.00×10^{-6}	6.00×10^{-6}	6.00×10^{-6}	6.00×10^{-6}	6.00×10^{-6}
EL	3.36×10^{-3}	0	1	9.98×10^{-1}	3.36×10^{-3}	3.91×10^{-1}	0	3.36×10^{-3}	3.36×10^{-3}	3.25×10^{-1}	3.32×10^{-3}	9.71×10^{-1}	0	5.51×10^{-1}	1	1.12×10^{-1}
EL1	3.36×10^{-3}	0	9.98×10^{-1}	9.98×10^{-1}	3.36×10^{-3}	3.90×10^{-1}	0	3.36×10^{-3}	3.36×10^{-3}	3.24×10^{-1}	3.31×10^{-3}	9.69×10^{-1}	0	5.51×10^{-1}	1	1.12×10^{-1}
EL11	7.00×10^{-4}	0	2.08×10^{-1}	2.08×10^{-1}	7.00×10^{-4}	8.14×10^{-2}	0	7.00×10^{-4}	7.00×10^{-4}	6.76×10^{-2}	6.90×10^{-4}	2.02×10^{-1}	0	8.53×10^{-1}	8.83×10^{-2}	1.02×10^{-2}
EL12	1.20×10^{-3}	1.18×10^{-3}	2.39×10^{-2}	7.54×10^{-3}	7.00×10^{-4}	3.67×10^{-3}	1.18×10^{-3}	1.20×10^{-3}	1.20×10^{-3}	3.25×10^{-3}	1.20×10^{-3}	7.36×10^{-3}	1.18×10^{-3}	2.38×10^{-1}	3.61×10^{-3}	0
EL13	1.38×10^{-3}	1.31×10^{-3}	2.39×10^{-2}	2.39×10^{-2}	1.38×10^{-3}	1.01×10^{-2}	1.31×10^{-3}	1.38×10^{-3}	1.38×10^{-3}	8.65×10^{-3}	1.38×10^{-3}	2.33×10^{-2}	1.31×10^{-3}	5.27×10^{-2}	3.84×10^{-2}	1
EL14	1.80×10^{-4}	1.71×10^{-4}	2.95×10^{-3}	2.95×10^{-3}	1.80×10^{-4}	1.26×10^{-3}	1.71×10^{-4}	1.80×10^{-4}	1.80×10^{-4}	1.07×10^{-3}	1.80×10^{-4}	2.87×10^{-3}	1.71×10^{-4}		4.50×10^{-3}	1
EL15	2.02×10^{-3}	2.02×10^{-3}	2.12×10^{-3}	2.12×10^{-3}	2.02×10^{-3}	2.06×10^{-3}	2.02×10^{-3}	2.02×10^{-3}	2.02×10^{-3}	2.05×10^{-3}	2.02×10^{-3}	2.11×10^{-3}	2.02×10^{-3}	3.32×10^{-3}	2.16×10^{-3}	1.11×10^{-1}
EL16	2.03×10^{-3}	0	6.03×10^{-1}	6.03×10^{-1}	2.03×10^{-3}	2.36×10^{-1}	0	2.03×10^{-3}	2.03×10^{-3}	1.96×10^{-1}	2.00×10^{-3}	5.86×10^{-1}	0	5.07×10^{-1}	1	1
EL17	8.08×10^{-4}	0	2.40×10^{-1}	2.40×10^{-1}	8.08×10^{-4}	9.59×10^{-2}	0	8.08×10^{-4}	8.08×10^{-4}	7.80×10^{-2}	7.97×10^{-4}	2.33×10^{-1}	0	8.08×10^{-1}	8.08×10^{-4}	8.08×10^{-4}
EL2	8.23×10^{-6}	0	2.45×10^{-3}	2.45×10^{-3}	8.23×10^{-6}	9.57×10^{-4}	0	8.23×10^{-6}	8.23×10^{-6}	7.95×10^{-4}	8.11×10^{-6}	2.38×10^{-3}	0	8.23×10^{-6}	8.23×10^{-6}	8.23×10^{-6}
EL3	1.41×10^{-2}	0	0	1.41×10^{-2}	1.41×10^{-2}	1.41×10^{-2}	0	9.92×10^{-1}	0	3.30×10^{-1}	1.40×10^{-2}	1.41×10^{-2}	1.41×10^{-2}	1.41×10^{-2}	1.41×10^{-2}	1.41×10^{-2}
FL1	1.48×10^{-4}	1.00×10^{-4}	2.12×10^{-4}	1.43×10^{-4}	1	5.65×10^{-3}	0	3.46×10^{-4}	1.00×10^{-4}	1	0	4.27×10^{-1}	0	8.82×10^{-1}	1.43×10^{-2}	1.69×10^{-3}
FL11	1.00×10^{-4}	1.00×10^{-4}	1.00×10^{-4}	1.00×10^{-4}	1	1.00×10^{-4}	0	1.00×10^{-4}	1.00×10^{-4}	6.77×10^{-1}	0	2.89×10^{-2}	0	1.00×10^{-4}	1.00×10^{-4}	1.00×10^{-4}
FL2	1.48×10^{-4}	1.00×10^{-4}	2.12×10^{-4}	1.43×10^{-4}	1	5.65×10^{-3}	0	3.46×10^{-4}	1.00×10^{-4}	1	0	4.27×10^{-1}	0	8.82×10^{-1}	1.43×10^{-2}	1.69×10^{-3}
FL3	3.46×10^{-3}	1.00×10^{-4}	1	1	1	3.91×10^{-1}	0	3.46×10^{-3}	3.46×10^{-3}	1	3.32×10^{-3}	4.27×10^{-1}	0	5.52×10^{-2}	1	1.12×10^{-1}
FL4	1.48×10^{-4}	1.00×10^{-4}	2.12×10^{-4}	1.43×10^{-2}	3.36×10^{-3}	5.65×10^{-3}	0	3.46×10^{-3}	3.36×10^{-4}	1	0	4.27×10^{-1}	0	8.82×10^{-1}	1.43×10^{-2}	1.69×10^{-3}
FL41	3.36×10^{-3}	0				3.91×10^{-1}		3.36×10^{-3}	3.36×10^{-4}	3.25×10^{-1}	3.32×10^{-3}	9.71×10^{-1}	0	5.51×10^{-1}	1	1.12×10^{-1}
FL42	1.48×10^{-7}	1.00×10^{-4}	2.12×10^{-4}	1.43×10^{-2}	2.07×10^{-4}	2.41×10^{-2}	6.70×10^{-5}	3.46×10^{-4}	1.00×10^{-4}	4.27×10^{-2}	0	4.27×10^{-2}	0	8.82×10^{-1}	1.43×10^{-2}	1.69×10^{-3}
F	2.00×10^{-7}	2.00×10^{-7}	2.00×10^{-7}	2.00×10^{-7}	2.00×10^{-7}	2.00×10^{-7}	5.25×10^{-3}	2.00×10^{-7}	2.00×10^{-7}	1.35×10^{-3}	0	5.77×10^{-7}	5.25×10^{-3}	2.00×10^{-7}	2.00×10^{-7}	2.00×10^{-7}
MA	8.60×10^{-3}	5.25×10^{-3}	1	1	8.60×10^{-3}	1	5.25×10^{-3}	8.60×10^{-3}	8.60×10^{-3}	3.28×10^{-1}	8.55×10^{-3}	9.71×10^{-1}	5.25×10^{-3}	6.01×10^{-2}	1	1.17×10^{-1}
MA1	8.60×10^{-3}	5.25×10^{-3}	1	1	8.60×10^{-3}	6.53×10^{-1}	5.25×10^{-3}	8.60×10^{-3}	8.60×10^{-3}	3.28×10^{-1}	8.55×10^{-3}	9.71×10^{-1}	5.25×10^{-3}	5.72×10^{-2}	1	1.14×10^{-1}
MA11	3.00×10^{-3}	3.00×10^{-3}	1.40×10^{-3}	3.00×10^{-3}	3.00×10^{-3}	3.49×10^{-1}	3.00×10^{-3}	3.00×10^{-3}	3.00×10^{-3}	3.28×10^{-1}	3.00×10^{-3}	9.71×10^{-1}	3.00×10^{-3}	6.01×10^{-2}	1	1.17×10^{-1}
MA111	1.40×10^{-3}	1.40×10^{-3}	1.40×10^{-3}	1.40×10^{-3}	1.40×10^{-3}	1.63×10^{-1}	1.40×10^{-3}	1.40×10^{-3}	1.40×10^{-3}	1.40×10^{-3}	1.40×10^{-3}	1.40×10^{-3}	1.40×10^{-3}	1.40×10^{-3}	3.00×10^{-3}	3.00×10^{-3}
MA112	1.60×10^{-3}	1.60×10^{-3}	1.33×10^{-3}	1.60×10^{-3}	1.60×10^{-3}	1.86×10^{-1}	1.60×10^{-3}	1.60×10^{-3}	1.60×10^{-3}	1.60×10^{-3}	1.60×10^{-3}	1.60×10^{-3}	1.60×10^{-3}	1.60×10^{-3}	1.40×10^{-3}	1.40×10^{-3}
MA1121	1.33×10^{-3}	1.33×10^{-3}	1.33×10^{-3}	1.33×10^{-3}	1.33×10^{-3}	1.55×10^{-1}	1.33×10^{-3}	1.33×10^{-3}	1.33×10^{-3}	1.33×10^{-3}	1.33×10^{-3}	1.33×10^{-3}	1.33×10^{-3}	1.33×10^{-3}	1.60×10^{-3}	1.60×10^{-3}
MA1122	6.70×10^{-5}	6.70×10^{-5}	6.70×10^{-5}	6.70×10^{-5}	6.70×10^{-5}	7.79×10^{-3}	6.70×10^{-5}	6.70×10^{-5}	6.70×10^{-5}	6.70×10^{-5}	6.70×10^{-5}	6.70×10^{-5}	6.70×10^{-5}	6.70×10^{-5}	1.33×10^{-3}	1.33×10^{-3}
MA1123	2.07×10^{-4}	2.07×10^{-4}	2.07×10^{-4}	2.07×10^{-4}	2.07×10^{-4}	2.36×10^{-2}	2.07×10^{-4}	2.07×10^{-4}	2.07×10^{-4}	2.07×10^{-4}	2.07×10^{-4}	2.07×10^{-4}	2.07×10^{-4}	2.07×10^{-4}	6.70×10^{-5}	6.70×10^{-5}
MA2	8.60×10^{-3}	5.25×10^{-3}	1	1	8.60×10^{-3}	1	5.25×10^{-3}	8.60×10^{-3}	8.60×10^{-3}	3.28×10^{-1}	8.55×10^{-3}	9.71×10^{-1}	5.25×10^{-3}	6.01×10^{-2}	2.07×10^{-4}	1.17×10^{-1}
MA21	5.62×10^{-3}	2.26×10^{-3}	1	1	5.62×10^{-3}	1.21×10^{-1}	2.26×10^{-3}	5.62×10^{-3}	5.62×10^{-3}	3.26×10^{-1}	5.57×10^{-3}	9.71×10^{-1}	2.26×10^{-3}	5.72×10^{-2}	1	1.14×10^{-1}
MA211	2.70×10^{-4}	2.70×10^{-4}	1.04×10^{-3}	2.70×10^{-4}	1.04×10^{-3}	3.14×10^{-2}	1.04×10^{-3}	1.04×10^{-3}	1.04×10^{-3}	1.04×10^{-3}	1.04×10^{-3}	1.04×10^{-3}	1.04×10^{-3}	1.04×10^{-3}	1.04×10^{-3}	3.00×10^{-3}
MA2111	2.70×10^{-4}	2.70×10^{-4}	2.70×10^{-4}	2.70×10^{-4}	2.70×10^{-4}	3.14×10^{-2}	2.70×10^{-4}	2.70×10^{-4}	2.70×10^{-4}	2.70×10^{-4}	2.70×10^{-4}	2.70×10^{-4}	2.70×10^{-4}	2.70×10^{-4}	2.70×10^{-4}	2.70×10^{-4}
MA2112	1.62×10^{-4}	1.62×10^{-4}	1.62×10^{-4}	1.62×10^{-4}	1.62×10^{-4}	1.88×10^{-2}	1.62×10^{-4}	1.62×10^{-4}	1.62×10^{-4}	1.62×10^{-4}	1.62×10^{-4}	1.62×10^{-4}	1.62×10^{-4}	1.62×10^{-4}	1.62×10^{-4}	1.62×10^{-4}
MA2113	6.09×10^{-4}	6.09×10^{-4}	6.09×10^{-4}	6.09×10^{-4}	6.09×10^{-4}	7.08×10^{-2}	6.09×10^{-4}	6.09×10^{-4}	6.09×10^{-4}	6.09×10^{-4}	6.09×10^{-4}	6.09×10^{-4}	6.09×10^{-4}	6.09×10^{-4}	6.09×10^{-4}	6.09×10^{-4}
MA212	4.28×10^{-3}	9.19×10^{-4}	1	1	4.28×10^{-3}	4.98×10^{-1}	9.19×10^{-4}	4.28×10^{-3}	4.28×10^{-3}	3.26×10^{-1}	4.23×10^{-3}	9.71×10^{-1}	9.19×10^{-4}	5.60×10^{-2}	1	1.13×10^{-1}
MA2121	3.37×10^{-4}	3.37×10^{-4}	3.37×10^{-4}	3.37×10^{-4}	3.37×10^{-4}	3.92×10^{-2}	3.37×10^{-4}	3.37×10^{-4}	3.37×10^{-4}	3.37×10^{-4}	3.37×10^{-4}	3.37×10^{-4}	3.37×10^{-4}	3.37×10^{-4}	3.37×10^{-4}	3.37×10^{-4}
MA21211	6.71×10^{-5}	6.71×10^{-5}	6.71×10^{-5}	6.71×10^{-5}	6.71×10^{-5}	7.80×10^{-3}	6.71×10^{-5}	6.71×10^{-5}	6.71×10^{-5}	6.71×10^{-5}	6.71×10^{-5}	6.71×10^{-5}	6.71×10^{-5}	6.71×10^{-5}	6.71×10^{-5}	6.71×10^{-5}
MA21212	6.70×10^{-5}	6.70×10^{-5}	6.70×10^{-5}	6.70×10^{-5}	6.70×10^{-5}	7.79×10^{-3}	6.70×10^{-5}	6.70×10^{-5}	6.70×10^{-5}	6.70×10^{-5}	6.70×10^{-5}	6.70×10^{-5}	6.70×10^{-5}	6.70×10^{-5}	6.70×10^{-5}	6.70×10^{-5}
MA21213	2.03×10^{-4}	2.03×10^{-4}	2.03×10^{-4}	2.03×10^{-4}	2.03×10^{-4}	2.36×10^{-2}	2.03×10^{-4}	2.03×10^{-4}	2.03×10^{-4}	2.03×10^{-4}	2.03×10^{-4}	2.03×10^{-4}	2.03×10^{-4}	2.03×10^{-4}	2.03×10^{-4}	2.03×10^{-4}
MA2122	3.94×10^{-3}	5.82×10^{-4}	1	1	3.94×10^{-4}	4.59×10^{-1}	5.82×10^{-4}	3.94×10^{-4}	3.94×10^{-4}	3.25×10^{-1}	3.90×10^{-3}	9.71×10^{-1}	5.82×10^{-4}	5.56×10^{-2}	1	1.13×10^{-1}
MA22121	5.82×10^{-4}	5.82×10^{-4}	3.02×10^{-4}	5.82×10^{-4}	5.82×10^{-4}	6.77×10^{-2}	5.82×10^{-4}	5.82×10^{-4}	5.82×10^{-4}	5.82×10^{-4}	5.82×10^{-4}	5.82×10^{-4}	5.82×10^{-4}	5.82×10^{-4}	5.82×10^{-4}	5.82×10^{-4}
MA213	3.02×10^{-4}	3.02×10^{-4}	2.80×10^{-4}	3.02×10^{-4}	3.02×10^{-4}	3.51×10^{-2}	3.02×10^{-4}	3.02×10^{-4}	3.02×10^{-4}	3.02×10^{-4}	3.02×10^{-4}	3.02×10^{-4}	3.02×10^{-4}	3.02×10^{-4}	3.02×10^{-4}	3.02×10^{-4}
MA2131	2.80×10^{-4}	2.80×10^{-4}	2.80×10^{-4}	2.80×10^{-4}	2.80×10^{-4}	3.26×10^{-2}	2.80×10^{-4}	2.80×10^{-4}	2.80×10^{-4}	2.80×10^{-4}	2.80×10^{-4}	2.80×10^{-4}	2.80×10^{-4}	2.80×10^{-4}	2.80×10^{-4}	2.80×10^{-4}
MA2132	2.23×10^{-5}	2.23×10^{-5}	2.23×10^{-5}	2.23×10^{-5}	9.98×10^{-1}	2.59×10^{-3}	2.23×10^{-5}	2.23×10^{-5}	2.23×10^{-5}	2.23×10^{-5}	2.23×10^{-5}	2.23×10^{-5}	2.23×10^{-5}	2.23×10^{-5}	2.23×10^{-5}	2.23×10^{-5}
T	1.00×10^{-4}	1.00×10^{-4}	1.00×10^{-4}	1.00×10^{-4}	1	1.00×10^{-4}	1.00×10^{-4}	1.00×10^{-4}	1.00×10^{-4}	6.76×10^{-1}	0	2.89×10^{-2}	1.00×10^{-4}	1.00×10^{-4}	1.00×10^{-4}	1.00×10^{-4}
SFT_FAILURE	1.48×10^{-4}	2.12×10^{-4}	1.00×10^{-4}	1.43×10^{-2}	1	5.65×10^{-3}		3.46×10^{-3}	1.00×10^{-4}		0	4.27×10^{-2}	2.23×10^{-5}	8.82×10^{-1}	1.43×10^{-2}	1.69×10^{-3}

Table D.1: Occurrence/exceedance/failure probabilities of the nodes for all scenarios.

References

[1] G.A. Torres-Alves, O. Morales-Nápoles, and S.N. Jonkman. Simulation of hydrodynamic loads for a submerged floating tunnel using a copula-based model. In *Bridge Maintenance, Safety, Management, Life-Cycle Sustainability, and Innovations. IABMAS 2020.*, pages 844–852. CRC Press, 2021.

[2] G.A Torres-Alves, O Morales-Nápoles, and S.N Jonkman. Bayesian Networks for Estimating Hydrodynamic Forces on a Submerged Floating Tunnel. In *31st European Safety and Reliability Conference*, pages 2518–2524. Research Publishing Services, 2021.

[3] G.A. Torres-Alves, C.M.P. 't Hart, O. Morales-Nápoles, and S.N. Jonkman. Structural reliability analysis of a submerged floating tunnel under copula-based traffic load simulations. *Engineering Structures*, 269:114752, 2022.

[4] G.A. Torres-Alves, O. Morales-Nápoles, and S.N. Jonkman. A vine-copula model for simulation of extreme metocean loads and estimation of hydrodynamic forces for a submerged floating tunnel at the Qiongzhou Strait. Under Review, 2024.

[5] G.A. Torres-Alves, O. Morales-Nápoles, and S.N. Jonkman. Bayesian Networks to assess the risk and reliability of a submerged floating tunnel. Under Review, 2024.

[6] Giulio Martire. *The Development of Submerged Floating Tunnels as an innovative solution for waterway crossings*. PhD thesis, Università degli Studi di Napoli Federico II, 2010.

[7] Anette Fjeld and Tore H. Søreide. Feasibility study for crossing the Sognefjord-Submerged floating tunnel. Report 11774-ROO-R-001, Reinertsen Olav Olsen Group, 2012.

[8] Shunji Kanie. Feasibility studies on various SFT in Japan and their technological evaluation. *Procedia Engineering*, 4:13–20, 2010.

[9] Sungsoo Lim, Daniil Popov, Nauman Raza, Fahad Pervaiz, and Mazen Al-Qadi. Feasibility study of submerged floating crossing. Student report, Delft University of Technology, 2018.

[10] Arianna Minoretti, Anders Myhr, Stein Haugerud, J Sekse, and T.F Egeland. The submerged floating tube bridge: The invisible bridge crossing the bjørnafjord. *IABSE Stockholm 2016*, 09 2016.

[11] Kjersti Dunham. Coastal Highway Route E39 – Extreme Crossings. *Transportation Research Procedia*, 14:494–498, 12 2016.

[12] Donna Ahrens. Chapter 10 submerged floating tunnel, a concept whose time has arrived. *Tunnelling and Underground Space Technology*, 12(2):317–336, 1997. Immersed and Floating Tunnels, Second Edition.

[13] F.M. Mazzolani, B. Faggiano, and G. Martire. Design aspects of the AB prototype in the Qiandao Lake. *Procedia Engineering*, 4:21 – 33, 2010. ISAB-2010.

[14] Xu Long, Fei Ge, Lei Wang, and Youshi Hong. Effects of fundamental structure parameters on dynamic responses of submerged floating tunnel under hydrodynamic loads. *Acta Mechanica Sinica/Lixue Xuebao*, 25:335–344, 06 2009.

[15] Bolin Jiang, Bo Liang, and Shanshan Wu. Feasibility study on the submerged floating tunnel in Qiongzhou Strait, China. *Polish Maritime Research*, 25:4–11, 2018.

[16] S.K. Chakrabarti. *Handbook of Offshore Engineering*. Number V.1 in Elsevier ocean engineering book series. Elsevier, 2005.

[17] Richard Lunniss and Jonathan Baber. *Immersed Tunnels*. CRC Press, 1st edition, 2013.

[18] J.A Hakkaart, A Lancelotti, H Ostlid, R Marazza, and K.A Nyhus. Chapter 6: Submerged floating tunnels. *Tunnelling and Underground Space Technology*, 8(2):265–285, 1993. Special Issue. Immersed and Floating Tunnels.

[19] Michele Baravalle and Jochen Köhler. Risk and Reliability Based Calibration of Design Codes for Submerged Floating Tunnels. *Procedia Eng.*, 166(1877):247–254, 2016.

[20] Jian-yun Chen, Jing Li, Sheng-nan Sun, and Zhi-bin Su. Experimental and numerical analysis of submerged floating tunnel. *Journal of Central South University*, 19:2949–2957, 2012.

[21] Shi Deng, Haojie Ren, Yuwang Xu, Shixiao Fu, Torgeir Moan, and Zhen Gao. Experimental study of vortex-induced vibration of a twin-tube submerged floating tunnel segment model. *Journal of Fluids and Structures*, 94:102908, 2020.

[22] Gyu-Jin Kim, Sangmin Lee, Mujong Kim, Hyo-Gyoung Kwak, and Jung-Wuk Hong. Characterization of single and dual SFT through a hydraulic experiment under regular and irregular waves. *Ocean Engineering*, 263:112365, 2022.

[23] Qinxi Li, Shuping Jiang, and Xiang Chen. Experiment on pressure characteristics of submerged floating tunnel with different section types under wave condition. *Polish Maritime Research*, 25(s3):54–60, 2018.

[24] YG Qin and XJ Zhou. Experimental study of dynamic behavior of submerged floating tunnel under current effect. *J. Railw. Transp. Res. Dev*, 26:69–77, 2009.

[25] Sung il Seo, Hyung suk Mun, Jin ho Lee, and Jin ha Kim. Simplified analysis for estimation of the behavior of a submerged floating tunnel in waves and experimental verification. *Marine Structures*, 44:142–158, 2015.

[26] G. Ferro, H. Ostlid, F. Mazzolani, T. Soreide, K. Nyhus, and A. Fiorentino. Appendix A: "Submerged floating tunnels analysis project" (Edited and condensed version). *Tunnelling and Underground Space Technology*, 12(2):337–346, 1997.

[27] Walter C. Grantz P.E. Conceptual study for a deep water, long span, submerged floating tunnel (SFT) crossing. *Procedia Engineering*, 4:61–70, 2010. ISAB-2010.

[28] Wanhai Xu, Yexuan Ma, Guangjun Liu, Mingliu Li, Ang Li, Menglei Jia, Ziqi He, and Zunfeng Du. A review of research on tether-type submerged floating tunnels. *Applied Ocean Research*, 134:103525, 2023.

[29] Fatih Tosunoglu and Vijay P. Singh. Multivariate modeling of annual instantaneous maximum flows using copulas. *Journal of Hydrologic Engineering*, 23:04018003, 2018.

[30] Alireza Daneshkhah, Renji Remesan, Omid Chatrabgoun, and Ian P. Holman. Probabilistic modeling of flood characterizations with parametric and minimum information pair-copula model. *Journal of Hydrology*, 540:469–487, 2016.

[31] C. Jiang, L. Xiong, L. Yan, J. Dong, and C.-Y. Xu. Multivariate hydrologic design methods under nonstationary conditions and application to engineering practice. *Hydrology and Earth System Sciences*, 23(3):1683–1704, 2019.

[32] Erika Spissu, Abdul Rawoof Pinjari, Ram Pendyala, and Chandra R. Bhat. A copula-based joint multinomial discrete-continuous model of vehicle type choice and miles of travel. *Transportation*, 36(4):403–422, 2009.

[33] Chandra R. Bhat and Naveen Eluru. A copula-based approach to accommodate residential self-selection effects in travel behavior modeling. *Transportation Research Part B: Methodological*, 43(7):749 – 765, 2009.

[34] Yajie Zou and Yunlong Zhang. A copula-based approach to accommodate the dependence among microscopic traffic variables. *Transportation Research Part C: Emerging Technologies*, 70:53 – 68, 2016.

[35] Changqing Gong and Dan M. Frangopol. Reliability of steel girder bridges with dependent corrosion growth. *Engineering Structures*, 224:111125, 2020.

[36] Xing Fu, Hong-Nan Li, Gang Li, Zhi-Qian Dong, and Mi Zhao. Failure analysis of a transmission line considering the joint probability distribution of wind speed and rain intensity. *Engineering Structures*, 233:111913, 2021.

[37] Zhi wei Wang, Wen ming Zhang, Gen min Tian, and Zhao Liu. Joint values determination of wind and temperature actions on long-span bridges: Copula-based analysis using long-term meteorological data. *Engineering Structures*, 219:110866, 2020.

[38] R. Jane, L. Dalla Valle, D. Simmonds, and A. Raby. A copula-based approach for the estimation of wave height records through spatial correlation. *Coastal Engineering*, 117:1–18, 2016.

[39] Yi Zhang, Chul-Woo Kim, Michael Beer, Huliang Dai, and Carlos Guedes Soares. Modeling multivariate ocean data using asymmetric copulas. *Coastal Engineering*, 135:91–111, 2018.

[40] Tiago Fazeres-Ferradosa, Francisco Taveira-Pinto, Erik Vanem, Maria Teresa Reis, and Luciana das Neves. Asymmetric copula–based distribution models for met-ocean data in offshore wind engineering applications. *Wind Engineering*, 42(4):304–334, 2018.

[41] G.A Torres-Alves and O. Morales-Nápoles. Reliability analysis of flood defenses: The case of the Nezahualcoyotl dike in the Aztec city of Tenochtitlan. *Reliability Engineering & System Safety*, 203:107057, 2020.

[42] Abe Sklar. Fonctions de répartition à n dimensions et leurs marges. *Publications de l'Institut de Statistique de l'Université de Paris*, 8:229–231, 1959.

[43] Harry Joe. *Dependence Modeling with Copulas*. Chapman and Hall/CRC, 2014.

[44] Harry Joe. *Multivariate Models and Multivariate Dependence Concepts*. Chapman & Hall/CRC Monographs on Statistics & Applied Probability. Taylor & Francis, 1997.

[45] Fabrizio Durante, José Quesada-Molina, and Manuel Úbeda Flores. A method for constructing multivariate copulas. In *New Dimensions in Fuzzy Logic and Related Technologies - Proceedings of the 5th EUSFLAT 2005 Conference*, volume 1, pages 191–195, 01 2007.

[46] R.B. Nelsen. *An Introduction to Copulas*. Lecture Notes in Statistics. Springer New York, 2013.

[47] Mimi Zhang and Tim Bedford. Vine copula approximation: a generic method for coping with conditional dependence. *Statistics and Computing*, 28(1):219–237, 2017.

[48] Roger M. Cooke. Markov and entropy properties of tree-and vine-dependent variables. In *Proceedings of the ASA Section on Bayesian Statistical Science*, 01 1997.

[49] Tim Bedford and Roger M. Cooke. Vines-a new graphical model for dependent random variables. *The Annals of Statistics*, 30(4):1031–1068, 2002.

[50] Dorota Kurowicka and Roger Cooke. A parameterization of positive definite matrices in terms of partial correlation vines. *Linear Algebra and its Applications*, 372:225 – 251, 2003.

[51] Dorota Kurowicka and Roger Cooke. *Uncertainty Analysis With High Dimensional Dependence Modelling*. Uncertainty Analysis with High Dimensional Dependence Modelling. Wiley Series in Probability and Statistics, 2006.

[52] Dorota Kurowicka and Harry Joe. *Dependence Modeling: Vine Copula Handbook*. World Scientific Publishing Co. Pte. Ltd., 2010.

[53] C. Czado. *Analyzing Dependent Data with Vine Copulas: A Practical Guide With R*. Lecture Notes in Statistics. Springer International Publishing, 2019.

[54] J. Dißmann, E.C. Brechmann, C. Czado, and D. Kurowicka. Selecting and estimating regular vine copulae and application to financial returns. *Computational Statistics & Data Analysis*, 59:52–69, 2013.

[55] O. Morales-Nápoles. *Bayesian Belief Nets and Vines in Aviation Safety and other Applications.* PhD thesis, Delft University of Technology, 02 2010.

[56] O Morales-Nápoles, M. Rajabi-Bahaabadi, G.A Torres-Alves, and C.M.P 't Hart. Chimera: An atlas of regular vines on up to 8 nodes. *Scientific Data*, 10(1), 2023.

[57] O. Morales-Nápoles. Counting vines. In *Dependence Modeling Vine Copula Handbook*, chapter 9, pages 189–218. World Scientific Publishing Co. Pte. Ltd., 2010.

[58] H. Akaike. A new look at the statistical model identification. *IEEE Transactions on Automatic Control*, 19(6):716–723, 1974.

[59] H. Vernieuwe, S. Vandenberghe, B. De Baets, and N. E. C. Verhoest. A continuous rainfall model based on vine copulas. *Hydrology and Earth System Sciences*, 19(6):2685–2699, 2015.

[60] Xinyu Jiang, Lijiao Yang, and Hirokazu Tatano. Assessing spatial flood risk from multiple flood sources in a small river basin: A method based on multivariate design rainfall. *Water*, 11:1031, 05 2019.

[61] George Pouliasis, Gina Alexandra Torres-Alves, and Oswaldo Morales-Nápoles. Stochastic modeling of hydroclimatic processes using vine copulas. *Water*, 13(16), 2021.

[62] B. Gräler, M. J. van den Berg, S. Vandenberghe, A. Petroselli, S. Grimaldi, B. De Baets, and N. E. C. Verhoest. Multivariate return periods in hydrology: A critical and practical review focusing on synthetic design hydrograph estimation. *Hydrology and Earth System Sciences*, 17(4):1281–1296, 2013.

[63] M. Carmen Domínguez, Mario Gómez Díaz, and María Concepción Ausín Olivera. Vine copula models for predicting water flow discharge at King George Island, Antarctica. Report 23812, Universidad Carlos III de Madrid. Departamento de Estadística, 10 2016.

[64] W. S. Jäger and O. Morales Nápoles. A vine-copula model for time series of significant wave heights and mean zero-crossing periods in the north sea. *ASCE-ASME Journal of Risk and Uncertainty in Engineering Systems, Part A: Civil Engineering*, 3(4), 2017.

[65] Ruben de Nie, Georgios Leontaris, Don Hoogendoorn, and A. R. M. Wolfert. Offshore infrastructure planning using a vine copula approach for environmental conditions: An application for replacement maintenance of tidal energy infrastructure. *Structure and Infrastructure Engineering*, 15(5):600–617, 2019.

[66] Hugh A Watson et al. Launch control safety study. *Bell labs*, 1961.

[67] Qamar Mahboob and Daniel Straub. Comparison of fault tree and Bayesian networks for modeling safety-critical components in railway systems. In *Advances in Safety, Reliability and Risk Management: Proceedings of the European Safety and Reliability Conference (ESREL 2011)*, pages 89–95. CRC Press, 08 2011.

[68] Yinan Cai and Michael W. Golay. A dynamic Bayesian network-based emergency decision-making framework highlighting emergency propagations: Illustrated using the Fukushima nuclear accidents and the Covid-19 pandemic. *Risk Analysis*, n/a(n/a), 2022.

[69] Prabal Das and Kironmala Chanda. Bayesian Network based modeling of regional rainfall from multiple local meteorological drivers. *Journal of Hydrology*, 591:125563, 2020.

[70] D. Paprotny and O. Morales-Nápoles. Estimating extreme river discharges in europe through a Bayesian network. *Hydrology and Earth System Sciences*, 21(6):2615–2636, 2017.

[71] A. Sebastian, E.J.C. Dupuits, and O. Morales-Nápoles. Applying a Bayesian network based on Gaussian copulas to model the hydraulic boundary conditions for hurricane flood risk analysis in a coastal watershed. *Coastal Engineering*, 125:42–50, 2017.

[72] Luis Carlos Ortega Chamorro and Julio Eduardo Cañón Barriga. Urban risks due to climate change in the Andean municipality of Pasto, Colombia: A Bayesian network approach. *Risk Analysis*, n/a(n/a), 2023.

[73] H.C.W. van Verseveld, A.R. van Dongeren, N.G. Plant, W.S. Jäger, and C. den Heijer. Modelling multi-hazard hurricane damages on an urbanized coast with a Bayesian network approach. *Coastal Engineering*, 103:1–14, 2015.

[74] Rita L. Sousa and Herbert H. Einstein. Risk analysis during tunnel construction using Bayesian networks: Porto metro case study. *Tunnelling and Underground Space Technology*, 27(1):86–100, 2012.

[75] Judea Pearl. *Probabilistic Reasoning in Intelligent Systems: Networks of Plausible Inference.* Morgan Kaufmann Publishers Inc., San Francisco, CA, USA, 1988.

[76] N. Fenton and M. Neil. *Risk Assessment and Decision Analysis with Bayesian Networks (2nd ed.).* Chapman and Hall/CRC., 2018.

[77] Indrani Hazel Govender, Ullrika Sahlin, and Gordon C. O'Brien. Bayesian network applications for sustainable holistic water resources management: Modeling opportunities for South Africa. *Risk Analysis*, 42(6):1346–1364, 2022.

[78] Pedro Antão and C. Guedes Soares. Analysis of the influence of human errors on the occurrence of coastal ship accidents in different wave conditions using Bayesian Belief Networks. *Accident Analysis & Prevention*, 133:105262, 2019.

[79] Pedro Antão and C. Soares. Analysis of the influence of waves in the occurrence of accidents in the Portuguese coast using Bayesian belief networks. *Journal of KONBiN*, 13(1):105–116, 2010.

[80] Marcelo Ramos Martins, Adriana Miralles Schleder, and Enrique López Droguett. A methodology for risk analysis based on hybrid Bayesian networks: Application to the regasification system of liquefied natural gas onboard a floating storage and regasification unit. *Risk Analysis*, 34(12):2098–2120, 2014.

[81] A. M. Hanea, D. Kurowicka, and R. M. Cooke. Hybrid method for quantifying and analyzing Bayesian belief nets. *Quality and Reliability Engineering International*, 22(6):709–729, 2006.

[82] E. Ragno, M. Hrachowitz, and O. Morales-Nápoles. Applying non-parametric Bayesian networks to estimate maximum daily river discharge: potential and challenges. *Hydrology and Earth System Sciences*, 26(6):1695–1711, 2022.

[83] Anca Hanea. *Algorithms for non-parametric Bayesian belief nets*. Doctoral thesis, Delft University of Technology, 2008.

[84] Anca Hanea, Oswaldo Morales Nápoles, and Dan Ababei. Non-parametric Bayesian networks: Improving theory and reviewing applications. *Reliability Engineering & System Safety*, 144:265–284, 2015.

[85] Barry R. Cobb, Rafael Rumí, and Antonio Salmerón. Bayesian Network models with discrete and continuous variables. In Peter Lucas, José A. Gámez, and Antonio Salmerón, editors, *Advances in Probabilistic Graphical Models*, pages 81–102, Berlin, Heidelberg, 2007. Springer Berlin Heidelberg.

[86] Ibrahim Alkhairy, Samantha Low-Choy, Justine Murray, Junhu Wang, and Anthony Pettitt. Quantifying conditional probability tables in bayesian networks: Bayesian regression for scenario-based encoding of elicited expert assessments on feral pig habitat. *Journal of Applied Statistics*, 47(10):1848–1884, 2020.

[87] Bill Cooper, Andrew Saulter, and Peter Hodgetts. *Guidelines for the use of metocean data through the life cycle of a marine renewable energy development*. CIRIA publication. CIRIA, 2008.

[88] Kin Sik Liu and Johnny C. L. Chan. Climatological characteristics and seasonal forecasting of tropical cyclones making landfall along the south China coast. In *Monthly Weather Review*, volume 131, pages 1650 – 1662, Boston MA, USA, 2003. American Meteorological Society.

[89] Bolin Jiang, Bo Liang, and Shanshan Wu. Feasibility study on the submerged floating tunnel in Qiongzhou Strait, China. *Polish Maritime Research*, 25:4–11, 2018.

[90] Wu Shengzhong, Chen Xiang, Li Qinxi, and Cao Gengren. Research on type selection of submerged floating tunnel of Qiongzhou Strait. *Procedia Engineering*, 166:307–316, 2016.

[91] Global Times. First tunnel across Qiongzhou Strait. *Global Times*, 08 2018.

[92] Copernicus Climate Change Service (C3S)(2017):ERA5. Fifth generation of ECMWF atmospheric reanalyses of the global climate. copernicus climate change service climate data store (CDS). Date of access July 2019.

[93] Copernicus Marine Environment Monitoring Service. Date of Access: July 2019. `http://marine.copernicus.eu/`.

[94] Robert J. Hijmans. *raster: Geographic Data Analysis and Modeling*, 2020. R package version 3.3-13.

[95] R Core Team. *R: A Language and Environment for Statistical Computing*. R Foundation for Statistical Computing, Vienna, Austria, 2020.

[96] Sofia Caires. Extreme value analysis: wave data. Technical Report 57, World Meteorological Organization/JCOMM, 2011. Geneva, Switzerland.

[97] AHJM Vervuurt, JP Pruiksma, RDJM Steenbergen, WMG Courage, S. Miraglia, and O. Morales-Nápoles (TUD). Statische belastingen herijking verkeersbelastingen voor brugconstructies op basis van WIM analyses van April 2013 (IQ-2014-33c). Report, TNO, 2015.

[98] Miguel Angel Mendoza-Lugo, Oswaldo Morales-Nápoles, and David Joaquín Delgado-Hernández. A Non-parametric Bayesian network for multivariate probabilistic modelling of Weigh-in-Motion system data. *Transportation Research Interdisciplinary Perspectives*, 13:100552, 2022.

[99] Paul Koot, Miguel Angel Mendoza-Lugo, Dominik Paprotny, Oswaldo Morales-Nápoles, Elisa Ragno, and Daniël T.H. Worm. PyBanshee version (1.0): A Python implementation of the MATLAB toolbox BANSHEE for non-parametric Bayesian networks with updated features. *SoftwareX*, 21:101279, 2023.

[100] Christian Ingerslev. Immersed and floating tunnels. *Procedia Engineering*, 4:51–59, 12 2010.

[101] Miguel Angel Mendoza-Lugo, David Joaquín Delgado-Hernández, and Oswaldo Morales-Nápoles. Reliability analysis of reinforced concrete vehicle bridges columns using non-parametric Bayesian networks. *Engineering Structures*, 188:178 – 187, 2019.

[102] Habib Tabatabai, Hani Titi, and Jian Zhao. WIM-based assessment of load effects on bridges due to various classes of heavy trucks. *Engineering Structures*, 140:189–198, 2017.

[103] Oswaldo Morales-Nápoles and Raphaël D.J.M. Steenbergen. Analysis of axle and vehicle load properties through Bayesian networks based on weigh-in-motion data. *Reliability Engineering & System Safety*, 125:153 – 164, 2014. Special issue of selected articles from ESREL 2012.

[104] Oswaldo Morales-Nápoles and Raphaël D. J. M. Steenbergen. Large-scale hybrid Bayesian network for traffic load modeling from Weigh-in-Motion system data. *Journal of Bridge Engineering*, 20(1):04014059, 2015.

[105] Schepsmeier, Stöber, Brechmann, Gräler, Nagler, and Erhardt. VineCopula: statistical inference of vine copulas. https://cran.r-project.org/web/packages/VineCopula/index.html, 2018.

[106] A. Nestegård, S.A. Haugerud, J. Solemsli, K.B. Engebretsen, K. Wåsjø, and A. Myhr. K3- k4 design basis report - bjornafjord submerged floating tunnel. Technical report, Norconsult, 2016.

[107] EN. *EN 1990. Eurocode: Basis of structural design*, Brussels, 2002. CEN.

[108] M.R. Leadbetter. On a basis for 'peaks over threshold' modeling. *Statistics & Probability Letters*, 12(4):357–362, 1991.

[109] Nejc Bezak, Mitja Brilly, and Mojca Šraj. Comparison between the peaks-over-threshold method and the annual maximum method for flood frequency analysis. *Hydrological Sciences Journal*, 59(5):959–977, 2014.

[110] Pamela S. Naden. *Analysis and use of peaks-over-threshold data in flood estimation*, pages 131–143. Springer Netherlands, Dordrecht, 1992.

[111] Max Rydman. Application of the peaks-over-threshold method on insurance data, 2018.

[112] Leo H. Holthuijsen. *Waves in Oceanic and Coastal Waters*. Cambridge University Press, 2007.

[113] M. A. Ribatet. A user's guide to the POT package (Version 1.1-7), 08 2006.

[114] Anthony C. Davison and Richard L. Smith. Models for exceedances over high thresholds. *Journal of the royal statistical society series b-methodological*, 52:393–425, 1990.

[115] Marko Katalinić and Joško Parunov. Uncertainties of estimating extreme significant wave height for engineering applications depending on the approach and fitting technique—Adriatic Sea case study. *Journal of Marine Science and Engineering*, 8(4), 2020.

[116] Kjersti Aas, Claudia Czado, Arnoldo Frigessi, and Henrik Bakken. Pair-copula constructions of multiple dependence. *Insurance: Mathematics and Economics*, 44(2):182 – 198, 2009.

[117] P. Stoica and Y. Selen. Model-order selection: a review of information criterion rules. *IEEE Signal Processing Magazine*, 21(4):36–47, 2004.

[118] Kenneth P. Burnham and David R. Anderson. Multimodel inference: Understanding AIC and BIC in model selection. *Sociological Methods & Research*, 33(2):261–304, 2004.

[119] Kenneth P. Burnham, David R. Anderson, and Kathryn P. Huyvaert. AIC model selection and multimodel inference in behavioral ecology: some background, observations, and comparisons. *Behavioral Ecology and Sociobiology*, 65:23–35, 2010.

[120] J.N. Newman. *Marine Hydrodynamics*. Mit Press. Wei Cheng Cultural Enteroprise Company, 1977.

[121] P. Boccotti. *Wave Mechanics and Wave Loads on Marine Structures*. Elsevier Science, 2014.

[122] C. M.P. 't Hart, D. J. Peters, O. Morales-Nápoles, and S. N. Jonkman. Target reliability for submerged floating tunnels. In Hiroshi Yokota and Dan M. Frangopol, editors, *Bridge Maintenance, Safety, Management, Life-Cycle Sustainability and Innovations - Proceedings of the 10th International Conference on Bridge Maintenaince, Safety and Management, IABMAS 2020*, Bridge Maintenance, Safety, Management, Life-Cycle Sustainability and Innovations - Proceedings of the 10th International Conference on Bridge Maintenance, Safety and Management, IABMAS 2020, pages 857–863. CRC Press / Balkema - Taylor & Francis Group, 2021. 10th International Conference on Bridge Maintenaince, Safety and Management, IABMAS 2020 ; Conference date: 11-04-2021 Through 15-04-2021.

[123] ISO 2394. *General Principles on Reliability for Structures*, volume 2015. ISO. Joint Committee on Structural Safety, Geneva, Switzerland, 2015.

[124] JCSS. JCSS Probabilistic Model Code, 1999.

[125] Norwegian Technology Standards Institution. Actions and Action Effects. Standard, Norwegian Technology Standards Institution, Oslo, Norway, 1999.

[126] A. Sperotto, J.L. Molina, S. Torresan, A. Critto, M. Pulido-Velazquez, and A. Marcomini. A Bayesian networks approach for the assessment of climate change impacts on nutrients loading. *Environmental Science & Policy*, 100:21–36, 2019.

[127] Qingwen Lu, Ping an Zhong, Bin Xu, Feilin Zhu, Yufei Ma, Han Wang, and Sunyu Xu. Risk analysis for reservoir flood control operation considering two-dimensional uncertainties based on Bayesian network. *Journal of Hydrology*, 589:125353, 2020.

[128] Dominik Paprotny, Oswaldo Morales-Nápoles, Daniël T.H. Worm, and Elisa Ragno. Banshee−a matlab toolbox for non-parametric Bayesian networks. *SoftwareX*, 12:1–7, 2020.

[129] O Morales-Nápoles, D Worm, P van den Haak, A Hanea, A Courage, and A Miraglia. Reader for course: Introduction to Bayesian Networks. Technical report, The Netherlands Organisation for applied scientific research (TNO), Delft, The Netherlands, 2013.

[130] Oswaldo Morales-Nápoles, David Joaquín Delgado-Hernández, David De-León-Escobedo, and Juan Carlos Arteaga-Arcos. A continuous Bayesian network for earth dams' risk assessment: methodology and quantification. *Structure and Infrastructure Engineering*, 10(5):589–603, 2014.

[131] Julwan Hendry Purba. A fuzzy-based reliability approach to evaluate basic events of fault tree analysis for nuclear power plant probabilistic safety assessment. *Annals of Nuclear Energy*, 70:21–29, 2014.

[132] Jin Wang, Fang Wang, Shanqi Chen, Jiaqun Wang, Liqin Hu, Yuan Yin, and Yican Wu. Fault-tree-based instantaneous risk computing core in nuclear power plant risk monitor. *Annals of Nuclear Energy*, 95:35–41, 2016.

[133] Fang Zhao, Shuliang Zou, Shoulong Xu, Junlong Wang, Tao Xu, and Dewen Tang. Safety analysis of marine nuclear reactor in severe accident with dynamic fault trees based on cut sequence method. *Nuclear Engineering and Technology*, 54(12):4560–4570, 2022.

[134] M. Mazzoleni, Y. Maccarana, and F. Previdi. A comparison of data-driven fault detection methods with application to aerospace electro-mechanical actuators. *IFAC-PapersOnLine*, 50(1):12797–12802, 2017. 20th IFAC World Congress.

[135] Jian Hao, Yingchao Song, Peizhe Zhang, Haojie Liu, Shun Jia, Yujie Zheng, and Xioafeng Zhang. Failure analysis of scraper conveyor based on fault tree and optimal design of new scraper with polyurethane material. *Journal of Materials Research and Technology*, 18:4533–4548, 2022.

[136] Favour Ikwan, David Sanders, and Mohamed Hassan. Safety evaluation of leak in a storage tank using fault tree analysis and risk matrix analysis. *Journal of Loss Prevention in the Process Industries*, 73:104597, 2021.

[137] Matthias Schubert, Niels Peter Høj, Arild Ragnøy, and Harald Buvik. Risk assessment of road tunnels using Bayesian networks. *Procedia - Social and Behavioral Sciences*, 48:2697–2706, 2012. Transport Research Arena 2012.

[138] Fan Wang, Heng Li, Chao Dong, and Lieyun Ding. Knowledge representation using non-parametric Bayesian networks for tunneling risk analysis. *Reliability Engineering & System Safety*, 191:106529, 2019.

[139] A. Bobbio, L. Portinale, M. Minichino, and E. Ciancamerla. Improving the analysis of dependable systems by mapping fault trees into Bayesian networks. *Reliability Engineering & System Safety*, 71(3):249–260, 2001.

[140] Özkan Uğurlu, Ercan Köse, Umut Yıldırım, and Ercan Yüksekyıldız. Marine accident analysis for collision and grounding in oil tanker using fta method. *Maritime Policy & Management*, 42(2):163–185, 2013.

[141] Norsys Software Corp. Netica and Netica API: For Java on Windows 5.04. Bayesian Network Software from Norsys, 2022.

[142] H. Hersbach, B. Bell, P. Berrisford, G. Biavati, A. Horányi, J. Muñoz Sabater, J. Nicolas, C. Peubey, R. Radu, I. Rozum, D. Schepers, A. Simmons, C. Soci, D. Dee, and J-N. Thépaut. ERA5 hourly data on single levels from 1959 to present. copernicus climate change service (C3S) Climate Data Store (CDS). (2018) Accessed on July 2022.

[143] National Geophysical Data Center / World Data Service (NGDC/WDS). NCEI/WDS Global Significant Earthquake Database. NOAA National Centers for Environmental Information. Date of access: June 2022.

[144] Pedro Antão and C. Guedes Soares. Fault-tree models of accident scenarios of RoPax vessels. *International Journal of Automation and Computing*, 3(2):107–116, 2006.

[145] Jichuan Kang, Liping Sun, and C. Guedes Soares. Fault tree analysis of floating offshore wind turbines. *Renewable Energy*, 133:1455–1467, 2019.

[146] Bruce R. Ellingwood. Mitigating risk from abnormal loads and progressive collapse. *Journal of Performance of Constructed Facilities*, 20(4):315–323, 2006.

[147] Qingsheng Miao, Xinyang Yue, Jinkun Yang, Zhifeng Wang, Shanshan Xu, Yang Yang, and Siqi Chu. Characteristics analysis and risk assessment of extreme water levels based on 60-year observation data in Xiamen, China. *Journal of Ocean University of China*, 21(2):315–322, 2022.

[148] Rui Huang, Baoguo Liu, Jinglai Sun, Yu Song, and Mingyuan Yu. A multistate Bayesian Network-based approach for risk analysis of tunnel collapse. *Arabian Journal for Science and Engineering*, 47(4):4893–4911, 2022.

[149] Torgeir Moan and Mathias Eidem. *Floating Bridges and Submerged Tunnels in Norway—The History and Future Outlook*, pages 81–111. Springer, 2020.

[150] Proceedings from the Fifth International Symposium on Tunnel Safety and Security. *Submerged Floating Tunnels, a New Tunnel Concept, Creating New Challenges in Tunnel Safety and Security*, SP Rapport, Norway, 03 2012. SP Fire Research.

[151] Yiqiang Xiang, Chengxi Liu, Chunfeng Chao, and Huishi Liu. Risk analysis and assessment of public safety of submerged floating tunnel. *Procedia Engineering*, 4:117–125, 2010.

[152] Mari Krogness Forsnes. *Risk assessment of strait crossing bridges*. Master thesis, Norwegian University of Science and Technology, 2015.

[153] Konrad Bergmeister and Sandro Francesconi. Causes and frequency of incidents in tunnels. Technical report D1.2a, Autostrada del Brennero SpA, 2004.

Acknowledgments

Firstly, I acknowledge that this research is part of the Submerged Floating Tunnel Technical Joint Research Team that is led by the Chinese engineering and construction company China Communications Construction Co., Ltd. (CCCC) and supported by both public and private companies (such as TU Delft, Tunnel Engineering Consultants-TEC, among others). This thesis marks the culmination of a significant chapter in my life. In 2019, I embarked on this journey, and despite the challenges along the way and a pandemic later, I am finally here. This path has proven to be the most enduring and enriching experience of my life.

I will start by thanking my daily supervisor and promotor **Dr. Ir. Oswaldo Morales-Nápoles**. Our collaboration started during my master's thesis and for the past 7 years, you have not only served a role as a supervisor but evolved into a valuable colleague, mentor, and friend. I consider myself fortunate to have had your full support throughout my Ph.D. journey, granting me the freedom to explore my research interests. I am grateful for our conversations, ranging from Mexican culture to delving into the probabilistic intricacies even in the simplest aspects of life. Oswaldo's influence has transformed me into a probabilistic enthusiast. It has been a pleasure working with and learning from you. I look forward to continue working together.

I want to express my gratitude to my promotor, **Dr. Ir. Bas Jonkman**, for the valuable discussions we had during my Ph.D. I am thankful for your insightful perspective, which opened my eyes and mind to diverse viewpoints. This led to improvements in the work presented in this thesis. I appreciate your consideration for the well-being of your students. I would like to thank the independent members of my doctoral committee. Thank you for your time and interest in my research.

To my colleagues at the Hydraulic engineering department, thank you for the camaraderie and positive vibes. Your friendly presence made the journey more enjoyable. To the SFT team members at TU Delft, **Marcel**, **Roelof**, **Dirk Jan**. It was an enriching experience working with each one of you. **Marcel**, I'm grateful for the collaboration on our paper. Working with you was not only productive but also a pleasure. Thanks for your contributions and our great teamwork.

To my office mates, **Miguel**, **Pengxu**, and **Danny**. Thank you for the hundreds of coffee and tea cups shared after lunch at our coffee machine on the second floor. Thank you for the laughs shared, and the words of support and encouragement we gave to each other during these years. **Miguel**, I want to express my gratitude for the cheerful blend of chisme catch-ups and profound conversations we've shared. Your support during the isolated times of COVID has been invaluable. I cherish the "stupid questions" sessions where we created a safe space to explore new ideas. **Dr. Peng**, thank you for always lighting up the office with your laughs. Your positivity was like a breath of fresh air during tough times. To the PSOR crew, thank you for the laughs and the beers we shared. Your company was my weekly getaway, and I always looked forward to it after a long week.

Living in a foreign country has given new significance to the saying "friends are the family you chose". To my second family, thank you for transforming the Netherlands into my home: **Arturo**, mi pana, mi ñaño, what an incredible friend life gave me. Despite the distance, we have been able to keep our friendship fresh, like we were never apart. Thank you for the long voice notes to catch up about our lives. Thank you for always being there, for understanding, for the karaoke nights, thank you for all the conversations about life. We grew up together. To **Rasa**, my dear friend and the honorary third member of our house. Our initial connection over a shared love for good food, trashy reality TV shows, drag queens, and pop divas quickly blossomed into a profound friendship. You arrived at my life at the perfect time. Thank you for being my confidant, for countless hours of conversations and laughter. Your friendship stands as one of the most valuable connections I've ever had; **Claudia**, from the spontaneous creation of "Las Fit" on a tipsy Saturday night to becoming one of my dearest friends, our journey has been nothing short of amazing. Thanks for being my perpetual "so low" date and the ultimate mixologist extraordinaire; **Ale**, **Arturo**, and little **Meli**. Thank you for being my Mexican family. Your welcoming home, shared laughter, and meals together have made me feel right at home. Thank you for adding board games to my plethora of existing hobbies. Those long and dark winters would not have been the same without you.

To the Latin crew, **Fernando**, **Claudia**, **Juan**, **Thomas**, **Lore**, **Menno**, and **Jakub**: thank you for the birthdays and celebrations we've had together. Your friendship brings a sense of home to every gathering. Our shared moments, filled with laughter are memories that I hold close to my heart.

To my dear family –**Mom, Karen, and Brian**– thank you for being the fuel that propels me forward. Your constant presence and comforting refuge have been my anchor through thick and thin. I am fortunate to have such a wonderful family. I aim to continue making you proud with every step I take. Cachito, this is for you. All of this is for you.

To my beloved abuelita Mercedes and tia Cuca, the matriarchs of our family. Your support has shaped my path in ways I can't express enough gratitude for. Thank you for the heartwarming conversations filled with love and encouragement.

Last but certainly not least, to **Gaby**, luz de mis ojos. What can I say that I haven't expressed in all these years? Thank you for your support and patience. Your open arms, especially during my moments of defeat, have been my sanctuary. Thank you for celebrating every achievement, big or small, and for the Mexican meals that have become my comfort food. Our home is a testament to the beautiful life we are building together. Thanks for the love, understanding, and freedom you've generously given me that I never thought possible. I can not wait for tomorrow to embark on the next chapter of our lives together.

Gina
Delft, September 2024

Curriculum Vitæ

13/05/1991	Born in Cuenca, Ecuador

Education

2023	Ph.D. in Hydraulic Engineering. Delft University of Technology.
2016-2018	MSc. in Civil Engineering, Hydraulic Structures section. Delft University of Technology, The Netherlands. Thesis: *'Reliability Analysis of the Nezahualcoyotl Dike in the Aztec City of Tenochtitlan'.*
2008-2013	BSc Civil Engineering. University of Cuenca.

Employment

2023-present	Junior Researcher, TNO. Delft, The Netherlands.
2019-2023	Ph.D. Candidate, Department of Hydraulic Engineering, Delft University of Technology, Delft, The Netherlands.
2015-2016	Freelance Engineer. Design of private projects. Cuenca, Ecuador.
2014-2016	Junior Engineer, PROMAS. University of Cuenca. Cuenca, Ecuador.
2012	Junior Engineer, SIPETROL. Cuenca, Ecuador.

Awards

2015	Senescyt Scholarship Universities of Excellence.

List of Publications

Journal Publications

1. **G.A. Torres-Alves**, *Oswaldo Morales-Nápoles, and S.N. Jonkman.* Bayesian Networks to assess the risk and reliability of a Submerged floating tunnel'. Structure and Infrastructure Engineering. *Under Review.*

2. **G.A. Torres-Alves**, *and Oswaldo Morales-Nápoles.* Vine-Copula model for simulation of extreme metocean loads and estimation of hydrodynamic forces for a submerged floating tunnel at the Qiongzhou Strait'. Marine Structures. *Under Review.*

3. **G.A. Torres-Alves**, *C.M.P. 't Hart, O. Morales-Nápoles, and S.N. Jonkman.* 'Structural reliability analysis of a submerged floating tunnel under copula-based traffic load simulations'. Engineering Structures, 269:114752, 2022. *Published.*

4. *George Pouliasis,* **G.A. Torres-Alves**, *and Oswaldo Morales-Nápoles.* Stochastic Modeling of Hydroclimatic Processes Using Vine Copulas. Water 13.16 (2021), p. 1-19. issn: 2073-4441. doi: 10.3390/913w13162156. url: `https://www.mdpi.com/2073-4441/13/16/2156`. *Published.*

5. **G.A. Torres-Alves** and *Oswaldo Morales-Nápoles.* Reliability analysis of flood defenses: The case of the Nezahualcoyotl dike in the Aztec city of Tenochtitlan'. In: Reliability Engineering & System Safety (2020), p. 107057. issn: 0951-8320. doi: https://doi.org/10.1016/j.ress.2020.107057. url: `https://www.sciencedirect.com/science/article/pii/S0951832020305585`. *Published.*

6. *O. Morales Nápoles, C.M.P. 't Hart,* **G.A. Torres-Alves,** *E. Perrone, E. Ragno.* A simulation study of fitting regular vines on up to 8 nodes. *Not Submitted yet.*

7. *O. Morales Nápoles, M. Rajabi-Bahaabadi,* **G.A. Torres-Alves,** *and & C.M.P. 't Hart.* Chimera: An atlas of regular vines on up to 8 nodes. Scientific Data, 10(1), 33. *Published.*

8. **G.A. Torres-Alves**, *M.A. Mendoza Lugo, O. Morales-Nápoles, & E.Ragno.* Non-stationary probabilities of the smallest marathon times for Brazilian, Mexican, Ethiopian, and Kenyan male runners. *Not Submitted yet.*

9. *T. de Kok, H. Niazi,* **G. A. Torres-Alves,** *B. van Es, O. Morales-Nápoles, & B. van Prooijen.* Temporal Variability in Nature-based Hybrid Flood Defenses: A Dynamic Bayesian Network. Coastal Engineering. *Under Review.*

Conference Proceedings

📄 10. **G.A. Torres-Alves**, *O. Morales-Nápoles, P. Mares-Nasare* Reliability analysis for overturning and sliding of lacustrine dikes: The Nezahualcoyotl's dike case. Proceedings of the 33rd European Safety and Reliability Conference (ESREL 2023). Conference date: 03-09-2023 to 08-09-2023. *Published.*

📄 11. *Miguel Angel Mendoza-Lugo*, **G.A. Torres-Alves**, *O. Morales-Nápoles* Reliability analysis of the ancient Nezahualcoyotl's dike. Investigating failure due to overtopping using an improved hydrological model. Proceedings of the 33rd European Safety and Reliability Conference (ESREL 2023). Conference date: 03-09-2023 to 08-09-2023. *Published.*

📄 12. **G.A. Torres-Alves**, *O. Morales-Nápoles, & S.N. Jonkman.* Bayesian Networks for Estimating Hydrodynamic Forces on a Submerged Floating Tunnel. Proceedings of the 31st European Safety and Reliability Conference, ESREL 2021 (pp 2518-2524). Ed. by Bruno Castanier, Marko Cepin, Marko, David Bigaud, Christophe Berenguer. Conference date: 19-09-2021 to 23-09-2021. isbn: 978-981-18-2016-8. doi: `https://doi.org/10.3850/978-981-18-2016-8_292-cd`. *Published.*

📄 13. **G.A. Torres-Alves**, *O. Morales-Nápoles, & S.N. Jonkman.* Simulation of hydrodynamic loads for a submerged floating tunnel using a copula-based model. Bridge Maintenance, Safety, Management, Life-Cycle Sustainability and Innovations - Proceedings of the 10th International Conference on Bridge Maintenance, Safety and Management, IABMAS 2020 (pp. 844-852). Ed. by H. Yokota, & D. M. Frangopol. CRC Press / Balkema - Taylor & Francis Group. Conference date: 11-04-2021 to 15-04-2021. isbn: 9780367232788. doi: `https://doi.org/10.1201/9780429279119-112`. *Published.*

📄 14 *O. Morales-Nápoles, D. Paprotny, A. Couasnon*, **G.A. Torres-Alves**, *S. Sanjaya.* Non-Parametric Bayesian Networks for estimation of Maximum River Discharges. 14th International Conference on Hydroinformatics. 2020. *Published.*